# Oncology and Translational Medicine

Volume 5 • Number 3 • June 2019



Oncology and Translational Medicine Volume 5 • Number 3 • June 2019 pp 103-151



邮发代号：38-121
ISSN 2095-9621

GENERAL INFORMATION
≫otm.tjh.com.cn

ISSN 2095-9621
CN 42-1865/R

# Oncology and Translational Medicine

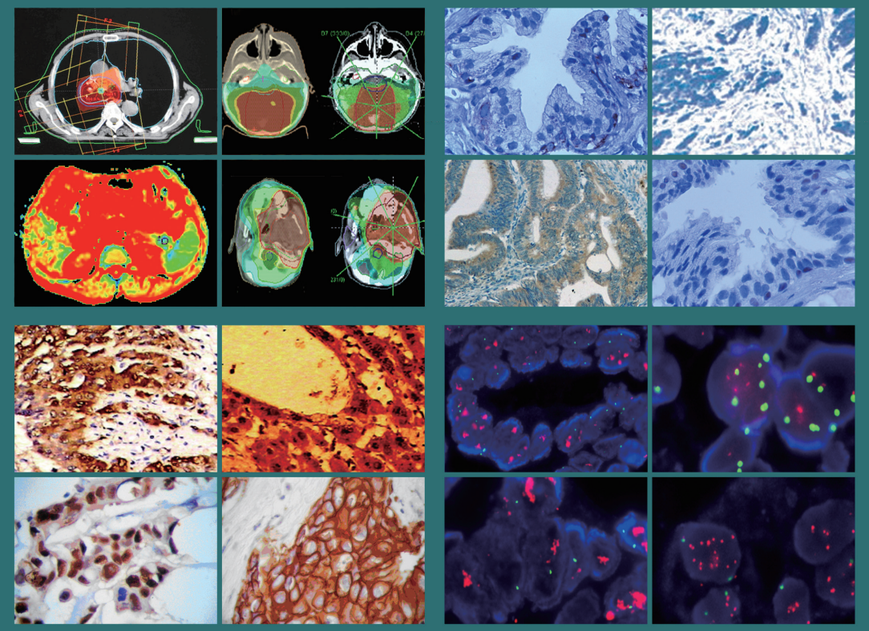

Volume 5
Number 3
June 2019

# Oncology and Translational Medicine

**Oncology and Translational Medicine**
*June 2019 Volume 5 Number 3*

## Contents

# Oncology and Translational Medicine

## Aims & Scope

***Oncology and Translational Medicine*** is an international professional academic periodical. The Journal is designed to report progress in research and the latest findings in domestic and international oncology and translational medicine, to facilitate international academic exchanges, and to promote research in oncology and translational medicine as well as levels of service in clinical practice. The entire journal is published in English for a domestic and international readership.

## Copyright



## Supervised by

Ministry of Education of the People's Republic of China.

## Administered by

Tongji Medical College, Huazhong University of Science and Technology.

## Submission information

Manuscripts should be submitted to:
**http://otm.tjh.com.cn**
**dmedizin@sina.com**

## Subscription information

ISSN edition: 2095-9621
CN: 42-1865/R

■ Subscription rates
Subscription may begin at any time. Remittances made by check, draft or express money order should be made payable to this journal. The price for 2017 is as follows: US $ 30 per issue; RMB ￥28.00 per issue.

## Database

***Oncology and Translational Medicine*** is abstracted and indexed in EMBASE, Index Copernicus, Chinese Science and Technology Paper Citation Database (CSTPCD), Chinese Core Journals Database, Chinese Journal Full-text Database (CJFD), Wanfang Data; Weipu Data; Chinese Academic Journal Comprehensive Evaluation Database.

## Business correspondence

All matters relating to orders, subscriptions, back issues, offprints, advertisement booking and general enquiries should be addressed to the editorial office.

***Mailing address***
Editorial office of
*Oncology and Translational Medicine*
Tongji Hospital
Tongji Medical College
Huazhong University of Science and Technology
Jie Fang Da Dao 1095
430030 Wuhan, China
Tel.: +86-27-69378388
Email: dmedizin@sina.com

**Printer**
Changjiang Spatial Information Technology Engineering Co., Ltd. (Wuhan)
Hangce Information Cartorgraphy Printing Filial, Wuhan, China
Printed in People's Republic of China

## Managing director



## Executive editors

Oncology and Translational Medicine
DOI 10.1007/s10330-019-0335-5

June 2019, Vol. 5, No. 3, P103–P108

ORIGINAL ARTICLE

# Quantitative monitoring and mutations of ctDNA before and after non-small cell lung cancer radical surgery*

**Xiangqi Chen[1], Tingyan Lin[1], Zhisen Gao[1], Jiangjiang Xu[3], Rui Feng[2], Sheng Yang[2], Shuchen Chen[3], Mingqiang Kang[3] (✉)**

[1] Department of Respiratory, Fujian Medical University Union Hospital, Fuzhou 350001, China
[2] Department of Oncology, the Union Hospital of Fujian Medical University, Fuzhou 350001, China
[3] Department of Thoracic surgery, Fujian Medical University Union Hospital, Fuzhou 350001, China

## Abstract

**Objective** The aim of this study was to study the quantitative expression of circulating tumour DNA (ctDNA) in patients with non-small cell lung cancer (NSCLC) before and after radical operation and to explore the correlation between gene mutations in non-small cell lung cancer tissues and those in ctDNA.

**Methods** We randomly assigned 5 NSCLC patients from the Department of Thoracic Surgery of Fujian Medical University Union Hospital. All the patients had undergone radical surgery. Venous blood samples were collected from the 5 NSCLC patients at two time points (before the operation and 21–37 days after the operation) for monitoring ctDNA levels. This was done by isolating plasma from venous blood using high velocity centrifugation, extracting DNA from the plasma using the QIAamp Circulating Nucleic Acid kit, and then quantifying the ctDNA levels. The results were analyzed using the Wilcoxon Rank Sum Test. Moreover, the ctDNA levels were compared with those of carcinoembryonic antigen (CEA), which was detected simultaneously with the ctDNA. Then, DNA samples from the tumor tissues and peripheral blood cells and ctDNA were sequenced using the Hiseq2000 sequencing platform (Illumina) and the mutant genes were screened out. Mutations that occurred within the tumor tissues were used as positive control, whereas those found in the pre-operative blood cells were used as a negative control. Based on the mutational analysis of ctDNA genes, a total of 508 cancer-related genes were screened.

**Results** The median values of the pre- and post-operative ctDNA levels in the 5 patients with NSCLC were 0.612 (0.518–0.876) and 0.430 (0.372–0.612) ng/μL, respectively. There was a significant difference between the two groups ($P < 0.05$). The pre-operative CEA level was slightly higher than the post-operative level ($P > 0.05$). In one of the cases, LC tissues showed multiple mutations, consistent with pre-operative ctDNA. Moreover, isogenic mutations of the same type were not detected in post-operative ctDNA or peripheral blood cells.

**Conclusion** Mutations found in the lung cancer (LC) ctDNA gene were consistent with the mutation type of LC tissue. Hence, the quantitative and qualitative analysis of ctDNA is a promising novel molecular biomarker for the evaluation of tumor burden changes in NSCLC.

Received: 17 March 2019
Revised: 5 April 2019
Accepted: 20 May 2019

**Key words:** ctDNA; non-small cell lung cancer (NSCLC); mutant genes; molecular markers

✉ Correspondence: Mingqiang Kang. Email: drkang2011@163.com
* Supported by grants from the Key Specialty Discipline Construction Program of Fujian and Nation, P.R.C and Fujian Provincial Department of Health's Key Middle-aged and Young Talents Program (No. 2013-ZQN-JC-14).

Lung cancer (LC) is a type of malignant cancer with a very high mortality rate worldwide. In China, its morbidity and mortality rates are the highest and non-small cell lung cancer (NSCLC) is the most common form of this disease. ctDNA is a type of circulating cell-free DNA (ccfDNA) fragment found in the plasma or serum and it is released due to tumor cell apoptosis, necrocytosis, or proactive release [1–2]. ccfDNA is extracellular in nature and is found at extremely low levels in normal human tissues. In 1977, Leon et al. discovered that the DNA levels in the plasma of tumor patients was greatly increased and based on this revelation, several studies further investigated the applications of ccfDNA for the early diagnosis of tumors, real-time monitoring of therapeutic effects, and prediction of relapse [3]. ccfDNA levels were also found to be abnormally increased in patients with ovarian, gastric, and breast cancers [4–6]. Newman et al. reported that the ctDNA level can reflect the changes in the tumor burden in early or terminal NSCLC after various types of treatments [7]. Therefore, ctDNA is a promising novel molecular biomarker for the early diagnosis and evaluation of malignant tumors.

## Materials and methods

### Clinical data and inclusion criteria for relevant mutant genes

All patients included in the study had no previous history of other tumors, distant organ metastasis, chronic liver, kidney, endocrine and immune system diseases before the operation, and had not received any radiotherapy, chemotherapy or immunotherapy (Table 1).

According to the catalog of somatic mutations in cancer (COSMIC) database, the genes that qualified the inclusion criteria (a total of 508 genes) referred to the high frequency mutant genes in various tumors and signaling pathways related to cancer occurrence and development.

### Methods

*Separation of tumor, plasma and blood cell samples*

Venous blood (5 mL) was drawn into EDTA-coated anticoagulant tubes, centrifuged for 10 min at 1600 g (4 °C), and the supernatant containing the plasma was separated. The blood cells were collected and stored at –80 °C. The plasma was further centrifuged for 10 min at 16000 g (4 °C) to remove the residual cells and stored at –80 °C until further use.

Fresh tissues were removed immediately after tumor resection, approximately 0.5 $cm^3$ of tumor tissue mass was cut and then, these samples were stored at -80 °C.

*Extraction of sample DNA and quantitative determination of ctDNA*

DNA extraction from all the tissues and peripheral blood cell samples was performed using QIAGEN QIAamp DNA and blood mini kits (QIAGEN, USA), according to the manufacturer's instructions.

The extraction of free DNA from the plasma was performed using the QIAamp circulating nucleic acid kit, according to the manufacturer's instructions, and the extracted DNA was quantified using the Qubit (Invitrogen, the Quant-iTTM dsDNA HS Assay Kit) quantometer.

*Detection of gene mutations*

A customized chip 140119_HG19_CAN_panel_EZ_HX3 (1.7M) was obtained from Roche and was used to capture sequence hybridization. Hiseq2000 sequencing platform (Illumina) was used for sequencing. GATK (2.3.9) and other software were used to identify somatic SNV, INDEL and CNV.

*Quantitative determination of CEA*

Venous blood (3 mL) was drawn, and CEA was detected using automated immunoassay system (E601, Roche) using the original reagents according to the manufacturer's instructions.

## Results

### ctDNA And CEA levels in patients with NSCLC

As shown in Table 2, the median values of pre- and post-operative ctDNA levels in the five patients with NSCLC were 0.612 (0.518–0.876) and 0.430 (0.372–0.612) ng/μL, respectively. The pre-operative ctDNA level was significantly higher than the post-operative level ($P < 0.05$; Table 2).

The median values of pre- and post-operative CEA levels in the five patients were 3.90 (2.25–6.20) and 1.90 (1.55–4.95) ng/mL, respectively. The pre-operative CEA

**Table 1** Clinical data of five patients with non-small cell lung cancer (*n*)

| No. | Gender | Age (years) | Pathology | TNM Stage* | Clinical stage |
|---|---|---|---|---|---|
| 1 | Female | 59 | Invasive adenocarcinoma | T1N2M0 | IIa |
| 2 | Male | 62 | Median differentiated squamous carcinoma | T2N0M0 | Ib |
| 3 | Male | 56 | Median differentiated squamous carcinoma | T2N1M0 | IIb |
| 4 | Male | 61 | High differentiated squamous carcinoma | T1N1M0 | IIa |
| 5 | Male | 61 | Invasive adenocarcinoma | T2N0M0 | Ib |

* TNM staging was developed by American Joint Committee on Cancer (AJCC) and Union for International Cancer Control (UICC) in 2002

**Table 2** Concentrations of ctDNA and CEA

| Group | ctDNA (ng/μL) (Quartile range) | CEA (ng/mL) (Quartile range) |
|---|---|---|
| Before operation | 0.612 (0.518–0.876) | 3.90 (2.25–6.20) |
| After operation | 0.430 (0.372–0.612) | 1.90 (1.55–4.95) |
| *Z* | –2.023 | –0.944 |
| *P* | 0.043* | 0.345** |

* Comparison of pre- and post-operative ctDNA levels after 28 days in five patients with non-small cell lung cancer ($P < 0.05$); ** Comparison of the first and second CEA levels in patients with non-small cell lung cancer ($P > 0.05$)

level was slightly higher than the post-operative level ($P > 0.05$).

Although there was a difference in the detection time of ctDNA and CEA before operation, all patients had non-excised lung tumor tissue before operation. The median detection time of both indices in blood samples after the operation was 26 days, assuming that the sampling occurred at the same time.

Pre-operative ctDNA and CEA levels were higher than the post-operative levels, but only the ctDNA levels showed significant difference ($P < 0.05$; Table 2). The comparison of pre- and post-operative ctDNA and CEA levels in five patients is shown in Fig. 1.

## Mutations found in NSCLC tissue, peripheral blood cells, and ctDNA

The samples from five patients showed several mutant genes in tumor tissues as well as pre- and postoperative ctDNA (Table 3). A total of 85 mutant genes were detected, with 42 genes detected in the lung tumor tissue, 26 in pre-operative ctDNA, 15 in post-operative ctDNA, and two in pre-operative peripheral blood cells. No mutant genes were found in the post-operative peripheral blood. The mutant genes found were either

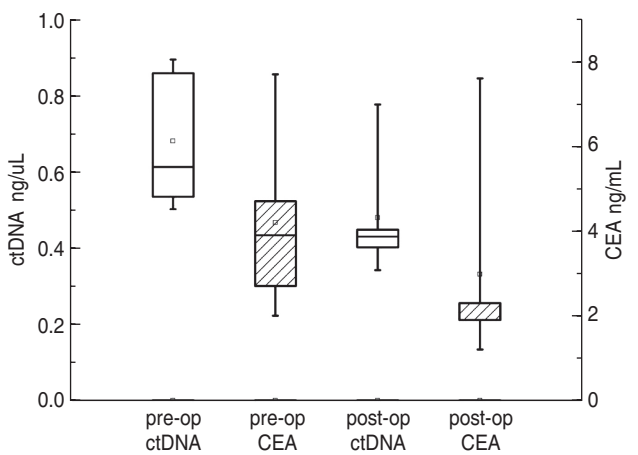


**Fig. 1** Comparison of pre- and post-operative ctDNA and CEA levels in five patients

**Table 3** Number of mutant genes detected in samples

| No. | Pre-operative ctDNA | Post-operative ctDNA | Tumor tissue | Peripheral blood cells |
|---|---|---|---|---|
| 1 | 4 | 1 | 3 | 0 |
| 2 | 9 | 2 | 12 | 0 |
| 3 | 6 | 0 | 5 | 0 |
| 4 | 4 | 6 | 17 | 1 |
| 5 | 3 | 6 | 5 | 1 |

oncogenes or tumor suppressor genes involved in tumor cell signal transduction, regulation of gene transcription, cell proliferation, differentiation, apoptosis, migration, invasion, and metastasis (Table 3).

The mutations in the pre-operative ctDNA were compared with those found in the tumor tissues, post-operative ctDNA and pre-operative blood cells, and the results were as follows: LC tissue showed mutations consistent with pre-operative ctDNA in one case (case no. 2), and the gene and the site location of the mutations were found to be similar. There were eight pairs of identical mutant genes between tumor tissues and pre-operative ctDNA (TP53, PTEN, KMT2D, TET2, CDK12, PRPF40B, RUNX1T1, and NTRK3) in this patient. Moreover, after excision of LC tissue, the same type of isogenic mutation was not detected in ctDNA of this patient. A consistent gene mutation (ASXL1) was also detected between pre- and post-operative ctDNA in one case (No. 5). However, this mutation was not detected in the tumor tissue or peripheral blood cells, suggesting that it might not be derived from the excised tumor tissue.

The average numbers of mutant genes found in the four sample types were in the following order: tumor tissue > pre-operative ctDNA > post-operative ctDNA > peripheral blood cells. There were significant differences in the number of mutant genes between the tumor tissue and peripheral blood cells, and between pre-operative ctDNA and peripheral blood cells ($P < 0.05$). In case of the other pairwise comparisons, especially the pre- and post-operative ctDNA showed no statistical difference ($P > 0.05$).

No significant positive or negative correlation was found in the number of mutant genes in ctDNA and their individual levels. In only three cases, a uniform decrease was seen in the pre- and post-operative ctDNA levels, and two cases of these cases actually showed decreased level but increased number.

We detected three genes (KMT2D, EGFR and TP53) in this study that were amongst the top 20 mutanted genes for LC according to the COSMIC database. The TP53 mutation was detected in three cases, for one of which it was found in the pre-operative ctDNA. Four KMT2D mutations were detected in two cases. Besides the similar mutation types of KMT2D found in ctDNA and tumor, we also found two different types of mutations in KMT2D

in one of patient's tumor tissue. Two mutations in EGFR were detected, and the mutation of L858R, which is a drug target site, was also detected in the tumor tissues of two patients (Table 4).

## Discussion

LC is a malignant tumor with a high morbidity rate worldwide. While the preferred treatment for early-stage LC is surgical resection, only about 50% patients achieve a high long-term survival rate with a good quality of life. In particular, patients with NSCLC easily relapse and develop metastasis within a short duration after operation [8]. Since there are no sensitive tumor biomarkers available for imaging examination, the search for an efficacious, simple, and highly accurate clinical biomarker is a research hotspot in tumor biology.

Compared to the traditional protein tumor biomarkers, when ctDNA with specific mutations and other cancer-related genetic changes is used as a marker, the probability of false positivity is significantly reduced [9] and better specificity is also observed. Clinical tumor markers are easily influenced by other lesion factors. However, the half-life of ctDNA is shorter than those of protein markers, therefore, it represents the current status of the tumor [10] and is more appropriate for real-time monitoring of tumors. Detection of CEA levels in the serum is also very important for the evaluation of prognosis of LC. For example, Yang *et al* found that the CEA level continuously declined in patients with non-relapsed NSCLC after operation, and the post-operative CEA level greatly decreased within one month [11]. Tan *et al* reported that the post-operative CEA level was significantly different from the pre-operative level within seven days of operation [12]. Similarly, in our study, we noticed that the CEA level decreased as compared to the pre-operative level and could be detected up to 26 days after the operation. However, there was no significant difference between the two levels and this can perhaps be due to the small sample size. The ccfDNA level in the tumor samples is higher than in normal samples, as demonstrated by the studies on ctDNA and tumors [4–5]. Furthermore, ctDNA level shows obvious correlation with tumor cell burden [13]. Imberger et al. also found that the post-operative ctDNA levels was greatly reduced and even reached normal levels in patients with ovarian cancer after successful operation. However, increased ctDNA levels after operation might be caused by ineffective treatment or systemic disease [14]. Among the five cases investigated in our study, the post-operative ctDNA level was significantly reduced compared to pre-operative ctDNA level, consistent with the previous reports. Jung *et al* showed that the continuously increasing cfDNA level could reflect the possibility of a relapse earlier than that predicted using the CEA marker or imaging examination in patients who have undergone esophageal resection [15]. In our study, the quantitative comparison of pre- and post-operative ctDNA and CEA levels in NSCLC patients showed a decreasing trend, which was significantly different for ctDNA, suggesting that ctDNA was more sensitive for detection of surgical efficacy. Hence, the quantitative analysis of ctDNA has potential application

**Table 4** Genes mutated ≥ two times out of the 508 genes and their corresponding distribution (*n*)

| Gene | Total number of times | Number of cases/person | Tumor tissue/time | Pre-operative ctDNA/time | Post-operative ctDNA/time |
|---|---|---|---|---|---|
| TP53 | 4 | 3 | 3 | 1 | 0 |
| KMT2D | 4 | 2 | 2 | 1 | 1 |
| CHD4 | 3 | 2 | 1 | 0 | 2 |
| NTRK3 | 3 | 2 | 2 | 1 | 0 |
| GNAQ | 2 | 2 | 0 | 2 | 0 |
| ASXL1 | 2 | 1 | 0 | 1 | 1 |
| ABL2 | 2 | 2 | 1 | 1 | 0 |
| EGFR | 2 | 2 | 2 | 0 | 0 |
| NOTCH2 | 2 | 2 | 1 | 1 | 0 |
| PTEN | 2 | 1 | 1 | 1 | 0 |
| TET2 | 2 | 1 | 1 | 1 | 0 |
| NOTCH1 | 2 | 2 | 1 | 1 | 0 |
| PRPF40B | 2 | 1 | 1 | 1 | 0 |
| CDK12 | 2 | 1 | 1 | 1 | 0 |
| RUNX1T1 | 2 | 1 | 1 | 1 | 0 |
| EPHB2 | 2 | 2 | 1 | 0 | 1 |
| PTCH1 | 2 | 2 | 2 | 0 | 0 |
| KMT2C | 2 | 1 | 0 | 2 | 0 |
| AXL | 2 | 2 | 0 | 2 | 0 |

in the early diagnosis of LC; however, the evaluation of its clinical efficacy and the improvement of its relevance in translational medicine are required. However, in our study, the sample size was relatively small and future studies using larger sample sizes should be performed.

A total of 508 genes were analyzed in our study, including the highly comprehensive detection of genes relevant to LC. The genes detected were either oncogenes or tumor suppressor genes involved in tumor cell signaling transduction, regulation of gene transcription, cell proliferation, differentiation, apoptosis, migration, invasion, and metastasis. In this study, we found that the mutation frequency of TP53 was high. Previous studies have reported that point mutations of TP53 are detected in the ctDNA of patients with colorectal, lung, liver, breast, and head and neck cancers [16–17]. Recently, Chen *et al* reported that the co-exist of tumor mutations and ctDNA mutation was up to 26% of breast cancer cases [18]. Similarly, in our study, KMT2D gene was detected several times, which is one of the genes that shows high mutation rate, according to the COSMIC database. However, there are few reports about its effective mechanism in tumors, or co-existence of its mutation with tumor in ctDNA detection. Sahoo *et al* demonstrated that the mutation rate of EGFR was 30%–50% in Asian NSCLC patients [19]. Peng *et al* reported that the mutation rate of EGFR was 17.7% in plasma ctDNA in 96 pairs of LC [20] .Furthermore, Lee *et al* showed that the EGFR mutation type found in the plasma was the same as that found in the tumor with a coincidence rate of 59.6%, compared to the LC tissue [21]. Taken together, these three studies suggested that approximately half of the mutation-positive EGFR genes found in NSCLC patients could be detected using peripheral ctDNA: an EGFR gene mutation was detected in LC tissues in two cases, but no mutation was detected in ctDNA. Hence, the detection of the mutations in the ctDNA gene can be used for tumor efficiency monitoring, prognosis evaluation, prediction of disease progression and survival time, drug selection, and drug resistance. Due to the low sensitivity and specificity of single-gene diagnosis and evaluation, the presence of a mutant gene cannot be used as the sole marker for tumor diagnosis. However, a combination of quantitative and qualitative analyses of ctDNA with other tumor markers has shown higher accuracy for the diagnosis and prognosis of tumors, compared to a single indicator.

Notably, ctDNA is highly relevant in tumors, and the mutation of the LC ctDNA gene is found to be consistent with the mutation type of LC tissue, further proving the tumor derivation of ctDNA. When compared to traditional tumor markers, ctDNA is sensitive to tumor burden changes, which indicates that the quantitative and qualitative analysis of ctDNA is a promising novel molecular biomarker for the evaluation of tumor burden changes in NSCLC. Our study had some limitations, such as a small sample size and short follow-up period. Having said that, this was just a preliminary study. Further high quality, multicenter, clinical studies with large sample sizes focusing on the correlation of ctDNA and LC diagnosis are needed to provide a novel strategy for the prophylaxis and treatment of LC.

### Conflicts of interest

The authors declare no conflicts of interest.

## References


1. Lianos GD, Mangano A, Kouraklis G Roukos DH. Dynamic sequencing of circulating tumor DNA: novel noninvasive cancer biomarker. Biomark Med, 2014, 8: 629–632.
2. Jiang WF, Zhang HL. Enrichment and detection of circulating tumor cells in peripheral blood. Oncol Transl Med, 2011, 10: 240–244.
3. Leon SA, Shapiro B, Sklaroff DM, *et al*. Free DNA in the serum of cancer patients and the effect of the rapy. Cancer Res, 1977, 37: 646–650.
4. Cheng X, Zhang L, Chen Y, Qing C. Circulating cell-free DNA and circulating tumor cells, the “liquid biopsies” in ovarian cancer. J Ovarian Res, 2017,10: 75.
5. Todenhöfer T, Struss WJ, Seiler R, *et al*. Liquid Biopsy-Analysis of Circulating Tumor DNA (ctDNA) in Bladder Cancer. Bladder Cancer, 2018, 4: 19–29.
6. Gao J, Wang H, Zang W, *et al*. Circulating tumor DNA functions as an alternative for tissue to overcome tumor heterogeneity in advanced gastric cancer. Cancer Sci, 2017, 108: 1881–1887.
7. Newman AM, Bratman SV, To J *et al*. An ultrasensitive method for quantitating circulating tumor DNA with broad patient coverage. Nat Med, 2014, 20: 548–554.
8. Liu ZZ, Xie XD. Whole process control and precision therapy in lung cancer. Oncol Transl Med, 2017, 3: 91–92.
9. Ellen Heitzer, Peter Ulz, Jochen B. Circulating Tumor DNA as a Liquid Biopsy for Cancer. Clin Chem, 2015, 61: 112–123.
10. Zhao H, Chen KZ, Hui BG, *et al*. Role of circulating tumor DNA in the management of early-stage lung cancer. Thorac Cancer, 2018, 9: 509–515.
11. Yang D, Xia W, Ma R. Significance of observing serum tumor markers before and after operation of NSCLC. Chin J Surg Oncol (Chinese), 2014, 6: 25–27.
12. Tan W, Yang S, Bao Y, *et al*. Changes of serum NSE, CYFRA21-1 and CEA in patients with lung cancer before after operation and related clinical significance analysis. Int J Lab Med, 2012, 33:16–17.
13. Sausen M, Parpart S, Diaz LA. Circulating tumor DNA moves further into the spotlight. Genome Med, 2014, 6: 35.
14. Wimberger P, Roth C, Puntel K, *et al*. Impact of platinum-based chemotherapy on circulating nucleic acid levels, protease activities in blood and disseminated tumor cells in bone marrow of ovarian cancer patients. Int J Cancer, 2011,128: 2572–2580.
15. Jung K, Fleischhacker M, Rabien A. Cell-free DNA in the blood as a solid tumor biomarker-acriticalappraisal of the literature. Clin Chim Acta, 2010, 411: 1611–1624.
16. Park YR, Kim Y-M, Lee SW, *et al*. Optimization to detect TP53 mutations in circulating cell-free tumor DNA from patients with serous epithelial ovarian cancer. Obstet Gynecol Sci, 2018, 61: 328–336.
17. Wade M, Li YC, Wan GM. MDM2, MDMX and p53 in oncogenesis

and cancer therapy. Nat Rev Cancer, 2013, 13: 83–96.
18. Chen Z, Fang J, Buzin CH, *et al*. Analysis of cancer mutation signatures in blood by a novel ultra-sensitive assay: monitoring of therapy or recurrence in non-metastatic breast cancer. PloS One, 2009, 4: e7220.
19. Sahoo R, H arini VV, Babu VC, *et al*. Screening for EGFR mutations in lung cancer a report from India. Lung Cancer, 2011,73: 316–319.
20. Peng Q, Zhao J, Qin H, *et al*. Detection of EGFR mutation in peripheral blood and its clinical significance in lung cancer patients. Chin J Surg Oncol (Chinese), 2011, 38: 263–267.
21. Lee Y, Park S, Kim WS, *et al*. Correlation between progression-free survival, tumor burden, and circulating tumor DNA in the initial diagnosis of advanced-stage EGFR-mutated non-small cell lung cancer. Thorac Cancer, 2018: doi:10.1111/1759-7714.12793.

**DOI 10.1007/s10330-019-0335-5**
**Cite this article as:** Chen XQ, Lin TY, Gao ZS, *et al*. Quantitative monitoring and mutations of ctDNA before and after non-small cell lung cancer radical surgery. Oncol Transl Med, 2019, 5: 103–108.

Oncology and Translational Medicine
DOI 10.1007/s10330-019-0331-1

June 2019, Vol. 5, No. 3, P109–P113

ORIGINAL ARTICLE

# Application of malignant pleural effusion cell blocks in the diagnosis and personalized treatment of advanced non-small cell lung carcinoma*

**Wei Luan[1], Nier Cha[2], Yinzai He[2], Baoqing Jia[2] (✉)**

[1] Departments of Oncology, Inner Mongolia People's Hospital, Hohhot 010017, China
[2] Departments of Surgical Oncology, Inner Mongolia People's Hospital, Hohhot 010017, China

## Abstract

**Objective** The aim of the study was to investigate the efficacy of immunocytochemistry and related gene detection using cell block for the diagnosis and individualized treatment of advanced lung cancer.

**Methods** Sixty-five malignant pleural effusion specimens were collected to make cell blocks, which were used for hematoxylin and eosin (H&E) staining, immunocytochemical studies, and gene sequencing of the tumors to guide the individualized diagnoses and treatment of the given tumors.

**Results** The tumor cells in the cell block sections were abundant in number with high quality cellular structures, and the histological morphological characteristics were partially maintained. Immunocytochemical staining was helpful in identifying the cell origin and tumor classification, and amplification refractory mutation system (ARMS) was used to determine the mutation status of epidermal growth factor receptor (EGFR). Of the 65 samples, 50 had a diagnosis of adenocarcinoma, 7 were pulmonary squamous cells, 6 were small cell carcinoma of the lung, and 2 were mesothelioma. The morphological features of the tumors were as follows: acinar formation, papillary and single cells for adenocarcinoma; intercellular bridges for squamous cell carcinoma; and morphology of the small cells is similar to that of the smear. Correlating with the results of immunocytochemical staining and clinical data analysis, 40 cases were confirmed as pulmonary adenocarcinoma, with an additional 4 cases of breast cancer, 3 cases of ovarian adenocarcinoma, and 3 cases of colorectal adenocarcinoma. Of the 47 non-small cell lung carcinoma (NSCLC) patients, EGFR mutations were detected in 26 cases (55.3%) by ARMS, with four mutation types: exon 19 deletion (13 cases, 50.0%), exon 2l point mutations L858R (11 cases, 42.3%) and L861Q (1 case, 3.8%), and exon 18 point mutation G719X (1 case, 3.8%).

**Conclusion** Malignant pleural effusion cell blocks combined with immunocytochemical markers and molecular pathology are helpful for the diagnosis of advanced tumors, the identification of tumor properties and histological tumor origin, and the selection of individualized treatment for advanced lung cancer.

Received: 21 January 2019
Revised: 3 May 2019
Accepted: 3 June 2019

**Key words:** pleural effusion; cell block; immunocytochemistry; epidermal growth factor receptor (EGFR)

Due to the location of the tumor or the occurrence of complications, it is difficult for a considerable number of patients with advanced tumors to obtain their tumor tissues through intervention [1]. Only a few cases with surgery can provide large specimens, and most cases are diagnosed based on small biopsy materials, such as fiberoptic bronchoscopy, percutaneous lung core biopsy, endobronchial ultrasound-guided transbronchial needle aspirate (EBUS-TBNA), and cytological examination. In comparison, cytological specimens are relatively easy to obtain, so the use of cytological specimens for corresponding detection is significant for the diagnosis of tumors and the guidance of clinical personalized treatment. In this study, the application value of a modified cell paraffin block technique in the individualized diagnosis and treatment of advanced non-small cell lung cancer (NSCLC) by combining tumor-related specific protein and gene detection was discussed.

✉ Correspondence to: Baoqing Jia. Email: 13604715646@qq.com
* Supported by a grant from the Natural Sciences Foundation of Inner Mongolia (No. 2017MS08147).

## Materials and methods

### Materials

The 65 samples from patients with malignant pleural effusion that were treated in the Department of Oncology of the Inner Mongolia People's Hospital (China) were collected from January 2016 to December 2016, including 31 males and 34 females, aged 29–88 years old, with an average age of 60.14 (± 16.94) years old.

### Methods

The smear was prepared by conventional methods and stained with hematoxylin and eosin (H&E).

*Cell block production*

Specimen was refrigerated at 4 °C for two hours until visible precipitation formed. Supernatant was then removed, the precipitate was collected in a 50 mL tube, and centrifuged at 2000 r/min for five minutes, supernatant was removed, then was fixed in 15 mL of 10% neutral formaldehyde for two hours at room temperature, wrapped in filter paper, and submitted for dehydration, transparency, paraffin embedding, sectioning, and staining.

*Immunocytochemical staining*

The 3 μm-thick sections were prepared from the paraffin blocks, and the EnVision two-step staining method was carried out according to the instructions. Immunohistochemical antibodies were selected based on microscopic examination of morphology by smear and biopsy, evaluation of H&E sections, and corresponding clinical data for each case. For unknown origin of adenocarcinoma, a panel of antibodies with Napsin A, CDX-2, TTF-1, CK20, CK7, and Villin markers was selected. TTF-1, CA125, CDX-2, and GCDFP-15 can be used as organ-specific antibodies for lung adenocarcinoma, ovarian epithelial cancer, digestive tract adenocarcinoma, and breast cancer, respectively. For cases of mesothelial cells, Calretinin, WT-1, and D2-40 were added. The primary and secondary antibodies used were all purchased ready-to-use from Beijing Zhongshan Jinqiao Biotechnology Co., Ltd. (China), and the positive and negative controls used were purchased from Beijing Zhongshan Jinqiao Biotechnology Co., Ltd. (China).

*Gene mutation detection*

Cell paraffin blocks were made into eight sections of 8 μm-thick sections, and DNA was extracted by using the QIAamp DNA FFPE Tissue Kit according to the described steps. The concentration and quality of extracted DNA products were determined by the Thermo ND-2000 nucleic acid and protein quantitative analyzer, and the OD260/OD280 ratio of the DNA was required to be between 1.8 and 2.0. EGFR gene mutation was detected by the Xiamen AiDe AMRS kit, and the specific steps were performed on the ABIStep-one fluorescence quantitative PCR instrument according to the instructions. A positive control and a negative control were set for each test, and the reaction volume was set to 25 μL.

### Statistical analysis

For the statistical analysis, the SPSS 17.0 software (IBM, USA) $\chi^2$ test analysis was used, and $P < 0.05$ for the difference was considered statistically significant.

## Results

### Cell smear and cell block sections

Of the 65 samples, 50 were diagnosed with adenocarcinoma, 7 with lung squamous cell carcinoma, 6 with small cell lung cancer, and 2 with mesothelioma. Compared with the smear, the tumor cells in the cell block section were abundant in both quantity and quality, and some histologic characteristics were maintained. The squamous cells are nests, with intercellular bridges (Fig. 1). The morphology of cells in neuroendocrine cancer cells in the smear and section were similar: small cells, with sparse or absent cytoplasm, irregular hyperchromatic nuclei, easy mitosis, often single cell shedding, and different from the background lymphocytes.

### Immunophenotype

The immunocytochemistry staining of cell block sections was accurate, and the granules were clear (Fig. 1 and Table 1).

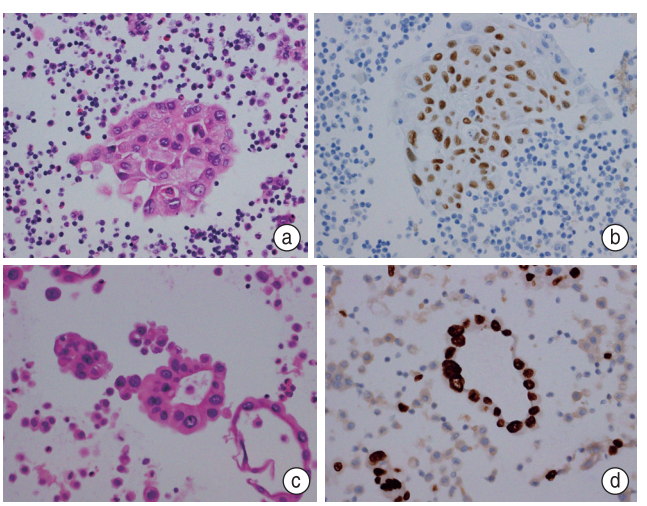


**Fig. 1** (a) Squamous cell carcinoma nest in cell block with dense eosinophilic cytoplasm, individual keratinization and intercellular bridges; (b) Immunohistochemistry revels that the tumor cells are positive for p40; (c) Adenocarcinoma in cell block with glandular lumen formation, bubbling cytoplasm, and intracytoplasmic mucin; (d) Immunohistochemistry analysis reveals the tumor cells are positive for TTF-1 (all H&E staining, 400×)

**Table 1** Immunocytochemical staining of 65 sample cell sections

| Antibodies | Lung cancer | | | Breast cancer | Ovarian cancer | Colorectal cancer | Pleural mesothelioma |
|---|---|---|---|---|---|---|---|
| | Adenocarcinoma | Squamous cell carcinoma | Small cell carcinoma | | | | |
| TTF-1 | + | – | – | – | – | – | – |
| Napsin A | + | – | – | – | – | – | – |
| CK5/6 | – | + | – | – | – | – | + |
| p40 | – | + | – | – | – | – | – |
| CgA | – | – | + | – | – | – | – |
| CK20 | +/– | – | – | – | – | + | – |
| CK7 | + | – | – | + | + | – | – |
| villin | + | – | – | – | – | + | – |
| Calretinin | – | – | – | – | – | – | + |
| D2-40 | – | – | – | – | – | – | + |
| WT-1 | – | – | – | – | – | – | + |
| CDX-2 | – | – | – | – | – | + | – |
| CA125 | – | – | – | – | + | – | – |
| GCDFP-15 | – | – | – | + | – | – | – |

### Gene mutation detection

In 47 NSCLC patients, EGFR mutation was detected in 26 cases (55.3%) by ARMS. Within these 26 samples, four mutation types were detected: exon 19 deletion (13 cases, 50.0%), exon 2l point mutations L858R (11 cases, 42.3%) and L861Q (1 case, 3.8%), and exon 18 point mutation G719X (1 case, 3.8%). All mutations were unipoint mutations and no multilocus mutations were found.

## Discussion

According to the United States National Cancer Institute Surveillance, Epidemiology and End Results (SEER) database, 57% of lung cancer patients have already developed distant metastases [2] at the first diagnosis. In China, this proportion is higher, as most of the lung cancer patients have been diagnosed at an advanced stage [3]. Small specimens, including malignant serosal effusion cells, are an important way to clarify the diagnosis of the disease. However, due to its small sample size, the specimen needs to be properly handled to provide accurate pathological and molecular diagnosis.

Converting serosal effusion cells into cell block is an effective method to improve the cytological diagnosis [4]. Cell block sections showed less background, high quality of staining, and uniform thickness, and histologic features could be observed in some cases. For example, glandular lumen or papillary structures appeared in sections of adenocarcinoma; nests, intercellular bridges, or keratinocytes could be seen in squamous cell carcinoma; and spindle/oval shaped cells, scattered or molding, in small cell carcinoma (Fig. 1). The cell block can be used for diagnosis and classification of tumor, which is almost compatible to histological diagnosis. At present, the thrombin method, agarose method, and cell precipitation method are commonly used to prepare cell blocks, but some of these methods require the addition of other enzymes to the material, which may have an impact on subsequent analysis. Some production processes are more cumbersome. In this study, cell blocks were prepared by cold precipitation, without adding additional enzymes, and the protein components contained in the hydrops were connected into a network scaffold, which was conducive to the adhesion between cells. This allowed for a convenient processing method, with no interference to the subsequent detection. Additionally, the number of harvested cells was large and the production efficiency was high. 10% neutral formaldehyde is one of the most commonly used fixative solutions, but DNA can be easily affected by the fixation time. Furthermore, sample DNA soaked in formaldehyde for days will be fragmented and cannot be used to effectively detect mutations. In this study, the fixation time of the sample is no more than two hours, which is optimal for cell nuclear structure stability and antigen retention [5].

Immunocytochemistry plays an important role in defining the pathological classification, origin and differential diagnoses of given tumors [6–7]. For mesenchymal tumors and neurogenic tumors, the primary tumor has no organ specificity; therefore, the significance of finding the primary tumor is limited. However, for epithelial-derived tumors, especially adenocarcinoma, the search for primary lesions is of great significance. Cytokeratin (CK) is a component of the cytoskeleton protein family of filaments and a reliable marker of epithelial differentiation. Some antibodies have a certain degree of organ specificity, such as TTF-1 expression mainly in lung and thyroid epithelial cells [8], CDX-2 and CK20 in the gastrointestinal epithelium, and CA-125 as the main marker of epithelial ovarian cancer,

especially serous carcinoma. However, single antibody detection can be difficult to use to determine the tumor origin of many metastatic tumors, while the combined use of antibodies can narrow down the potential sites of the primary tumor to a greater degree [9]. CK7 and CK20 can identify the origin of most adenocarcinomas, but there are still deficiencies in practical applications. Villin, as a cytoskeleton protein, plays an important role in the formation of brush border microvilli of many cells. Villin is relatively conserved in the process of tumor formation, and its combined application with CK7 and CK20 can help to clarify the primary lesions of adenocarcinoma, though it has no obvious value for squamous cell carcinoma and small cell carcinoma. Malignant mesothelioma is a kind of bidirectional differentiated malignant tumor, which can express both keratin and vimentin. Mesothelioma cells and the lining cells in the serosal cavity, are variable in morphology and often confused with other tumor cells. For the differential diagnosis between pleural epithelioid malignant mesothelioma, lung adenocarcinoma, and squamous cell carcinoma, there is no entirely specific marker at present, so at least two mesothelium markers and two epithelial markers should be selected [10]. Depending on the sensitivity and specificity of the antibody, the best markers at present for mesothelioma are Calretinin, CK5 or CK5/6, WT-1 and D2-40.

The molecular subclassification of NSCLC based on tumor oncogenes and molecular targeted therapy for corresponding genes has become the standard treatment for advanced NSCLC due to its remarkable efficacy and excellent safety in patients. EGFR is a transmembrane receptor, which is related to cell proliferation, metastasis, and apoptosis, along with signal transduction pathways. There are four major EGFR mutations: exon 19 deletion, exon 21 point mutation, exon 18 point mutation, and exon 20 insertion [11].

The most common types of EGFR mutations are deletion of exon 19 and exon 21 L858R point mutations. Both of these lead to tyrosine kinase domain activation and are EGFR-TKI sensitive mutations. Exon 18 G719X, exon 20 S768I, and exon 21 L861Q mutations also are gain-of-function mutations, while the exon 20 T790M mutation is related to acquired drug resistance of EGFR-TKI. There are many other types of mutations [12]; however, the clinical significance of those mutations remains unclear. The positive rate of EGFR gene mutation in lung adenocarcinoma patients is about 10% in Caucasian population, and about 50% in east Asian population [13]. Multiple clinical studies have demonstrated that NSCLC patients with EGFR gene mutations benefit from EGFR-TKI treatment significantly [3, 14–15]. For cytological specimens of NSCLC patients, the concentration of DNA from tumor cells is low, and the mutation rate is not high. The amplification refractory mutation system (ARMS) is of high sensitivity and can detect mutant DNA with concentrations as low as 1%, and is also a closed detection system with near-zero cross contamination. In this study, out of 47 NSCLC patients, EGFR mutations were detected in 26 patients by ARMS, which is in line with the published data.

Cell block has advantages in immunohistochemistry analysis and is superior to cytology analysis alone. However, there are some disadvantages to this method. For example, the number of tumor cells in some cell blocks are limited. Heterogeneity of tumors in a given cell block could have test results that may not be completely representative. Immunocytochemical staining may be nonspecific if apoptosis is occurring. Additionally, tumor cells are sometimes mixed with benign mesenchymal cells and inflammatory cells including histiocytes, which requires careful observation and identification. Furthermore, in order to improve the success rate of ARMS detection, it is suggested that the quality of DNA extracted be monitored every time. The OD260/OD280 ratio of qualified samples should be between 1.7 and 2.0, and samples with impure or inadequate concentration should be extracted again to avoid false negative results, as an insufficient amount of DNA will affect the test results for some specimens.

### Conflicts of interest

The authors indicate no potential conflicts of interest.

## References

1. de Mello RA, Madureira P, Carvalho LS, *et al*. EGFR and KRAS mutations, and ALK fusions: current developments and personalized therapies for patients with advanced non-small-cell lung cancer. Pharmacogenomics, 2013, 14: 1765–1777.
2. Howlader N, Noone AM, Krapcho M, *et al*. SEER cancer statistics review, 1975–2012, National Cancer Institute. Bethesda MD. http://seer.cancer.gov/csr/1975-2012/, based on November 2014 SEER data submission, posted to the SEER web site, April 2015.
3. Zhou C, Wu YL, Chen G, *et al*. Erlotinib versus chemotherapy as first-line treatment for patients with advanced EGFR mutation-positive non-small-cell lung cancer (OPTIMAL, CTONG-0802): a multicentre, open-label, randomised, phase 3 study. Lancet Oncol, 2011, 12: 735–742.
4. Varsegi GM, Shidham V. Cell block preparation from cytology specimen with predominance of individually scattered cells. J Vis Exp, 2009 Jul 21. pii: 1316. doi: 10.3791/1316.
5. Pine JW, McGough J, editors. Rosen's breast pathology. 3rd ed. Philadelphia: Lippincott Williams and Wilkins, 2009. 285–357.
6. Bhatia P, Dey P, Uppal R, *et al*. Cell blocks from scraping of cytology smear: comparison with conventional cell block. Acta Cytol, 2008, 52: 329–333.
7. Shivakumarswamy U, Arakeri SU, Karigowdar MH, *et al*. Diagnostic utility of the cell block method versus the conventional smear study in pleural fluid cytology. J Cytol, 2012, 29: 11–15.
8. Ordóñez NG. Value of thyroid transcription factor-1 immunostaining in tumor diagnosis: a review and update. Appl Immunohistochem Mol

Morphol, 2012, 20: 429–444.
9. Su YC, Hsu YC, Chai CY. Role of TTF-1, CK20, and CK7 immuohistochemistry for diagnosis of primary and secondary lung adenocarcinoma. Kaohsiung J Med Sci, 2006, 22: 14–19.
10. Husain AN, Colby T, Ordonez N, *et al*. Guidelines for pathologic diagnosis of malignant mesothelioma: 2012 update of the consensus statement from the International Mesothelioma Interest Group. Arch Pathol Lab Med, 2013, 137: 647–667.
11. Riely GJ, Politi KA, Miller VA, *et al*. Update on epidermal growth factor receptor mutations in non-small cell lung cancer. Clin Cancer Res, 2006, 12: 7232–7241.
12. Su KY, Chen HY, Li KC, *et al*. Pretreatment epidermal growth factor receptor (EGFR) T790M mutation predicts shorter EGFR tyrosine kinase inhibitor response duration in patients with non-small-cell lung cancer. J Clin Oncol, 2012, 30: 433–440.
13. Shi Y, Au JS, Thongprasert S, *et al*. A prospective, molecular epidemiology study of EGFR mutations in Asian patients with advanced non-small-cell lung cancer of adenocarcinoma histology (PIONEER). J Thorac Oncol, 2014, 9: 154–162.
14. Wu YL, Fukuoka M, Mok TS, *et al*. Tumor response and health-related quality of life in clinically selected patients from Asia with advanced non-small-cell lung cancer treated with first-line gefitinib: post hoc analyses from the IPASS study. Lung Cancer, 2013, 81: 280–287.
15. Kim HS, Park K, Jun HJ, *et al*. Comparison of survival in advanced non-small cell lung cancer patients in the pre- and post-gefitinib eras. Oncology, 2009, 76: 239–246.

**DOI 10.1007/s10330-019-0331-1**
**Cite this article as:** Luan W, Cha NE, He YZ, *et al*. Application of malignant pleural effusion cell blocks in the diagnosis and personalized treatment of advanced non-small cell lung carcinoma. Oncol Transl Med, 2019, 5: 109–113.

Oncology and Translational Medicine
DOI 10.1007/s10330-019-0344-4

June 2019, Vol. 5, No. 3, P114–P118

ORIGINAL ARTICLE

# Whole-brain radiation therapy alone vs. combined therapy with stereotactic radiosurgery for the treatment of limited brain metastases: A systematic review

**Chao Wan, Biao Chen (Co-first author), Yuanshi Liu, Ximing Xu (✉)**

Cancer Center, Renmin Hospital of Wuhan University, Wuhan 430060, China

## Abstract

**Objective** The aim of the study was to compare the efficacy and safety of whole brain radiotherapy (WBRT) used alone and combined with stereotactic radiosurgery (SRS) in the treatment of limited (1–4) brain metastases.

**Methods** We searched for randomized controlled and matched-pair analysis trials comparing WBRT plus SRS versus WBRT alone for brain metastases. The primary outcomes were the overall survival (OS), intracranial control (IC), and localcontrol (LC). The secondary outcome was radiation toxicity. The log hazard ratios (lnHRs) and their variances were extracted from published Kaplan-Meier curves and pooled using the generic inverse variance method in the RevMan 5.3 software. The non-pooled outcome measures were evaluated using descriptive analysis.

**Results** Three randomized controlled trials and two matched-pair analysis studies were included. There was no difference in the OS for limited brain metastases between the two groups [lnHR 0.91 (95% CI 0.76–1.09, $P$ = 0.32) *vs.* 0.72 (95% CI 0.44–1.19, $P$ = 0.20)]. The LC and IC were significantly higher in the combined treatment group [lnHR 0.69 (95% CI 0.55–0.86, $P$ = 0.001) *vs.* 0.41 (95% CI 0.29–0.58, $P$ < 0.0001)]. For patients with a single lesion, one trial showed a higher survival in the combined treatment group (median OS: 6.5 months *vs.* 4.9 months, $P$ = 0.04). The combined treatment was not associated with significantly higher incidence of radiation toxicity.

**Conclusion** Combined treatment with WBRT plus SRS should be recommended for patients with limited brain metastases based on the better LC and IC without increased toxicity. It should also be considered a routine treatment option for patients with solitary brain metastases based on the prolonged OS.

Received: 24 March 2019
Revised: 25 April 2019
Accepted: 17 May 2019

**Key words:** limited brain metastases; stereotactic radiosurgery (SRS); whole brain radiotherapy (WBRT); systematic review

It has been reported that 20%–40% of patients with cancer develop brain metastases. Patients with a limited number of metastatic lesions and well-controlled systemic disease may benefit from aggressive local therapeutic approaches in terms of a better prognosis. As a focal high-dose boost treatment, stereotactic radiosurgery (SRS) has been extensively employed in patients with brain metastases, either alone or combined with whole brain radiotherapy (WBRT). Clinical evidence has shown that adding SRS to WBRT was beneficial to patients with limited brain metastases [1–2]. This study investigated the effect of the addition of SRS to WBRT in the management of patients with 1 to 4 brain metastases.

## Methods

### Literature search

Studies comparing WBRT combined with SRS versus WBRT alone were searched in the following databases from inception up to January 2019: PubMed, Medline, Embase, the Cochrane Central Register of Controlled Trials, Wangfang Data, and Weipu.

✉ Correspondence to: Ximing Xu. Email: doctorxu120@aliyun.com

### Selection criteria

The literature type was restricted to randomized controlled trials or matched-pair analysis studies comparing combined WBRT plus SRS versus WBRT alone for the treatment of adult patients (age > 18 years) with newly diagnosed brain metastases (single or up to 4) confirmed by MRI.

### Data collection and analysis

Two investigators independently extracted study data following the inclusion criteria. Cases of conflicting opinion were resolved through discussion.

### Outcome measurement

The primary outcome measures were the overall survival (OS), local control (LC), and intracranial control (IC). The secondary outcome measure was the treatment-related toxicity.

### Statistical analysis

The generic inverse variance method in RevMan 5.3 software (The Cochrane Collaboration) was used for this meta-analysis. The outcome measures for data pooling were the log hazard ratios (lnHR) and their variances. A fixed-effect model was used when no heterogeneity was observed among the studies. Otherwise, a random effect model was adopted. The heterogeneity between the studies was assessed using the $Q$-test and $I^2$ statistic, and $P < 0.10$ and $I^2 > 50\%$ were considered to indicate heterogeneity between the studies.

## Results

### Studies' characteristics

The search strategy initially identified 126 articles. Irrelevant and duplicated studies were excluded after reading the abstracts. Finally, three randomized controlled trials and two matched-pair analysis studies with a total of 784 patients meeting our inclusion criteria were included. Table 1 shows the characteristics of each included study [3–7]. Patients had 1–4 brain metastases. The WBRT dosage schedules included 2.5 Gy × 15 F, 2.5 Gy × 12 F, 3 Gy × 10 F, and 2 Gy × 20 F, with a total of 30–40 Gy. The prescribed dose in SRS ranged from 14 Gy to 24 Gy depending on the tumor diameter and the number of brain lesions. Most dose prescriptions conformed to the Radiation Therapy Oncology Group guidelines.

### Primary outcomes

*Overall survival*

Three studies [3, 6–7] evaluated the OS in patients with 1 to 3 brain metastases, as shown in Fig. 1. There was no significant difference between the two treatment groups (HR 0.91, 95% CI 0.76–1.09). Three studies [3–5] reported the OS data for patients with 2 to 4 brain metastases. Similarly, there was no significant difference between the two treatment groups (HR 0.72, 95% CI 0.44–1.19; Fig. 2). For patients with a single brain metastasis, Andrews *et al* [3] reported that the OS was 6.5 months in the WBRT plus SRS group and 4.9 months in the WBRT alone group ($P$ = 0.0393). Rades *et al* [7] reported OS rates at 6, 12, 18, and 24 months of 83%, 64%, 34%, and 30%, respectively, in the WBRT plus SRS group, and 67%, 49%, 29%, and 18%, respectively, in the WBRT alone group ($P$ = 0.12).

*Local control*

All five studies evaluated the LC. The pooled data analysis found that the patients who underwent WBRT plus SRS had less chance of local failure than those who underwent WBRT alone (HR 0.69, 95% CI 0.55–0.86, $P$ = 0.001; Fig. 3).

*Intracranial control*

Three trials [3–5] evaluated the IC. The pooled data analysis revealed that the addition of SRS to WBRT significantly improved the IC of the treated lesions (HR 0.41, 95% CI 0.29–0.58, $P < 0.00001$; Fig. 4). Kondziolka *et al* [4] reported that the median time to any brain failure was 5 months in the WBRT alone group and 34 months in the combined treatment group ($P$ = 0.002).

### Secondary outcomes

Adverse events: Four trials [3–6] reported the treatment-related toxicities. The most common toxicities were nausea or vomiting and skin changes. Andrews *et al* [3]

**Table 1** Characteristics of the included studies

| Study type | | Group A | Group B | *n* | Radiation dose (Gy) WBRT | Radiation dose (Gy) SRS | PTV of SRS |
|---|---|---|---|---|---|---|---|
| Andrews [3] | RCT | 164 | 167 | 1–3 | 2.5 Gy × 15 F | $D_{max} \leq 2$ cm, 24 Gy; $2 < D_{max} \leq 3$ cm, 18 Gy; $3 < D_{max} \leq 4$ cm, 15 Gy | NR |
| Kondziolka [4] | RCT | 14 | 13 | 2–4 | 2.5 Gy × 12 F | 16 Gy | NR |
| Minniti [5] | MPA | 66 | 66 | 2–3 | 3 Gy × 10 F | $D_{max} \leq 2$ cm, 20 Gy; $D_{max} > 2$ cm, 18 Gy | PTV: GTV + 2 mm |
| El Gantery [6] | RCT | 21 | 21 | 1–3 | 3 Gy × 10 F | 14 – 20 Gy (mean = 14.6 Gy, median = 14 Gy) | PTV: GTV + 1 mm |
| Rades [7] | MPA | 168 | 84 | 1–3 | 3 Gy × 10 F or 2 Gy × 20 F | 4–8 Gy × 2–5 F | NR |

RCT: randomized controlled trial; MPA: matched-pair analysis; A: WBRT; B: WBRT + SRS; *n*: number of brain metastases; $D_{max}$: the broadest diameter of the metastases; PTV: planning target volume; GTV: contrast-enhanced gross tumor volume on MRI; NR: not reported

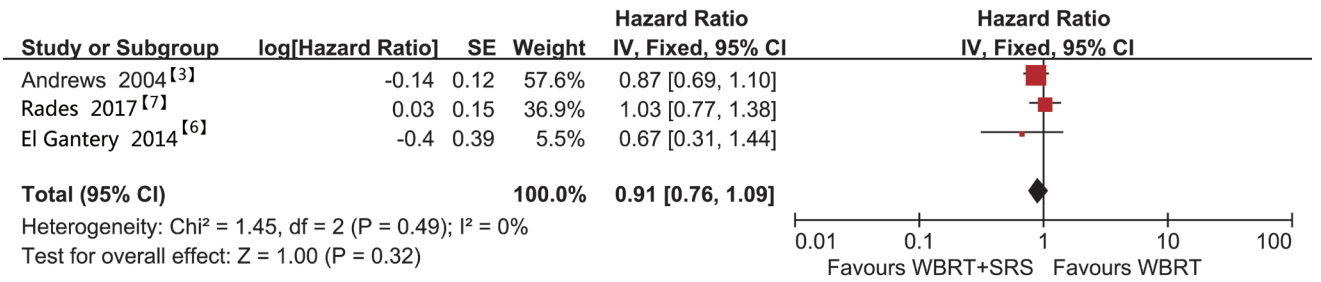


**Fig. 1** Overall survival per group in patients with 1 to 3 brain metastases

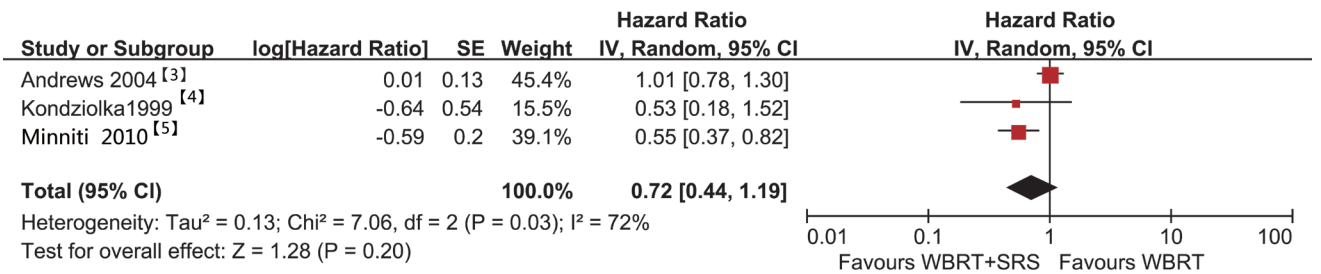


**Fig. 2** Overall survival per group in patients with 2 to 4 brain metastases

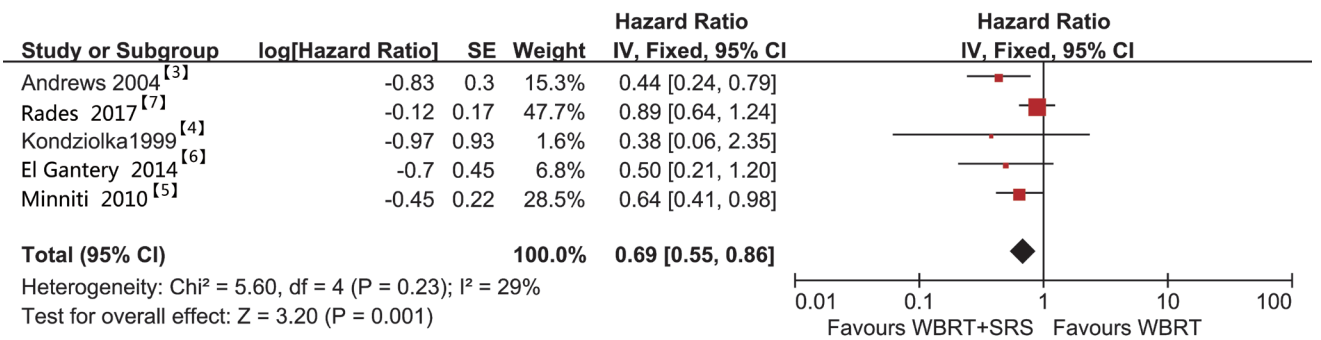


**Fig. 3** Local control

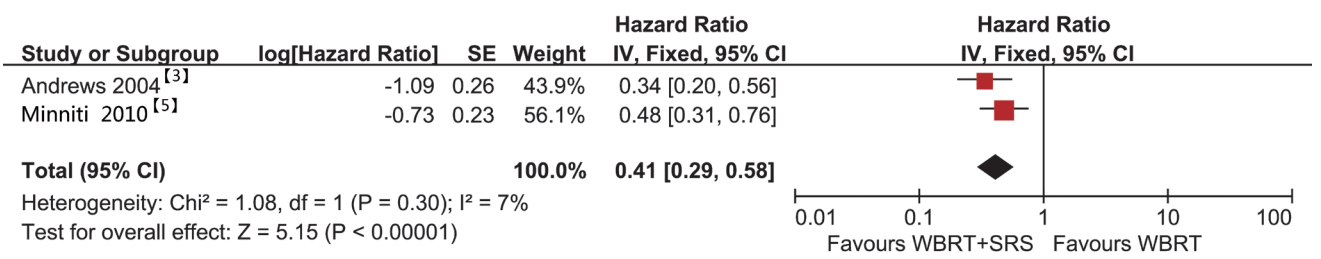


**Fig. 4** Intracranial control

reported rates of 43% grade 1, 18% grade 2, 2% grade 3, and 1% grade 4 acute toxicities in the SRS boost group versus 36%, 26%, 0%, and 0%, respectively, in the WBRT alone group. There were 2% grade 3 and 1% grade 4 late toxicities in the WBRT arm, and 3% grade 3 and 3% grade 4 late toxicities in the combined curative arm. El Gantery *et al* [6] reported 14% acute and 14% late toxicity rates in the SRS boost arm versus 14% and 9%, respectively, in the WBRT alone arm. These data suggested that the rates of acute and late toxicities were similar between the two groups. Kondziolka *et al* [4] reported no neurologic morbidity related to SRS except for mild scalp erythema and hair loss associated with WBRT. Minniti *et al* [5] reported that six patients developed radio necrosis and six patients experienced neurocognitive deficits in the WBRT plus SRS group. The radio necrosis lesions were controlled by the use of steroids or surgery. Five patients experienced neurocognitive deficits in the form of grade 2 confusion or grade 2 memory loss in the WBRT alone group.

## Discussion

Oligometastatic disease is defined as a maximum of five metastatic lesions for all disease sites, including no more than three active extracranial metastatic lesions. Small prospective and retrospective studies have suggested that aggressive consolidative therapy to the metastatic sites was associated with an improved OS in patients with oligometastatic non-small-cell lung carcinoma [8–9]. The current research findings are inconclusive as to whether patients who present with a limited burden of intracranial metastatic disease could benefit from a local consolidative therapy. The aim of this study was to systematically evaluate the benefit of adding SRS to WBRT in the treatment of limited brain metastases (1 to 4 brain metastases).

It has been determined that the combined treatment with WBRT and SRS significantly improved the LC compared to SRS alone in patients with intracranial oligometastatic disease. However, WBRT also leads to more pronounced neurocognitive impairment [10]. With the emerge of new methods to lower the risk of WBRT-induced neurocognitive decline [11–12], WBRT is still thought to bean essential part in the treatment of limited brain metastases. The present study also demonstrated that the addition of SRS to WBRT significantly improved the LC compared to WBRT alone for patients with limited lesions. However, the pooled data analysis showed no OS improvement with the use of combined treatment in patients with 1-4 brain metastases. For patients with solitary brain metastases, Andrews *et al* [3] concluded there was a survival advantage in the combined treatment group, whereas Rades *et al* [7] reported that the OS rates were not significantly different between the two groups. The study of Rades *et al* [7] was a small sample-size, matched-pair, retrospective study that may not be able to provide an adequate statistical power to detect a significant difference. In contrast, the study by Andrews *et al* [3] was a well-designed, large sample-size, randomized controlled trial; thus, the evidence rank was high. In view of this, we believe that the addition of SRS treatment to WBRT can improve the OS in patients with a single brain metastasis.

The analysis of the pooled data of the five trials revealed that the patients who underwent combined WBRT plus SRS treatment had a better control of the treated lesions, which indicated that the addition of SRS could improve the LC in patients with 1-4 brain metastases. There were three studies [3–5] that evaluated the IC. The data extracted from the study by Kondziolka *et al* [4] were not suitable for the pooling analysis. This study reported significant differences in the control of intracranial lesions favoring the combined treatment; the median time to intracranial failure was 5 months in the WBRT alone group and 34 months in the combined group ($P$ = 0.002). The pooled data from the other two studies [3, 5] revealed that the addition of SRS to WBRT led to a significant improvement in the IC. However, considering the beneficial effect of the addition of SRS on the LC, the pooled outcome maybe largely resulting from this effect and may not indicate that distant brain control would also benefit from the additional SRS treatment. As the study did not provide data on new cerebral distant metastases, whether the addition of SRS improves the distant brain control needs to be confirmed by further clinical trials.

With respect to the side effects of radio therapy, there was no significant difference in the acute or late toxicity rates between the two groups, which suggested that the toxic effects may not be affected by SRS. It is well known that WBRT may induce cognitive impairment. SRS has emerged as a focused treatment modality characterized by delivering a high-dose fraction of ionizing radiation to a discrete target volume. It was assumed to be associated with a high risk of radionecrosis, particularly when combined with WBRT. In the current study, the SRS dose ranged from 14 to 24 Gy due to the differences in the size and number of the brain lesions. However, only the study of Minniti *et al* [5] reported radionecrosis and neurocognitive deficits. This indicates that the prescribed dose of SRS in each of the included trials was safe, and the addition of SRS to WBRT therapy was not associated with an increase in toxicity.

There are several limitations in our review. First, two of the included matched-pair studies were retrospective in nature, which always presents a potential risk of a hidden selection bias. Second, the prescribed dose/fractionation regimens of SRS, pathological type of primary tumors,

and the diameter of the metastatic foci in each study were not homogenous. Moreover, most of the studies did not assess the functional outcome or quality of life, which are extremely important outcomes in the treatment of advanced cancer. All the above may have distorted our results.

Taken together, our data suggest that the addition of SRS to WBRT has a beneficial effect on the LC and IC without increasing the risk of toxicity. Moreover, the addition of SRS has the potential of improving the OS in patients with a single brain metastasis. Therefore, SRS combined with WBRT should be recommended as a suitable treatment option for patients with 1–4 brain metastases, particularly for patients with a single brain metastasis.

### Conflicts of interest

The authors indicate no potential conflicts of interest.

## References


1. Patil CG, Pricola K, Sarmiento JM, *et al*. Whole brain radiation therapy (WBRT) alone versus WBRT and radiosurgery for the treatment of brain metastases. Cochrane Database Syst Rev, 2012, Sep 12, (9): CD006121. doi: 10.1002/14651858.CD006121.pub3.
2. Tsao M, Xu W, Sahgal A. A meta-analysis evaluating stereotactic radiosurgery, whole-brain radiotherapy, or both for patients presenting with a limited number of brain metastases. Cancer, 2012, 118: 2486–2493.
3. Andrews DW, Scott CB, Sperduto PW, *et al*. Whole brain radiation therapy with or without stereotactic radiosurgery boost for patients with one to three brain metastases: phase III results of the RTOG 9508 randomised trial. Lancet, 2004, 363: 1665–1672.
4. Kondziolka D, Patel A, Lunsford LD, *et al*. Stereotactic radiosurgery plus whole brain radiotherapy versus radiotherapy alone for patients with multiple brain metastases. Int J Radiat Oncol Biol Phys, 1999, 45: 427–434.
5. Minniti G, Salvati M, Muni R, *et al*. Stereotactic radiosurgery plus whole-brain radiotherapy for treatment of multiple metastases from non-small cell lung cancer. Anticancer Res, 2010, 30: 3055–3061.
6. El Gantery MM, Abd El Baky HM, El Hossieny HA, *et al*. Management of brain metastases with stereotactic radiosurgery alone versus whole brain irradiation alone versus both. Radiat Oncol, 2014, 9: 116.
7. Rades D, Janssen S, Bajrovic A, *et al*. A matched-pair analysis comparing whole-brain radiotherapy with and without a stereotactic boost for intracerebral control and overall survival in patients with one to three cerebral metastases. Radiat Oncol, 2017, 12: 69.
8. Petty WJ, Urbanic JJ, Ahmed T, *et al*. Long-term outcomes of a phase 2 trial of chemotherapy with consolidative radiation therapy for oligometastatic non-small cell lung cancer. Int J Radiat Oncol Biol Phys, 2018, 102, 527–535.
9. Mitchell KG, Farooqi A, LudmirE B, *et al*. Improved overall survival with local consolidative therapy in oligometastatic non-small cell lung cancer: results from a cohort of 194 patients with synchronous disease. Int J Radiat Oncol Biol Phys, 2019, Thoracic Cancers Symposium Abstracts.
10. Brown PD, Jaeckle K, Ballman KV, *et al*. Effect of radiosurgery alone vs radiosurgery with whole brain radiation therapy on cognitive function in patients with 1 to 3 brain metastases: A randomized clinical trial. JAMA, 2016, 316: 401–409.
11. Shaw MG, Ball DL. Treatment of brain metastases in lung cancer: strategies to avoid/reduce late complications of whole brain radiation therapy. Curr Treat Options Oncol, 2013, 14: 553–567.
12. Gondi V, Pugh SL, Tome WA, *et al*. Preservation of memory with conformal avoidance of the hippocampal neural stem-cell compartment during whole-brain radiotherapy for brain metastases (RTOG 0933): a phase II multi-institutional trial. J Clin Oncol, 2014, 32: 3810–3816.


**DOI 10.1007/s10330-019-0344-4**
**Cite this article as:** Wan C, Chen B, Liu YS, *et al*. Whole-brain radiation therapy alone vs. combined therapy with stereotactic radiosurgery for the treatment of limited brain metastases: A systematic review. Oncol Transl Med, 2019, 5: 114–118.

Oncology and Translational Medicine
DOI 10.1007/s10330-019-0356-6

June 2019, Vol. 5, No. 3, P119–P122

ORIGINAL ARTICLE

# Identifying peptides that specifically bind to MDA-MB-468 breast cancer cells*

**Xiaoli Dai (✉), Qing Zhang, Huili Zhang, Hongtao Xu**

Clinical Medical College, Jiangsu Medical Vocational College, Yancheng 224005, China

## Abstract

**Objective** To use phage display technique to screen for small polypeptides that specifically bind to MDA-MB-468 cells.

**Methods** A random heptapeptide phage display library was used for *in vitro* screening against target MDA-MB-468 cells. SC1180 cells were used for subtractive selection. High-affinity phage DNA was extracted, and peptides were sequenced.

**Results** (1) The original library capacity of the polypeptide library was $2 \times 10^{13}$ pfu/mL, and phage titer was determined over 4 rounds. The average library capacity was $1.8 \times 10^{13}$ pfu/mL. (2) Subtractive screening showed that the phage library volume of each round was $1.8 \times 10^{12}$ pfu/mL, and that there was an enrichment effect in each subsequent round. Screening was stopped after the fourth round. (3) PCR results showed that the size of 39 products (78.0%) and 11 products (22%), were 300 bp and 258 bp, respectively. Thirty positive phages were selected for DNA extraction and sequencing, and the corresponding amino acid sequence was LMTRXSK. The sequence had no homology with known genes or proteins.

**Conclusion** Using the phage display technique, we identified that the short polypeptide, LMTRXSK, specifically binds MDA-MB-468 human breast cancer cells.

Received: 7 May 2019
Revised: 8 June 2019
Accepted: 17 June 2019

**Key words:** phage; breast cancer; specific binding peptide

Breast cancer occurs primarily in women (approximately 99% of cases) and is caused by malignant tumors in the epithelial tissue of the breast. In situ breast cancer is not fatal, but cancer cells can aberrantly alter their surrounding networks and can spread through the whole body through vascular or lymphatic channels [2–3]. Treatments can be targeted at the cellular or molecular levels, targeting known carcinogenic sites. This is advantageous in killing only cancer cells, and can avoid toxic side effects from traditional radiotherapy and chemotherapy methods [4–5]. Therefore, identification of target sites in cancer tissues has become an important topic in cancer therapy research. To explore targeted therapy for breast cancer, we used phage display technology to screen for small molecular polypeptides that specifically bind to MDA-MB-468 human breast cancer cells.

## Materials and methods

### Cell lines and main reagents

Human breast cancer cells (MDA-MB-468) and wild-type human breast cells (SC1180) were purchased from Kingsley Biotechnology Co. Ltd (USA). Phage display heptapeptide library kit was purchased from New England Biolabs (NEB, USA). M13 phage single-strand DNA rapid extraction kit was purchased from Booxis (Tianjin) Biotechnology Co. Ltd (China). Dulbecco's Modified Eagle Medium (DMEM), Dulbecco's phosphate buffered saline (DPBS), and HEP were purchased from Gibco-BRL (USA). PCR primers were synthesized by Shanghai Yingjun Biotechnology Co. Ltd (China).

### *In vitro* screening of phage display

✉ Correspondence to: Xiaoli Dai. Email: houxiangcai254@163.com
* Supported by a grant from the Jiangsu Provincial Health and Family Planning Commission (No. H201640).

### heptapeptide library

MDA-MB-468 and SC1180 cells were cultured in DMEM medium containing 10% fetal bovine serum (FBS) in culture dishes treated with poly-lysine. MDA-MB-468 cells were incubated with bovine serum albumin (BSA) solution for 1 h. Then, phage was added to display the heptapeptide library, and the phage was eluted with 0.2 M glycine. The eluent was moved into the cell culture dish containing SC1180 cells. After 1 h, the supernatant, which now contained the screened phage, was purified by polyethylene glycol (PEG) method, and was used in the next round of screening. In the second, third and fourth rounds, incubation time of peptide library and MDA-MB-468 cells was reduced to 40 min, 30 min, and 20 min, respectively. Adsorption time of eluent and SC1180 cells was increased to 70 min, 90 min, and 105 min, respectively.

### PCR amplification of phage DNA

The volume of the screened products in the fourth round were 20 L. The metal bath was centrifuged for 3 min after 10min. The supernatant (1 L) was used as the template. The PCR mixture contained: 0.5 L dNTP (concentration 10 mmol/L), 0.25 L DNA polymerase (5 U/L), 2.5 L reaction buffer, 1 L upstream primer, 1 L downstream primers, and 1 L DNA template. PCR conditions were: (1) 94°C for 2 min, (2) 30 cycles of 56°C for 30 s, 94°C for 30 s, 68°C for 30 s, (3) 68°C for 5 min.

### Sequencing of phage clones

Nucleic acids were extracted with the positive clone kit. DNA was sequenced by Shanghai Yingjun Biotechnology Co. Ltd. (China) using the 96 g primer, 5'-hoccctcatagttagcgtaacg-3'. Homology of polypeptide sequences with known protein sequences was analyzed using NCBI BLAST website.

## Results

### Phage polypeptide library capacity determination

The original library capacity of the polypeptide library was $2 \times 10^{13}$ pfu/mL, and phage titer was determined over 4 rounds of screening. The average library capacity was $1.8 \times 10^{13}$ pfu/mL, shown in Fig. 1.

### Phage peptide library enrichment effect

Cancerous MDA-MD-468 cells were used as the target cells, while the wild-type SC1180 cells were used to adsorb phages for subtraction selection. Phage library in each round was maintained at $1.8 \times 10^{12}$ pfu/mL, and an enrichment effect was observed in each subsequent round.

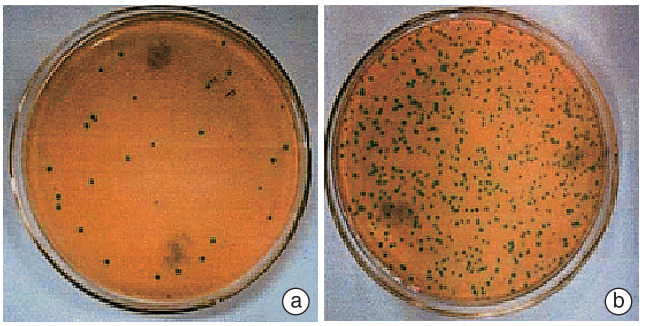


**Fig. 1** Phage titer determination. (a) Phage titer determination after the first round of screening; (b) Phage titer determination after the fourth round of screening

**Table 1** Recycling amount and enrichment effect of 4 rounds of selection

| Times | Inputs (pfu) | Recycled (pfu) | The recovery rate | Enrichment of multiple |
|---|---|---|---|---|
| 1 | $1.8 \times 10^{12}$ | $4.0 \times 10^{5}$ | $2.22 \times 10^{-7}$ | – |
| 2 | $1.8 \times 10^{12}$ | $2.5 \times 10^{6}$ | $1.39 \times 10^{-6}$ | 6.3 |
| 3 | $1.8 \times 10^{12}$ | $1.7 \times 10^{7}$ | $9.44 \times 10^{-6}$ | 6.8 |
| 4 | $1.8 \times 10^{12}$ | $2.0 \times 10^{7}$ | $1.11 \times 10^{-5}$ | 1.2 |

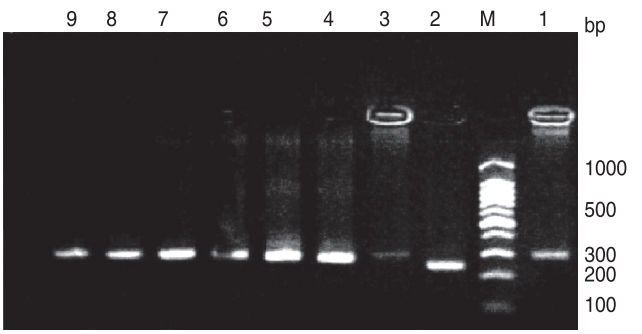


**Fig. 2** PCR electrophoresis of bacteriophage DNA

By the fourth round, there was no significant difference from the third round, so the screening was suspended. Phage enrichment in breast cancer cells increased by approximately 51 times (Table 1).

### PCR amplification of phage DNA

The sizes of 39 products (78.0%) and 11 products (22%), were 300 bp and 258 bp, respectively (Fig. 2).

### Sequence analysis of positive phage DNA

Thirty positive phages were selected for DNA extraction and sequencing. DNA sequences were analyzed with Chromas software. The DNA sequence translated to the amino acid sequence, LMTRXSK. The sequence showed no homology with known genes and proteins (Fig. 3).

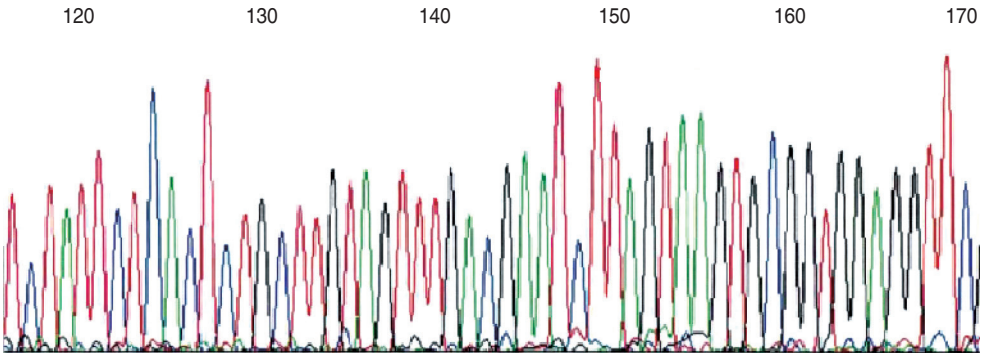


**Fig. 3** Results of PCR product sequencing

## Discussion

Increasing incidence of cervical spondylosis, malignant tumors, cardiovascular disease, and cerebrovascular disease in women correlates with increasing undertaking of high-pressure roles in society [6–7]. Breast cancer is caused by one of the most common types of malignant tumors in women. In some regions in the world, the incidence of breast cancer is second only to lung cancer, but the fatality rate ranks first among malignant tumors [8]. Compared to Europe and America, the incidence of breast cancer in China is higher, however, the cure rate is lower. The survival rate of patients has improved due to advancements in surgical techniques and chemotherapy regimens. However, there have been no recent breakthroughs in improving patient survival [9–10]. Therefore, more research is being focused on looking for targeted therapies with stronger specificity and fewer side effects.

Phage display is an experimental technique in which peptides are displayed on the phage surface, and the target peptides are then extracted and isolated [11]. A variety of malignant tumor-targeting peptides have been validated, and have been used in early diagnosis or targeted treatment of malignant tumors [12]. Phage display is an experimental technique in which peptides are displayed on the phage surface and the target peptides are extracted and isolated [13]. In this study, MDA-MB-468 breast cancer cells were targeted, and wild-type SC1180 cells were selected as adsorption cells to screen for specific peptides that bind human breast cancer cells. After four rounds of screening, phage enrichment in breast cancer cells increased by about 51 times, indicating that phage specifically bound to MDA-MB-468 was enriched. DNA extraction and sequencing of 30 positive phages revealed that the amino acid sequence of the peptide was LMTRXSK.

In conclusion, this study used phage display technology to screen and identify a small molecule polypeptide, LMTRXSK, that can specifically bind to MDA-MB-468 human breast cancer cells. This may be a potential candidate for breast cancer diagnosis and targeted therapy.

## References

1. Leung YK, Govindarajah V, Cheong A, *et al*. Gestational high-fat diet and bisphenol A exposure heightens mammary cancer risk. Endocr-Relat Cancer, 2017, 24: 345–358.
2. Lin W, Modiano JF, Ito D. Stage-specific embryonic antigen: determining expression in canine glioblastoma, melanoma, and mammary cancer cells. J Vet Sci, 2017, 18: 101–104.
3. Roy S, Banerjee S, Chakraborty T. Vanadium quercetin complex attenuates mammary cancer by regulating the P53, Akt/mTOR pathway and downregulates cellular proliferation correlated with increased apoptotic events. Biometals, 2018, 31: 647–671.
4. Matsuda N, Lim B, Wang X, *et al*. Early clinical development of epidermal growth factor receptor targeted therapy in breast cancer. Expert Opin Investig Drugs, 2017, 26: 463–479.
5. Kiderlen M, van de Velde CJH, Liefers GJ, *et al*. Targeted therapy in older women with breast cancer – What's the target? Eur J Surg Oncol, 2017, 43: 944–948.
6. Li R, Zhang L, Yang JX, *et al*. Analysis of inpatient payments of breast cancer patients with different medical insurance coverages in China (mainland) in 2011–2015. Chin J Cancer Res, 2017, 29: 419–425.
7. Dinegde NG, Xuying L. Awareness of Breast Cancer among Female Care Givers in Tertiary Cancer Hospital, China. Asian Pac J Cancer Prev, 2017, 18: 1977–1983.
8. Zhang NQ, Ho SC, Mo XF, *et al*. Glucosinolate and isothiocyanate intakes are inversely associated with breast cancer risk: a case-control study in China. Br J Nutr, 2018, 119: 957–964.
9. Li Q, Yang Z, Fan J, *et al*. A nation-wide multicenter 10-year (1999-2008) retrospective study of chemotherapy in Chinese breast cancer patients. Oncotarget, 2017, 8: 75864–75873.
10. Wu J, Fang M, Zhou X, *et al*. Paraoxonase 1 gene polymorphisms are associated with an increased risk of breast cancer in a population of Chinese women. Oncotarget, 2017, 8: 25362–25371.
11. Sakamoto K, Kamada Y, Sameshima T, *et al*. K-Ras(G12D)-selective inhibitory peptides generated by random peptide T7 phage display technology. Biochem Biophys Res Commun, 2017, 484: 605–611.
12. Jafari B, Hamzeh-Mivehroud M, Moosavi-Movahedi AA, *et al*. Identification of novel single-domain antibodies against FGF7 using

phage display technology. SLAS Discov, 2018, 23: 193–201.
13. Arab A, Robati RY, Nicastro J, *et al*. Phage-based nanomedicines as new immune therapeutic agents for breast cancer. Curr Pharm Des, 2018, 24: 1195–1203.

**DOI 10.1007/s10330-019-0356-6**
**Cite this article as:** Dai XL, Zhang Q, Zhang HL, *et al*. Identifying peptides that specifically bind to MDA-MB-468 breast cancer cells. Oncol Transl Med, 2019, 5: 119–122.

Oncology and Translational Medicine
DOI 10.1007/s10330-019-0342-2

June 2019, Vol. 5, No. 3, P123–P130

ORIGINAL ARTICLE

# Significant association between IL-18 and OCT4 gene polymorphisms in susceptibility and clinical characteristics of prostate cancer*

**Shaojun Nong[1] (✉), Yangbo Guan[1], Zhiwei Wang[1], Zhongqing Wei[2], Yueping Zhang[1], Jian Ni[1], Chongsheng He[1], Limin Ma[1], Shujun Zhou[1], Wenguang Li[1]**

[1] Department of Urological Surgery, The Affiliated Hospital of Nantong University, Nantong 226001, China
[2] Department of Urological Surgery, The Second Affiliated Hospital of Nanjing Medical University, Nanjing 210011, China

## Abstract

**Objective** Recent studies have shown abnormal expression of octamer-binding transcription factor 4 (OCT4) and interleukin-18 (IL-18) to be related to cancer. However, the molecular mechanisms by which the IL-18 and OCT4 gene polymorphisms are associated with prostate cancer remain unclear. In this study, we aimed to determine whether the presence of IL-18 and OCT4 polymorphisms were associated with size, grade, tumor, nodes and metastasis (TNM) stage, or survival in patients with prostate cancer.

**Methods** Polymorphisms in OCT4 and IL-18 genes were evaluated to determine susceptibility to prostate cancer in 120 patients. A control group consisted of 125 Chinese participants. Genotyping was performed using TaqMan allelic discrimination assays, and statistical analysis was performed using SPSS.

**Results** No association was found between OCT4 and IL-18 gene polymorphisms and prostate cancer susceptibility. For OCT4 AA and IL-18-607 CC genotypes, there was a significant association with higher tumor grade ($P$ = 0.03 and $P$ = 0.025) and stage ($P$ = 0.04 and $P$ = 0.001). The OCT4 and IL-18-137 GG genotype was correlated with higher tumor grade ($P$ = 0.028) and stage ($P$ = 0.008). Furthermore, OCT4 AA was significantly more frequent in patients with lymph node metastasis ($P$ = 0.02) and distant metastasis ($P$ = 0.01). The Cox proportional hazard model showed that tumor grade and stage grouping were independent prognostic factors but IL-18 and OCT4 polymorphisms were not.

**Conclusion** The OCT4 gene may have a profound effect on prostate cancer risk. Polymorphism variants in the IL-18 (IL-18-607 and IL-18-137) and OCT4 genes may be associated with poor prognoses for individuals with prostate cancer.

Received: 17 March 2019
Revised: 10 April 2019
Accepted: 28 May 2019

**Key words:** clinical characteristics; interleukin-18 (IL-18); octamer-binding transcription factor 4 (OCT4); polymorphism; prostate cancer

Initially, most patients with prostate cancer respond favorably to anti-androgen treatments or surgery. However, tumors frequently recur and progress towards the castration-resistant (CR) stage; for which therapeutic options are scarce. It has been suggested tumor initiation and progression is driven by small populations of cells endowed with stem-like properties: cancer stem cells (CSCs) [1]. Interestingly, CSCs may share properties, such as utilization of molecular pathways typically used by pluripotent embryonic stem cells (ESCs), with normal stem cells [1–2]. The prognostic significance of ESC gene expression signatures in solid tumors, including prostate cancer, has been successfully demonstrated [2–4]. Stem cell-like pluripotency has been successfully induced in differentiated fibroblasts upon reprogramming by transfecting a limited number of genes, including octamer-binding transcription factor 4 (OCT4) and Nanog [5]. Octamer-binding transcription factor 4 is a key transcription factor required to maintain the self-renewal and pluripotency of embryonic stem cells, and it enhances

✉ Correspondence to: Shaojun Nong. Email: shaojunnong@sina.com
* Supported by grants from the China Postdoctoral Science Foundation (No. 2014M139951) and the Science and Technology Project of Nantong, Jiangsu Province (No. MS22016043).

tumorigenesis in CSCs [6]. Increased expression of OCT4 is associated with low differentiation, tumor, nodes and metastasis (TNM) staging, and tumor recurrence in certain types of cancer, making OCT4 a promising biomarker for the diagnosis and prognosis of cancer in patients [7–9].

Recently, research showed that prostate tumor cells could secrete interleukin-18 (IL-18) in response to IFN-γ in the tumor microenvironment and that IL-18 could function as an autocrine or paracrine factor for the tumor [10]. Previously, we suggested IL-18 may play an important role in prostate cancer growth and metastasis, and we found that it correlated with serum IL-18 and VEGF in patients with prostate cancer. IL-18 proangiogenic functions are essential for tumor growth [11–12]. The IL-18 gene is located on chromosome 11q22 and functional gene polymorphisms -607A/C and -137G/C are found in its promoter region [13]. Our researchers found a change from C allele to A allele at position -607 and a change from G to C at position -137 of the IL-18 promoter region in prostate cancer patients [14]. These findings suggest IL-18 acts as a direct regulator of the self-renewal capacity of CSCs; however, the exact role of IL-18 in the regulation of CSC characteristics is not fully understood.

To further understand the role of IL-18 we recruited 245 participants, consisting of 120 patients with prostate cancer and 125 healthy individuals. The goal was to determine whether IL-18 and OCT4 gene polymorphisms, and their interaction with prostate cancer-related risk factors, are associated with susceptibility and clinicopathological development of prostate cancer among Chinese men.

## Patients and methods

### Patients

A total of 120 patients with prostate cancer who had undergone a radical prostatectomy between 2005 and 2011 at the Department of Urological Surgery, The Affiliated Hospital of Nantong University in China were evaluated. We excluded patients with infectious diseases and diabetes mellitus in order to eliminate the influence of other diseases. None of the patients with prostate cancer had received chemotherapy, hormonal therapy, or radiotherapy before surgery. Patient age ranged from 58–85 years and included 80 non-metastatic and 40 metastatic cases. The tumor stage was classified according to Whitmore-Jewett stage and was graded according to Gleason score. Patients were divided into low (≤ 6) and high (> 6) Gleason scores. Patient and tumor characteristics are listed in Table 1. Bone metastases were assessed by bone x-ray and bone scan, and extraosseous metastases were assessed by surgical biopsy. Recurrence was defined as a significant elevation of prostate-specific antigen (PSA) and/or new symptoms due to local tumor recurrence. The control group was comprised of 125 healthy volunteers who visited the general health check-up division at The Affiliated Hospital of Nantong University. Selection criteria for controls were no evidence of any personal or family history of cancer or other serious illnesses. Follow-up time ranged from 6 to 38 months with a median of 16 months after surgery. This study was performed with the approval of the ethics committee of Chinese Human Genome.

**Table 1** Clinicopathological characteristics of prostate cancer patients

| Characteristics | *n* | % |
|---|---|---|
| Age (years) | | |
| Mean | 70.43 ± 11.14 | |
| Range | 58–85 | |
| Tumor stage | | |
| A | 5 | 4.2 |
| B | 67 | 55.8 |
| C | 10 | 8.3 |
| D | 38 | 31.7 |
| Lymph node metastasis | | |
| Negative | 70 | 58.3 |
| Positive | 50 | 41.7 |
| Metastasis | | |
| Negative | 80 | 66.7 |
| Positive | 40 | 33.3 |
| Grade | | |
| ≤6 | 63 | 52.5 |
| >6 | 57 | 47.5 |

### DNA extraction

Genomic DNA was extracted from EDTA-anticoagulated peripheral blood leukocytes by the salting-out method. Blood (5 mL) was mixed with Triton lysis buffer (0.32 M sucrose, 1% Triton X-100, 5 mM $MgCl_2$, $H_2O$, and 10 mM Tris-HCl, pH 7.5). Leucocytes were spun down and washed with $H_2O$. The pellet was incubated with proteinase K at 56 °C and subsequently salted out at 48 °C using a saturated NaCl solution. Precipitated proteins were removed by centrifugation. The DNA in the supernatant fluid was dissolved in 300 mL $H_2O$.

### IL-18 genotype

The genotyping of the two IL-18 polymorphisms was performed using predesigned TaqMan SNP Genotyping Assays (Applied Biosystems, USA). The Assays-on-Demand SNP genotyping kit (Applied Biosystems, USA) was used for the PCR. Single-nucleotide polymorphism (SNP) amplification assays were performed according to the manufacturer's instructions. A 25 μL sample of reaction solution containing 10 ng of DNA was mixed with 12.5 μL of 2x TaqMan Universal PCR Mix (Applied Biosystems, USA) and 1.25 μL of predeveloped assay reagent from the SNP genotyping product (Applied

Biosystems, USA), containing two primers and two TaqMan MGB probes. Reaction conditions consisted of preincubation at 50 °C for 2 min and at 95 °C for 10 min, followed by 40 cycles at 95 °C for 15 s and at 60 °C for 1 min. Amplifications and analysis were performed in an ABI Prism 7500 Sequence Detection System (Applied Biosystems, USA), running SDS 1.4 software for allelic discrimination (Applied Biosystems, USA). The following SNPs were typed: IL-18-137 G/C (rs187238) and IL-18-607 A/C (rs1946518).

### OCT4 genotype

The TagSNPs were selected from the Haploview software 4.2 (Mark Daly's laboratory of Broad Institute, Britain) based on the GIH population data of HapMap (HapMap Data Rel 27 Phase II + III, Feb 09, on NCBI B36 assembly, dbSNP b126). TagSNPs that captured all known common SNPs (with minor allele frequencies of > 0.1) in the OCT4 genes, with a pairwise correlation $r^2$ > 0.8, were selected.

### Statistical analysis

SNP allele frequencies were tested against departure from Hardy-Weinberg equilibrium before analysis. Genotype frequencies were compared using the Pearson $\chi^2$ test for the 2 × 2 tables or Fisher's exact test when the expected frequency was $P < 0.05$. Patients were classified in a dichotomous manner for each of the following clinical parameters: tumor diameter, nuclear grade, tumor stage, lymph node metastasis, distant metastasis, stage grouping, and survival. The distribution of the polymorphism for each parameter was studied by analyzing genotype group and allele frequency. Odds ratios (ORs) and significance (*P*-values) were also calculated. The influence of each variable on survival was assessed by means of the Cox proportional hazard model. Values of $P < 0.05$ were considered significant. The SPSS statistical software package version 11.5 was used for all statistical analyses.

## Results

### Study subjects

The present study included 120 prostate cancer patients (mean age 70.43 ± 11.14 years) and 125 healthy controls (mean age 70.70 ± 9.41 years). The detailed baseline characteristics of the study subjects were given in Table 1.

### Correlation of IL-18 gene polymorphisms with the clinicopathological characteristics prostate cancer

This case-control study revealed similar frequencies in the distribution of IL-18-137 and -607 polymorphisms between healthy controls and patients with prostate cancer. Table 2 presented the genotype distributions and statistical analysis. The observed genotype frequencies were in accordance with Hardy-Weinberg equilibrium. The association of the IL-18 genotypes with tumor grade and stage are shown in Table 3. Genotype GG of IL-18-137 was associated with more advanced cancer stage (OR: 2.61; 95% CI: 1.15–5.37; $P = 0.008$) and with higher tumor grade (OR: 3.32; 95% CI: 1.16–8.17; $P = 0.028$). IL-18-137 G allele was correlated with more advanced stage (OR: 1.73; 95% CI: 1.04–3.42; $P = 0.027$) and with higher tumor grade (OR: 2.13; 95% CI: 0.98–4.12; $P = 0.040$). The IL-18-607 CC genotype was significantly more frequent in patients with more advanced cancer stage (OR: 3.82; 95% CI: 1.67–7.67; $P = 0.001$) and higher tumor grade (OR: 3.11; 95% CI: 1.05–10.25; $P = 0.025$). The IL-18-607 C allele was associated with more advanced cancer stage (OR: 2.37; 95% CI: 1.28–3.73; $P = 0.001$). The association of the IL-18 genotypes with lymph node metastasis and distant metastasis are shown in Table 4. The IL-18-137 G allele was significantly more frequent in patients with lymph node metastasis (OR: 3.82; 95% CI: 0.95–15.17; $P = 0.035$).The IL-18-607 CC genotype was associated with distant metastasis (OR: 2.71; 95% CI: 1.25–6.14; $P = 0.025$).

### Correlation of OCT4 gene polymorphisms with clinicopathological characteristics of prostate cancer

The observed genotype frequencies of the OCT4 gene polymorphisms studied in healthy controls were in accordance with Hardy–Weinberg equilibrium. No significant differences were observed in the frequency distribution of OCT4 polymorphisms between prostate cancer patients and healthy controls, both at the genotypic and allelic levels (Table 5). Genotype AA of

**Table 2** Association of IL-18 genotypes with tumor risk (*n*, %)

| IL-18 Polymorphisms | PC patients | Healthy controls | Odds ratio (95% CI) | *P* |
|---|---|---|---|---|
| -137 C/G Genotype | | | | |
| CC | 6 (5.0) | 10 (8.0) | 1.55 (0.45–4.05) | 0.522 |
| CG | 47 (39.2) | 40 (32.0) | 1.00 (Reference) | |
| GG | 67 (55.8) | 75 (60.0) | 0.78 (0.47–1.15) | 0.725 |
| Allele | | | | |
| C | 56 (23.3) | 75 (30.0) | 1.00 (Reference) | |
| G | 184 (76.7) | 175 (70.0) | 1.45 (0.75–1.87) | 0.072 |
| -607 A/C Genotype | | | | |
| AA | 13 (10.8) | 10 (8.0) | 1.22 (0.56–1.96) | 0.657 |
| AC | 61 (50.8) | 65 (52.0) | 1.00 (Reference) | |
| CC | 46 (38.3) | 50 (40.0) | 0.787 (0.61–1.33) | 0.322 |
| Allele | | | | |
| A | 114 (47.5) | 110 (44.0) | 1.00 (Reference) | |
| C | 126 (52.5) | 115 (46.0) | 1.36 (0.81–1.69) | 0.381 |

CI, confidence interval; $\chi^2$ Test or Fisher's exact test

**Table 3** Association of IL-18 genotypes with tumor stage and grade

| IL-18 Polymorphisms | Tumor stage (*n*, %) A–B | Tumor stage (*n*, %) C–D | Odds ratio (95% CI) | *P* | Tumor grade Odds (*n*, %) ≤ 6 | Tumor grade Odds (*n*, %) > 6 | Ratio (95% CI) | *P* |
|---|---|---|---|---|---|---|---|---|
| -137 C/G Genotype | | | | | | | | |
| CC | 4 (5.6) | 2 (4.2) | 1.25 (0.21–7.81) | 0.625 | 3 (4.7) | 3 (5.3) | 1.36 (0.15–16.27) | 0.620 |
| CG | 35 (48.6) | 14 (29.2) | 1.00 (Reference) | | 35 (55.6) | 11 (193) | 1.00 (Reference) | |
| GG | 33 (45.8) | 32 (66.7) | 2.61 (1.15–5.37) | 0.008 | 25 (39.7) | 43 (75.4) | 3.32 (1.16–8.17) | 0.028 |
| Allele | | | | | | | | |
| C | 35 (29.2) | 32 (24.8) | 1.00 (Reference) | | 55 (42.3) | 32 (26.2) | 1.00 (Reference) | |
| G | 85 (70.8) | 97 (75.2) | 1.73 (1.04–3.42) | 0.027 | 75 (57.7) | 90 (73.7) | 2.13 (0.98–4.12) | 0.040 |
| -607 A/C Genotype | | | | | | | | |
| AA | 8 (11.1) | 3 (6.2) | 0.83 (0.26–2.37) | 0.617 | 5 (7.9) | 4 (7.0) | 1.17 (0.27–5.05) | 0.782 |
| AC | 44 (61.1) | 21 (43.8) | 1.00 (Reference) | | 44 (69.8) | 29 (50.9) | 1.00 (Reference) | |
| CC | 20 (27.8) | 24 (50.0) | 3.82 (1.67–7.67) | 0.001 | 4 (22.2) | 24 (42.1) | 3.11 (1.05–10.25) | 0.025 |
| Allele | | | | | | | | |
| A | 57 (43.2) | 45 (35.4) | 1.00 (Reference) | | 35 (26.9) | 23 (17.7) | 1.00 (Reference) | |
| C | 75 (56.8) | 82 (64.6) | 2.37 (1.28–3.73) | 0.001 | 95 (73.1) | 107 (82.3) | 1.78 (0.87–4.52) | 0.153 |

**Table 4** Association of IL-18 genotypes with lymph node metastasis, metastasis, and stage grouping

| IL-18 Polymorphisms | Lymph nodemetastasis (*n*, %) Negative | Lymph nodemetastasis (*n*, %) Positive | Odds ratio (95% CI) | *P* | Metastasis (*n*, %) Negative | Metastasis (*n*, %) Positive | Ratio (95% CI) | *P* |
|---|---|---|---|---|---|---|---|---|
| -137 C/G Genotype | | | | | | | | |
| CC | 2 (2.9) | 1 (2.0) | 0.84 (0.88–1.12) | 0.672 | 2 (2.5) | 1 (2.5) | 2.81 (0.32–13.27) | 0.427 |
| CG | 30 (42.9) | 23 (46.0) | 1.00 (Reference) | | 35 (43.8) | 7 (17.5) | 1.00 (Reference) | |
| GG | 38 (54.2) | 26 (52.0) | 1.79 (0.33–8.35) | 0.436 | 43 (53.7) | 32 (80.01) | 1.98 (0.92–5.17) | 0.163 |
| Allele | | | | | | | | |
| C | 65 (43.3) | 5 (16.7) | 1.00 (Reference) | | 42 (25.1) | 11 (16.2) | 1.00 (Reference) | |
| G | 85 (56.7) | 25 (83.3) | 3.82 (0.95–15.17) | 0.035 | 125 (74.9) | 57 (83.8) | 1.57 (0.82-3.50) | 0.317 |
| -607 A/C Genotype | | | | | | | | |
| AA | 3 (4.3) | 2 (4.0) | 0.87 (0.89-1.03) | 0.343 | 5 (6.3) | 2 (5.0) | 2.47 (0.67-7.15) | 0.168 |
| AC | 40 (57.1) | 16 (32.0) | 1.00 (Reference) | | 47 (58.7) | 15 (37.5) | 1.00 (Reference) | |
| CC | 27 (38.6) | 32 (64.0) | 2.62 (0.68–9.67) | 1.52 | 28 (35.0) | 23 (57.5) | 2.71 (1.25-6.14) | 0.025 |
| Allele | | | | | | | | |
| A | 60 (46.2) | 5 (18.5) | 1.00 (Reference) | | 61 (34.7) | 21 (28.8) | 1.00 (Reference) | |
| C | 70 (53.8) | 22 (81.5) | 2.98 (0.89–8.93) | 0.057 | 115 (65.3) | 52 (71.2) | 1.45 (0.83-3.45) | 0.237 |

**Table 5** Association of Oct4 genotypes with tumor risk (*n*, %)

| IL-18 Polymorphisms | PC patients | Healthy controls | Odds ratio (95% CI) | *P* |
|---|---|---|---|---|
| Genotype | | | | |
| AA | 15 (12.5) | 10 (8.0) | 1.28 (0.54–1.95) | 0.648 |
| AC | 61 (50.8) | 64 (51.2) | 1.00 (Reference) | |
| CC | 44 (36.7) | 51 (40.8) | 0.877 (0.751–1.62) | 0.412 |
| Allele | | | | |
| A | 110 (45.8) | 105 (46.7) | 1.00 (Reference) | |
| C | 130 (54.2) | 120 (53.5) | 1.26 (0.97–1.89) | 0.401 |

CI, confidence interval; $\chi^2$ Test or Fisher's exact test

OCT4 was associated with more advanced cancer stage (OR: 1.40; 95% CI: 0.62–3.42; $P = 0.04$) and with higher tumor grade (OR: 0.81; 95% CI: 0.41–1.82; $P = 0.03$).The OCT4 Genotype AA was significantly more frequent in patients with lymph node metastasis (OR: 4.08; 95% CI:1.42–10.12; $P = 0.02$) and distant metastasis (OR: 1.81; 95% CI: 0.81–3.42; $P = 0.01$), shown in Table 6.

## Polymorphisms (IL-18 and OCT4) in cancer survival

Thirty-four patients died of cancer-related causes during the follow-up period. Fig. 1 and Fig. 2 showed the Kaplan-Meier curves calculated for cancer-specific survival for the IL-18-607 genotype (AC and CC) and OCT4 genotype (TT and CT + CC). Patients with the AC genotype showed a tendency towards more favorable cancer-specific survival than those with the CC genotype ($P = 0.075$; log-rank test). A Cox proportional hazard model demonstrated that tumor grade and stage grouping

**Table 6** Correlation of the Oct4 gene polymorphisms with prostate cancer clinicopathological characteristics (*n*, %)

| Oct4 | AA | AC + CC | OR (95% CI) | *P* | A | C | OR (95% CI) | *P* |
|---|---|---|---|---|---|---|---|---|
| Clincal stage | | | | | | | | |
| A + B | 41 (59.4) | 31 (60.8) | 1 (Reference) | 0.04 | 68 (56.7) | 81 (67.5) | 1 (Reference) | 0.55 |
| C + D | 28 (41.6) | 20 (39.2) | 1.40 (0.62–3.42) | | 52 (43.3) | 39 (32.5) | 1.18 (0.62–2.25) | |
| Grade | | | | | | | | |
| ≤ 6 | 32 (54.2) | 31 (51.8) | 1 (Reference) | 0.03 | 61 (50.8) | 67 (55.8) | 1 (Reference) | 0.35 |
| > 6 | 27 (45.8) | 30 (49.2) | 0.81 (0.41–1.82) | | 59 (49.2) | 53 (44.2) | 0.45 (0.39–1.21) | |
| lymphy node | | | | | | | | |
| Negative | 30 (57.7) | 40 (58.8) | 1 (Reference) | 0.02 | 65 (54.2) | 73 (60.8) | 1 (Reference) | 0.39 |
| Positive | 22 (42.3) | 28 (41.2) | 4.08 (1.42–10.12) | | 55 (45.8) | 47 (39.2) | 1.16 (0.45–2.17) | |
| Metastasis | | | | | | | | |
| Negative | 27 (56.3) | 57 (75.0) | 1 (Reference) | 0.01 | 83 (69.2) | 76 (63.3) | 1 (Reference) | 0.28 |
| Positive | 21 (43.7) | 19 (25.0) | 1.81 (0.81–3.42) | | 37 (30.8) | 44 (36.7) | 0.66 (0.25–1.71) | |

**Table 7** Multivariate analysis of overall survival in prostate cancer patients

| Variable | B | SE | Wald | *df* | *P* | Exp (B) |
|---|---|---|---|---|---|---|
| Tumor grade | 1.433 | 0.701 | 5.253 | 1 | 0.035 | 3.476 |
| Tumor Stage | 1.575 | 0.527 | 15.217 | 1 | 0.002 | 4.612 |
| IL18 -137 | –1.673 | 1.132 | 4.076 | 1 | 0.073 | 0.180 |
| IL18 -607 | 0.415 | 0.507 | 0.517 | 1 | 0.511 | 1.415 |

were independent prognosis factors (Table 7). However, IL-18 polymorphisms, at least in this series of patients, did not serve as independent prognosis factors.

## Discussion

CSCs are important in carcinogenesis and resistance to treatment and may lead to metastasis. The isolation of circulating stem cells involves cell sorting based on the presence of cell surface markers. The cell surface marker, OCT4 has been reported to be overexpressed in colorectal cancer and expression has been observed in bladder cell cancers [15–16]. Considering the role of OCT4 as a pluripotency factor, and possible role in the etiology of cancer, OCT4 was investigated as a marker for CSCs. Expression of OCT4 has been reported previously in benign prostate and cancer cell lines as evidence of CSC compartments. A subpopulation of telomerase-immortalized prostate epithelial cells that demonstrated stem cell properties expressed OCT4 protein [17]. Similarly, subpopulations of prostate cancer cells that were capable of reconstituting the original prostate tumor in vivo expressed OCT4 mRNA in cultures [18]. These observations suggest OCT4 is a marker for prostate CSCs. Therefore, in order to elucidate the role of OCT4 polymorphisms in cancer; polymorphisms in human prostate cancer were assessed.

Cytokine IL-18 is known to play a critical role in the development and progression of tumors, including prostate cancer tumors. Our results showed a strong association between increased expression of IL-18 and poor outcome in prostate cancer patients. Experimental studies have demonstrated IL-18 may promote

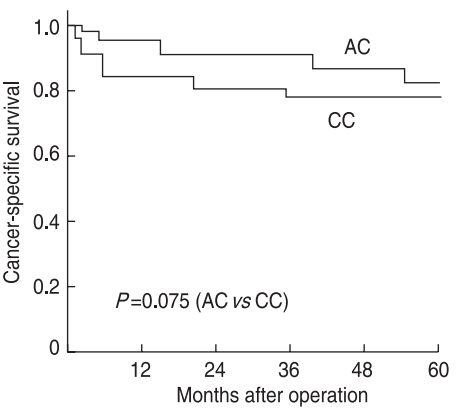


**Fig. 1** Kaplan-Meier overall survival estimate for IL-18-607 polymorphism. Differences between curves were evaluated by log-rank test [*P* = 0.075 (AC *vs* CC)]

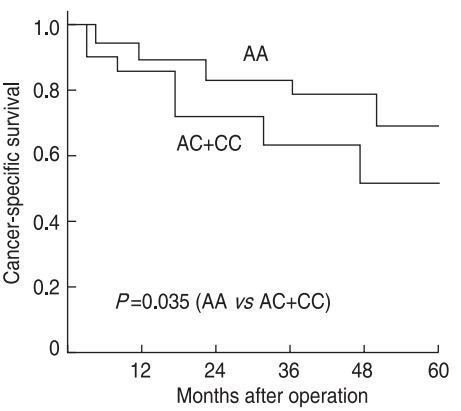


**Fig. 2** Kaplan-Meier overall survival estimate for OCT4 polymorphism. Differences between curves were evaluated by log-rank test [*P* = 0.035 (AA *vs* AC + CC)]

tumorigenesis, angiogenesis, and metastasis, and induce multi-drug resistance in cancer cell lines [19–21]. Moreover, emerging evidence suggests IL-18 has an important role in CSC phenotype and function. Finally, IL-18 has been found to enhance the tumorigenicity in glioblastomas, which is consistent with the increased capacity of CSCs to self-renew [22–23]. These findings suggest that IL-18 may act as a direct regulator of the self-renewal capacity of CSCs; however, the exact role of IL-18 in the regulation of CSC characteristics is not fully understood.

In the present study, we found no association between IL-18 and OCT4 polymorphisms and a higher risk of prostate cancer. However, as shown in other studies these polymorphisms were correlated with more advanced cancer stages [24–25]. Some studies have suggested IL-18 promoter polymorphisms are associated with prostate cancer and prostate cancer risk, although this was contradicted by other studies [26–28]. Our findings support the recent suggestion that pleiotropic cytokine IL-18 can exert both an anticancer and procancer influence [29]. In fact, IL-18 activities are influenced by the tumor microenvironment. So, IL-18 may exert antitumor activity by augmenting IFN-γ production, particularly in the presence of IL-12 [29]. However, recent data suggest a procancer activity for this multifunctional cytokine under certain conditions depending on the tumor immune response at different tumor sites, and genetic background [30]. Polymorphisms (IL-18 and OCT4) do not appear to be associated with prostate cancer susceptibility in our participants. This may be attributable to the different genetic backgrounds and environmental factors, such as different carcinogens, that initiate different cancers, and different carcinogen exposure. In addition, inadequacies in study design, such as nonrandom sampling and a limited sample size, should be considered. Selection bias in this hospital based, case-control study must also be considered. Finally, we cannot ignore that the observed association is dependent on linkage disequilibrium in the IL-18 gene, or on the effect of IL-18 on another peptide.

We found that a genotype related to higher production of IL-18 is associated with higher grade and stage of the tumor. IL-18 activates HIF (hypoxia-inducible factor-1alpha) and vascular endothelial growth factor, and may activate angiogenesis in tumor nests [29, 31]. Therefore, IL-18 polymorphisms may increase angiogenesis and provide adequate nutrients to transformed cells, promoting more advanced stage. Progression is also correlated with IL-18. High-production polymorphisms in IL-18 are associated with dedifferentiation of tumor cells, leading to a more advanced tumor grade and stage grouping. Elevated IL-18 expression was found to be correlated with the malignancy of skin cancers and with the progression of breast cancer [24, 32]. Therefore, IL-18 can directly promote proliferation by regulating proliferation stimulators. IL-18 was recently implicated in the migration of lung cancer and human melanoma cell lines through the region of interest generation method in mitogen-activated protein kinase pathway [33–34]. Our results were similar to previous findings that proinflammatory cytokines induce adhesion receptors of endothelial cells for cancer cell attachment, which is necessary for blood-borne metastasis [35]. The clinical importance of these parameters is worth investigating in patients with prostate cancer, especially for patients with bone metastasis; however, larger studies are needed. In the present study, polymorphisms related to IL-18 production were associated with the development of metastasis and lymph node involvement.

Our study revealed that the expression of OCT4 was correlated with tumor size and lymph node metastases. This study, and other research, may indicate an association between OCT4 nuclear accumulation and tumorigenesis [36]. In addition, OCT4 is more frequently located at the invasive front of tumors and correlates significantly with various aggressive behaviors and epithelial-mesenchymal transition (EMT) in nasopharyngeal carcinoma [37]. The expression of OCT4 in melanoma cells increases transmigration capacity, leading to high invasiveness and aggressiveness, while promoting cancer cell proliferation and formation [38–39]. Inversely, knockdown of OCT4 inhibits CSC cell motility and invasion and decreases hepatic colonization [40]. Patients with low OCT4 expression exhibit an improved overall survival rate [41]. This study provides support that polymorphisms related to OCT4 production were associated with the development of metastasis and lymph node involvement, suggesting OCT4 may be an effective therapeutic target for the treatment of cancer.

The association between overall survival and IL-18-607 polymorphism was also analyzed. Because the median survival (50% mortality) was not achieved, we cannot comment on the statistical influence of this variable as a prognostic factor. Although, polymorphisms related to IL-18 production were strongly correlated with more advanced stages of prostate cancer, explaining increased mortality ($P$ = 0.076). Cox analysis revealed IL-18 and Nanog polymorphisms are not independent risk factors for mortality. We propose that the influence of IL-18-607 polymorphism is more significant than that of IL-18-137, promoting high-risk phenotypes.

Cancer stem cells have been found to be regulated by mesenchymal stem cells through cytokine networks, including IL-6 and IL-8 [42]. Recent studies have demonstrated colon CSCs promote tumor formation and growth through the autocrine effect of certain cytokines, such as IL-8 and IL-4 [43–44]. A paracrine effect of mesenchymal stem cells in promoting tumor growth of CSCs by secreting cytokine IL-6 has also been revealed [45]. Additionally, IL-6 has been shown to enhance

tumorigenicity in glioblastoma, consistent with an increase in the CSCs self-renewal capacity [46]. Here, we show for the first time, the role of the combination of IL-18 and OCT4 gene polymorphisms in susceptibility, and clinical characteristics of prostate cancer. We found that polymorphisms of IL-18 and OCTt4 are associated with higher grade and stage of the tumor, development of metastasis, and lymph node involvement. These findings provide evidence to support that IL-18 may function as a direct mediator of CSCs self-renewal capacity. However, the exact role of IL-18 in the regulation of CSC characteristics requires further investigation.

### Conflicts of interest

The authors declare no conflicts of interest.

## References


1. Reya T, Morrison SJ, Clarke MF, *et al*. Stem cells, cancer, and cancer stem cells. Nature, 2001, 414: 105–111.
2. Ben-Porath I, Thomson MW, Carey VJ, *et al*. An embryonic stem cell-like gene expression signature in poorly differentiated aggressive human tumors. Nat Genet, 2008, 40: 499–507.
3. Markert EK, Mizuno H, Vazquez A, *et al*. Molecular classification of prostate cancer using curated expression signatures. Proc Natl Acad Sci USA, 2011,108: 21276–21281.
4. Schoenhals M, Kassambara A, De VJ, *et al*. Embryonic stem cell markers expression in cancers. Biochem Biophys Res Commun, 2009, 383: 157–162.
5. Takahashi K, Tanabe K, Ohnuki M, *et al*. Induction of pluripotent stem cells from adult human fibroblasts by defined factors. Cell, 2007, 131: 861–872.
6. Kim RJ and Nam JS. OCT4 expression enhances features of cancer stem cells in a mouse model of breast cancer. Lab Anim Res, 2011, 27: 147–152.
7. Dong Z, Zeng Q, Luo H, *et al*. Increased expression of OCT4 is associated with low differentiation and tumor recurrence in human hepatocellular carcinoma. Pathol Res Pract, 2012, 208: 527–533.
8. Li X, Wang J, Xu Z, *et al*. Expression of sox2 and oct4 and their clinical significance in human non-small-cell lung cancer. Int J Mol Sci, 2012, 13: 7663–7675.
9. Hatefi N, Nouraee N, Parvin M, *et al*. Evaluating the expression of oct4 as a prognostic tumor marker in bladder cancer. Iran J Basic Med Sci, 2012, 15: 1154–1161.
10. Lebel-Binay S, Thiounn N, De Pinieux G, *et al*. IL-18 is produced by prostate cancer cells and secreted in responseto interferons. Int J Cancer, 2003, 106: 827–835.
11. Nong SJ, Wen DG, Fan CB, *et al*. Clinical value of Serum Interleukin-18 in patients with prostate cancer. Chinese-German J Clin Oncol, 2007, 6: 574–578.
12. Nong SJ, Zhang YP, Zhou SJ, *et al*. Relationship between serum IL-18 and VEGF levels in patients with prostate cancer. Chinese-German J Clin Oncol, 2010, 9: 643–647
13. Giedraitis V, He B, Huang WX, *et al*. Cloning and mutation analysis of the human IL-18 promoter: a possible role of polymorphisms in expression regulation. J Neuroimmunol, 2001, 112: 146–152.
14. Nong SJ, Guan YB, Wang ZW, *et al*. Clinical study of Il-18 and NANOG gene polymorphisms in prostate cancer patients. Oncol Transl Med, 2018, 4: 247–255.
15. Padín-Iruegas ME, Herranz-Carnero M, Aguin-Losada S, *et al*. Prognostic value of changes in the expression of stem cell markers in the peripheral blood of patients with colon cancer. Oncol Rep, 2013, 29: 2467–2472.
16. Atlasi Y, Mowla SJ, Ziaee SA, *et al*. OCT-4, an embryonic stem cell marker, is highly expressed in bladder cancer. Int J Cancer, 2007, 120: 1598–1602.
17. Li H, Zhou J, Miki J, *et al*. Telomerase-immortalized non-malignant human prostate epithelial cells retain the properties of multipotent stem cells. Exp Cell Res, 2007, 314: 92–102.
18. Gu G, Yuan J, Wills M, *et al*. Prostate cancer cells with stem cell characteristics reconstitute the original human tumor *in vivo*. Cancer Res, 2007, 67: 4807–4815.
19. Hacker Elke, Muller Konrad, Whiteman David C, *et al*. Reduced expression of IL-18 is a marker of ultraviolet radiation-induced melanomas. Int J Cancer, 2008, 123: 227–231.
20. Zaki Mohammad Hasan, Vogel Peter, Body-Malapel Mathilde, *et al*. IL-18 Production downstream of the Nlrp3 Inflammasome confers protection against colorectal tumor formation. J Immunology, 2010,185: 4912–4920.
21. Loeffler M, e'Negrate G, Krajewska M, *et al*. IL-18-producing Salmonella inhibit tumor growth. Cancer Gene Therap, 2008,15: 787–794.
22. Zeng Changjun, Zhang Yanling, Park Su Cheol, *et al*. CD34(+) liver cancer stem cells were formed by fusion of hepatobiliary stem/progenitor cells with hematopoietic precursor-derived myeloid intermediates. Stem Cell Develop, 2015, 24: 2467–2478.
23. Huang Jianhua, Li Chonghui, Wang Yao, *et al*. Cytokine-induced killer (CIK) cells bound with anti-CD3/anti-CD133 bispecific antibodies target CD133(high) cancer stem cells *in vitro* and *in vivo*. Clin Immunology, 2013, 149 : 156–168.
24. Eissa SA, Zaki SA, El-Maghraby SM, *et al*. Importance of serum IL-18 and RANTES as markers for breast carcinoma progression. J Egypt Natl Canc Inst, 2005, 17: 51–55.
25. Farhat K, Hassen E, Bouzgarrou N, *et al*. Functional IL-18 promoter gene polymorphisms in Tunisian nasopharyngeal carcinoma patients. Cytokine, 2008, 43: 132–137.
26. Liu Y, Lin N, Huang L, *et al*. Genetic polymorphisms of the interleukin-18 gene and risk of prostate cancer. DNA Cell Biol, 2007, 26: 613–618.
27. Campa D, Hung RJ, Mates D, *et al*. Lack of association between -251 T > A polymorphism of IL8 and lung cancer risk. Cancer Epidemiol Biomarkers Prev, 2005, 14: 2457–2458.
28. Tulsyan S, Agarwal G, Lai P, *et al*. Balraj Mittal Significant association of combination of OCT4, NANOG, and SOX2 gene polymorphisms in susceptibility and response to treatment in North Indian breast cancer patients. Cancer Chemother Pharmacol, 2014, 74: 1065–1078.
29. Park S, Cheon S, Cho D. The dual effects of interleukin-18 in tumor progression. Cell Mol Immunol, 2007, 4: 329–335.
30. Vidal-Vanaclocha F, Mendoza L, Telleria N, *et al*. Clinical and experimental approaches to the pathophysiology of interleukin-18 in cancer progression. Cancer Metastasis Rev, 2006, 25: 417–434.
31. Kim J, Shao Y, Kim SY, *et al*. Hypoxia-induced IL-18 increases hypoxia-inducible factor-1alpha expression through a Rac1-dependent NF-kappaB pathway. Mol Biol Cell, 2008, 19: 433–444.
32. Park H, Byun D, Kim TS, *et al*. Enhanced IL-18 expression in common skin tumors. Immunol Lett, 200,79: 215–219.
33. Jiang DF, Liu WL, Lu YL, *et al*. Function of IL-18 in promoting

metastasis of lung cancer. Chin J Oncol (Chinese), 2003, 25: 348–352.
34. Jung MK, Song HK, Kim KE, *et al*. IL-18 enhances the migration ability of murine melanoma cells through the generation of ROI and the MAPK pathway. Immunol Lett, 2006,107: 125–130.
35. Li H, Ge C, Zhao FY, *et al*. Hypoxia-inducible factor 1 alpha-activated angiopoietin-like protein 4 contributes to tumor metastasis via vascular cell adhesion molecule-1/integrin beta 1 signaling in human hepatocellular carcinoma. Hepatology, 2011, 54: 910–919.
36. Al-Marzoqee FY, Khoder G, Al-Awadhi H, *et al*.Upregulation and inhibition of the nuclear translocation of Oct4 during multistep gastric carcinogenesis. Int J Oncol, 2012, 41: 1733–1743.
37. Luo W, Li S, Peng B, *et al*. Embryonic stem cells markers SOX2, OCT4 and Nanog expression and their correlations with epithelial-mesenchymal transition in nasopharyngeal carcinoma. PLoS One, 2013, 8: e56324.
38. Borrull A, Ghislin S, Deshayes F, *et al*. Nanog and Oct4 overexpression increases motility and transmigration of melanoma cells. J Cancer Res Clin Oncol, 2012,138: 1145–1154.
39. Cao L, Li C, Shen S, *et al*. OCT4 increases BIRC5 and CCND1 expression and promotes cancer progression in hepatocellular carcinoma. BMC Cancer, 2013, 13: 82.
40. Dai X, Ge J, Wang X, *et al*. OCT4 regulates epithelial-mesenchymal transition and its knockdown inhibits colorectal cancer cell migration and invasion. Oncol Rep, 2013, 29: 155–160.
41. Zhang Y, Zhang X, Wang X, *et al*. Inhibition of LDH-A by lentivirus-mediated small interfering RNA suppresses intestinal-type gastric cancer tumorigenicity through the downregulation of Oct4. Cancer Lett, 2012, 321: 45–54.
42. Liu S, Ginestier C, Ou SJ, *et al*. Breast cancer stem cells are regulated by mesenchymal stem cells through cytokine networks. Cancer Res, 2011, 71: 614–624.
43. Francipane MG, Alea MP, Lombardo Y, *et al*. Crucial role of interleukin-4 in the survival of colon cancer stem cells. Cancer Res, 2008, 68: 4022–4025.
44. Hwang WL, Yang MH, Tsai ML, *et al*. SNAIL regulates interleukin-8 expression, stem cell-like activity, and tumorigenicity of human colorectal carcinoma cells. Gastroenterology, 2011, 141: 279–291.
45. K S Tsai, S H Yang, Y P Lei, *et al*. Hung, Mesenchymal stem cells promote formation of colorectal tumors in mice. Gastroenterology, 2011,141: 1046–1056.
46. Inda MM, Bonavia R, Mukasa A, *et al*. Tumor heterogeneity is an active process maintained by a mutant EGFR-induced cytokine circuit in glioblastoma. Genes Dev, 2012, 24: 1731–1745.

**DOI 10.1007/s10330-019-0342-2**
**Cite this article as:** Nong SJ, Guan YB, Wang ZW, *et al*. Significant association between IL-18 and OCT4 gene polymorphisms in susceptibility and clinical characteristics of prostate cancer. Oncol Transl Med, 2019, 5: 123–130.

Oncology and Translational Medicine
DOI 10.1007/s10330-018-0297-7

June 2019, Vol. 5, No. 3, P131–P136

ORIGINAL ARTICLE

# Comparison of bone alignment and fiducial marker alignment for online cone-beam computed tomography-guided radiation therapy for prostate cancer

**Hussein M. Metwally** [1, 2] (✉)

[1] Clinical Oncology Department, Faculty of Medicine, Fayoum University, Cairo, Egypt
[2] Dar Al Fouad Hospital, Radiation Unit, Cairo, Egypt

## Abstract

**Objective** The aim of the study was to evaluate the coverage of the prostate when prostatic implanted fiducial markers are used to verify setup of the patients in comparison to the pelvic bones while using cone-beam computed tomography (CBCT).

**Methods** Seventeen patients with prostate cancer were included. For each patient, daily online CBCT was done. CT planning was matched with CBCT with the help of fiducial markers (3–5 markers) and another matching with done the help of pelvic bony landmarks. Registration of clinical target volume (CTV) 1 including prostate plus seminal vesicles and CTV2 including prostate only was done and were used to confirm the target volume during the process of matching. Delineation of the rectum on every CBCT was done. Two automatic margin representing planning target volume (PTV) were created. PTV1 was generated by adding 1 cm in all directions (PTV1a) and 0.7 cm in the posterior direction (PTV1b). PTV2 was generated by adding 0.5 cm in all directions (PTV2a) and 0.3 cm in the posterior direction (PTV2b). PTV1a was prescribed to receive 46 Gy in conventional fractionation with a boost dose of 30 Gy to PTV1b. The same dose was prescribed to PTV2a and PTV2b. Calculation of the percentage of intersection between CTV1 and CTV2 created on CBCT with the original CTV scan was done. A comparison between the two CTVs (CTV1 and CTV2) mean dose and the original delineated CTV was done. Then a comparison to the mean dose of the original CTV of PTV1a, PTV2a (CTV1a and CTV2a), and for PTV1b and PTV2b (CTV1b and CTV2b). Calculation of the mean rectal dose and also V60, V70 and V74 was done on the delineated rectum on every CBCT, and then a comparison to the planned original rectal dose.

**Results** The created CTV1 and CTV2 intersection percentage with the original CTV1 and CTV2 significantly increased by 85% (range, 65%–95%, $P < 0.05$), when fiducial markers were used. The main difference of the received mean dose was significantly less in comparison to pelvic bone alignment (0.03% to 2% vs 0.03% to 11.6% for PTV1a, $P < 0.006$; 0.01% to 1.8% vs 0.03% to 10.2% for PTV2a, $P < 0.014$; 0.08 to 2.11 vs 0.04 to 11.29 for PTV1b, $P < 0.015$ and 0.01 to 1.79 vs 0.01 to 9.69 for PTV2b, $P < 0.004$). With the use of less PTV margins, significant decrease of the rectal mean dose, V60, V70 and V74 by $P < 0.004$, $P < 0.004$, $P < 0.0005$ and $P < 0.009$, respectively. Reduction of the CTV1a and CTV1b mean dose by 1.13% and 0.28% in comparison to the initial CTV1a and CTV2a.

**Conclusion** A significant improvement of prostatic cancer patients alignment when fiducial markers are used, with more homogenous dose distribution, and with significant decrease in PTV margins. The delivered rectal dose is significantly less allowing prostate dose escalation.

Received: 4 September 2018
Revised: 14 December 2018
Accepted: 27 December 2018

**Key words:** cone-beam computed tomography (CBCT); prostate cancer; bone alignment; fiducial marker alignment

✉ Correspondence to: Hussein M. Metwally. Email: khelshahat@yahoo.com

The dose received via external beam radiotherapy represents a curative treatment option for patients of all ages with prostate cancer [1–2].

Three-dimensional conformal irradiation techniques and intensity-modulated radiotherapy (IMRT) are being used increasingly in prostate cancer radiotherapy (RT) to minimize radiation dose to surrounding organs and to improve tumor control by dose escalation [3–5]. These new treatment techniques depend greatly on the precise design of margins during treatment planning. The margins must be large enough to encompass the planning target volume (PTV) within the prescription isodose line and account for patient setup variations and internal organ movement but must be small enough to limit the risk of injury to nearby critical structures.

Offline adaptive radiotherapy strategies [6–10] have been shown to be efficient and robust for designing patient-specific margins using a limited number of observations of patient setup error and internal organ motion.

The introduction of enhanced or new imaging systems in radiation oncology treatment rooms, such as an in-room kilovoltage X-ray system for bony landmark localization and markers [11–13], ultrasound imaging for prostate localization [14–17], or in-room computed tomography (CT) to provide three-dimensional volumetric patient data [18], provides opportunities for more proactive online image guidance based on bony anatomy or soft-tissue registration.

Cone-beam CT (CBCT), implemented onboard a medical accelerator, offers imaging guidance capabilities with great potential for significantly improving treatment accuracy [19].

Many studies have assessed the feasibility and accuracy of implanted gold seeds in the prostate and proved it to be an accurate, feasible, and safe method [20–24].

In this study, we used two different methods to assess accuracy and advantages of using implanted fiducial markers in the prostate with CBCT compared with that using bony landmarks.

## Patients and methods

### Patient population

In this study, we examined the data of 17 patients, with median age of 66 years, who were diagnosed with localized prostate cancer. The stage of disease ranged between T1c and T3a, with a mean Gleason score of 7 ng/mL. All patients were treated in the Institute of Claudius Regaud (Paris, France) between 2007 and 2008 with conformal external beam radiotherapy.

### Fiducial marker implantation

Under local anesthesia, three to five fiducial markers were implanted in the prostate under ultrasound guidance. Implantation was performed at the same day of the planning CT. Patients also underwent pelvic magnetic resonance imaging (MRI) in the same treatment position to be used with the planning CT scan. No complication occurred in any of the patients during the procedure.

### Target volume definition and dosimetric calculations

MRI images were registered to the planning CT scan using semiautomatic fusion system based on the position of the implanted fiducial markers (advantage windows planning system; Sun Nuclear Corporation and Philips, Neu-Isenburg, Germany). Subsequently the images were transferred to the pinnacle planning system (Philips Healthcare, Fitchburg, WI, USA).

On the planning CT scan, with the aid of registered MRI images, target volumes were defined, and the clinical target volume (CTV) 1 (prostate seminal vesicles), CTV2 (prostate), PTV1a, and PTV2a were automatically generated to include CTV1 and CTV2, respectively with a margin of 1 cm all around and 0.7 mm posteriorly.

Organs at risk were defined as follows: the rectal wall with a thickness of 5 mm extending 2 cm above and below PTV1a [25–27]. No special measures were taken for the rectum, but the patients were advised to evacuate the rectum before each session. Bladder wall was defined with a thickness of 7 mm, and the patients were also advised to have a semi-full bladder throughout all the treatment steps.

Dosimetric plans were generated using five fields with angles of (0°, 45°, 90°, 270°, and 315°) by initially using PTV1a at 46 Gy, followed by PTV2a at 30 Gy.

### CBCT acquisition and image registration

All patients were treated using Varian linear accelerator equipped with online CBCT (OBI system; Varian Medical Systems, Inc., Palo Alto, CA, USA). CBCTs were acquired once weekly before treatment delivery throughout the whole treatment period. Only CBCTs with high quality were included in the study, resulting in an mean of five CBCTs for each patient. All CBCTs were transferred to the advantage windows planning system where semi-automatic fusion was performed for each CBCT with the original planning CT once using fiducial markers implanted inside the prostate and once using bony land markers as reference points for fusion. All fused images were transferred to the pinnacle planning system wherein the original contours for CTV1 and CTV2 were copied to each registered image and moved on each CT slice to fit the new prostate position acquired during treatment once with fiducial marker alignment and once with bony landmark alignment. The rectal wall was defined on each CBCT using the same protocol for the initial treatment plan.

### CTV comparison

Three different methods were used in this study to evaluate the accuracy of patient repositioning.

The first method was to identify the percentage of intersection between generated CTVs on each CBCT for each patient and original CTV whether for CTV1 or CTV2. The initial planning CT scan, including contours of the initial CTVs and generated CTVs on each CBCT, were transferred to the pinnacle treatment planning system (Koninklijke Philips N.V., USA) where the percentage of intersection between the initial CTVs and generated CTVs were calculated for fiducial marker registration and bony landmark alignment.

The second method was to assess the dose delivered to CTV1 and CTV2 throughout the treatment period when using fiducial marker and bone alignment. The mean dose received by generated CTVs with the position acquired using fiducial marker and bone landmark alignment was calculated and compared with that of the initial CTVs.

The third method was to evaluate the accessibility of further PTV reduction when using fiducial marker alignment and its effect on the dose received by the rectum. A new PTV was generated around the initial CTV with 0.5 cm all around and 0.3 cm posteriorly (PTV1b and PTV2b) [28]. Another plan was generated using the same angle distribution similar to the initial plan but with the use of PTV1b and PTV2b. The mean dose received by the generated CTVs and V74, V70, and V60 for the rectum defined on the registered CBCTs were calculated and compared with the initial doses received by the initial CTVs and rectum.

## Results

### Percentage of intersection

Calculating the percentage of the volume intersection between CTVs generated on CBCTS and initial CTV showed that the percentage of intersection significantly increased by 85% (rang 65% to 95%) and 86% (range 63% to 95%) for CTV1 and CTV2, respectively, when using fiducial markers as the source for image registration ($P <$ 0.001; Fig. 1).

### Dose calculation

The maximal variations of the mean dose delivered compared with the theoretical dose were significantly lower when using fiducial markers versus that using bony structures while using PTVa or PTVb for calculation.

For PTV1a and PTV2a, the range of variation for fiducial markers was 0.03%–2% and 0.01%–1.8%, whereas that for bone alignment was 0.03%–11.6% and 0.03%–10.2% ($P < 0.006$ and $P < 0.014$, respectively).

For PTV1b and PTV2b, we noted the same positive results in terms of fiducial marker alignment with a range of variation of 0.08–2.11 and 0.01–1.79 versus 0.04–11.29 and 0.01–9.69 ($P < 0.015$ and $P < 0.004$, respectively; Fig. 2).

Comparing the mean values of the mean dose, V74, V70, and V60 received by the contoured rectum on each CBCT with the initial theoretical doses planned to be received by the rectum dose showed that all the doses decreased significantly when using the smaller margin for the PTV with values of $P < 0.0042$, $P < 0.0009$, $P < 0.0005$, and $P < 0.0049$, respectively for volume dose. The mean dose received by the initial CTV1b and CTV2b decreased by 1.13% and 0.28%, respectively, compared with the mean dose received by the initial CTV1a and CTV2a. The percentage of reduction in dose delivered to the rectum was significantly greater than that of the CTV (57.27% versus 0.65%, $P < 0.0049$; Fig. 3).

## Discussion

It is well known that the simulation CT image setup used for treatment planning is a snapshot of the patient's anatomy, although perhaps a most atypical one, because this is the first time a patient is introduced to the position in which RT is going to be performed. Systematic displacements in the prostate position between the simulation CT scan and daily RT sessions occur and can significantly affect the delivered radiation dose in patients with prostate cancer. Direct target localization methods, such as daily US alignment, CBCT with bone alignment, and electronic portal images with the use of intra-prostatic fiducial markers, are commonly used to make adjustments according to this uncertainty [4, 25, 29–37].

Many studies have shown that prostate dose escalation improves freedom from biochemical and clinical progression [38–41].

Using the modern techniques of radiation therapy provides an advantage of prostate dose escalation while decreasing the side effects of the treatment [42]. However, using these modern techniques gave rise to another problem with reduction in treatment field sizes.

In this study, we tried to evaluate the benefits achieved when combining the use of implanted fiducial markers with online CBCT. Having the CBCTs registered to the original planning CT scan allowed us to calculate doses for CTVs and rectums generated on the CBCTs.

Our results showed that the use of this combination can provide a more accurate method in daily patient repositioning than that while using CBCT with bone alignment. This technique allowed a more homogenous dose to be delivered to the CTV throughout the treatment period.

Moreover, we suggest that being more precise in daily alignment of the patient allows for further reduction in PTV volumes. Using a PTV with margins of 5-mm all

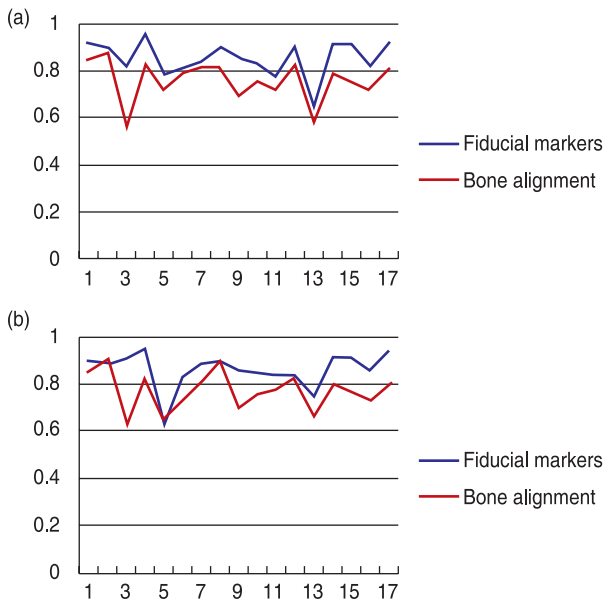


**Fig. 1** Percentage of intersection for CTV1 (a) and CTV2 (b) when using fiducial markers and bone alignment

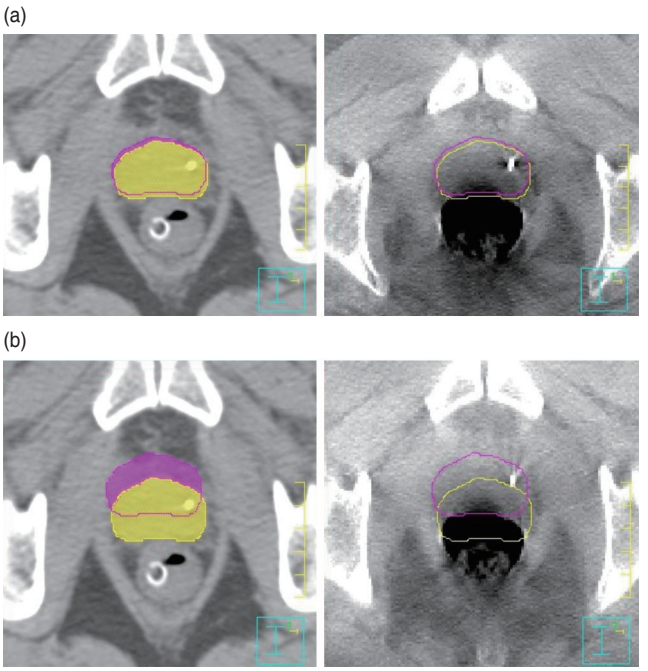


**Fig. 2** Difference in CTV position with fiducial marker alignment (a) and bone alignment (b).

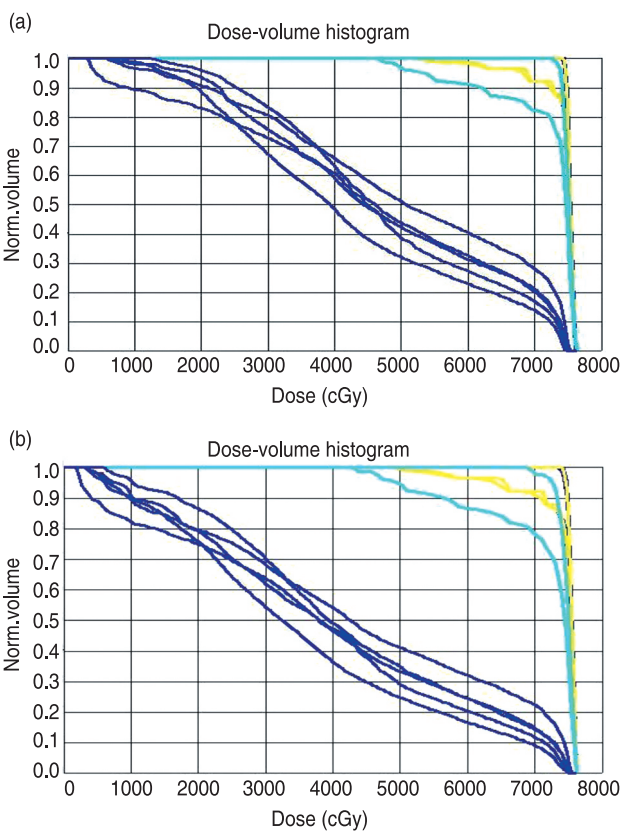


**Fig. 3** Difference in dose received by the rectum and CTV with PTV1 (a) and PTV2 (b)

around and 3 mm posteriorly significantly reduced the dose received by the rectum with minimal reduction to the dose received by the CTV. We believe that the reduction in PTV will allow us to perform prostate dose escalation without exceeding the relative dose thresholds for rectal toxicity/NTCP [22, 42–45].

Daily online matching based on planning for the system is automated. The automated match is visually inspected in each case by the staff. The staff performs a manual match in case of any mismatch. The orthogonal image pairs taken in the first three sessions give an independent validation of the positioning accuracy with the automatic system. This validation demonstrates a sub-millimeter accuracy of the automatic system for matching. However, good accuracy is degraded by intra-fraction movements during the treatment time. Each treatment session takes approximately 8–10 min.

Another point addressed by this study is the accuracy in dose delivery to the seminal vesicles. Our results showed that the accuracy of treatment delivery always increased in terms of CTV intersection and homogenous dose delivery when only treating the prostate. We do believe that repositioning of the seminal vesicles is an important issue that needs more research.

The US-guided fiducial marker insertion for radiotherapy in the present study is well tolerated in the majority of patients with prostate cancer. The severity of most symptoms was Grade 1 or 2. The symptoms in the majority of patients last < 2 weeks.

## Conclusion

A significant improvement of prostatic cancer patients alignment when fiducial markers are used, with more homogenous dose distribution, and with significant decrease in PTV margins. The delivered rectal dose is significantly less allowing prostate dose escalation.

## Conflicts of interest

The author indicates no potential conflicts of interest.

# References


1. Geinitz H, Zimmermann FB, Thamm R, *et al*. 3D conformal radiation therapy for prostate cancer in elderly patients. Radiother Oncol, 2005, 76: 27–34.
2. Nguyen TD, Poortmans PM, van der Hulst M, *et al*. The curative role of radiotherapy in adenocarcinoma of the prostate in patients under 55 years of age: a rare cancer network retrospective study. Radiother Oncol, 2005, 77: 286–289.
3. Pollack A, Zagars GK, Smith LG, *et al*. Preliminary results of a randomized radiotherapy dose-escalation study comparing 70 Gy with 78 Gy for prostate cancer. J Clin Oncol, 2000, 18: 3904–3911.
4. Pollack A, Zagars GK, Starkschall G, *et al*. Prostate cancer radiation dose response: results of the M. D. Anderson phase III randomized trial. Int J Radiat Oncol Biol Phys, 2002, 53: 1097–1105.
5. Yan D, Lockman D, Brabbins D, *et al*. An off-line strategy for constructing a patient-specific planning target volume in adaptive treatment process for prostate cancer. Int J Radiat Oncol Biol Phys, 2000, 48: 289–302.
6. Martinez AA, Yan D, Lockman D, *et al*. Improvement in dose escalation using the process of adaptive radiotherapy combined with three-dimensional conformal or intensity-modulated beams for prostate cancer. Int J Radiat Oncol Biol Phys, 2001, 50: 1226–1234.
7. Welsh JS, Patel RR, Ritter MA, *et al*. Helical tomotherapy: an innovative technology and approach to radiation therapy. Technol Cancer Res Treat, 2002, 1: 311–316.
8. van Herk M, Remeijer P, Rasch C, *et al*. The probability of correct target dosage: dose-population histograms for deriving treatment margins in radiotherapy. Int J Radiat Oncol Biol Phys, 2000, 47: 1121–1135.
9. Keller H, Tomé W, Ritter MA, *et al*. Design of adaptive treatment margins for non-negligible measurement uncertainty: application to ultrasound-guided prostate radiation therapy. Phys Med Biol, 2004, 49: 69–86.
10. Kitamura K, Shirato H, Shimizu S, *et al*. Registration accuracy and possible migration of internal fiducial gold marker implanted in prostate and liver treated with real-time tumor-tracking radiation therapy (RTRT). Radiother Oncol, 2002, 62: 275–281.
11. Millender LE, Aubin M, Pouliot J, *et al*. Daily electronic portal imaging for morbidly obese men undergoing radiotherapy for localized prostate cancer. Int J Radiat Oncol Biol Phys, 2004, 59: 6–10.
12. Zelefsky MJ, Crean D, Mageras GS, *et al*. Quantification and predictors of prostate position variability in 50 patients evaluated with multiple CT scans during conformal radiotherapy. Radiother Oncol, 1999, 50: 225–234.
13. Stroom JC, Koper PC, Korevaar GA, *et al*. Internal organ motion in prostate cancer patients treated in prone and supine treatment position. Radiother Oncol, 1999, 51: 237–248.
14. Beard CJ, Kijewski P, Bussière M, *et al*. Analysis of prostate and seminal vesicle motion: implications for treatment planning. Int J Radiat Oncol Biol Phys, 1996, 34: 451–458.
15. Roeske JC, Forman JD, Mesina CF, *et al*. Evaluation of changes in the size and location of the prostate, seminal vesicles, bladder, and rectum during a course of external beam radiation therapy. Int J Radiat Oncol Biol Phys, 1995, 33: 1321–1329.
16. Jaffray DA, Siewerdsen JH, Wong JW, *et al*. Flat-panel cone-beam computed tomography for image-guided radiation therapy. Int J Radiat Oncol Biol Phys, 2002, 53: 1337–1349.
17. Dehnad H, Nederveen AJ, van der Heide UA, *et al*. Clinical feasibility study for the use of implanted gold seeds in the prostate as reliable positioning markers during megavoltage irradiation. Radiother Oncol, 2003, 67: 295–302.
18. Kupelian PA, Willoughby TR, Meeks SL, *et al*. Intraprostatic fiducials for localization of the prostate gland: monitoring intermarker distances during radiation therapy to test for marker stability. Int J Radiat Oncol Biol Phys, 2005, 62: 1291–1296.
19. Langenhuijsen JF, van Lin EN, Kiemeney LA, *et al*. Ultrasound-guided transrectal implantation of gold markers for prostate localization during external beam radiotherapy: complication rate and risk factors. Int J Radiat Oncol Biol Phys, 2007, 69: 671–676.
20. Poggi MM, Gant DA, Sewchand W, *et al*. Marker seed migration in prostate localization. Int J Radiat Oncol Biol Phys, 2003, 56: 1248–1251.
21. Shirato H, Harada T, Harabayashi T, *et al*. Feasibility of insertion/implantation of 2.0-mm-diameter gold internal fiducial markers for precise setup and real-time tumor tracking in radiotherapy. Int J Radiat Oncol Biol Phys, 2003, 56: 240–247.
22. Fokdal L, Honoré H, Høyer M, *et al*. Dose-volume histograms associated to long-term colorectal functions in patients receiving pelvic radiotherapy. Radiother Oncol, 2005, 74: 203–210.
23. Heemsbergen WD, Hoogeman MS, Hart GA, *et al*. Gastrointestinal toxicity and its relation to dose distributions in the anorectal region of prostate cancer patients treated with radiotherapy. Int J Radiat Oncol Biol Phys, 2005, 61: 1011–1018.
24. Koper PC, Jansen P, van Putten W, *et al*. Gastro-intestinal and genito-urinary morbidity after 3D conformal radiotherapy of prostate cancer: observations of a randomized trial. Radiother Oncol, 2004, 73: 1–9.
25. Létourneau D, Martinez AA, Lockman D, *et al*. Assessment of residual error for online cone-beam CT-guided treatment of prostate cancer patients. Int J Radiat Oncol Biol Phys, 2005, 62: 1239–1246.
26. Serago CF, Chungbin SJ, Buskirk SJ, *et al*. Initial experience with ultrasound localization for positioning prostate cancer patients for external beam radiotherapy. Int J Radiat Oncol Biol Phys, 2002, 53: 1130–1138.
27. Trichter F, Ennis RD. Prostate localization using transabdominal ultrasound imaging. Int J Radiat Oncol Biol Phys, 2003, 56: 1225–1233.
28. Artignan X, Smitsmans MH, Lebesque JV, *et al*. Online ultrasound image guidance for radiotherapy of prostate cancer: impact of image acquisition on prostate displacement. Int J Radiat Oncol Biol Phys, 2004, 59: 595–601.
29. Fuss M, Cavanaugh SX, Fuss C, *et al*. Daily stereotactic ultrasound prostate targeting: inter-user variability. Technol Cancer Res Treat, 2003, 2: 161–170.
30. Boda-Heggemann J, Köhler FM, Küpper B, *et al*. Accuracy of ultrasound-based (BAT) prostate-repositioning: a three-dimensional on-line fiducial-based assessment with cone-beam computed tomography. Int J Radiat Oncol Biol Phys, 2008, 70: 1247–1255.
31. Bylund KC, Bayouth JE, Smith MC, *et al*. Analysis of interfraction

prostate motion using megavoltage cone beam computed tomography. Int J Radiat Oncol Biol Phys, 2008, 72: 949–956.
32. Zhang M, Moiseenko V, Liu M, *et al*. Internal fiducial markers can assist dose escalation in treatment of prostate cancer: result of organ motion simulations. Phys Med Biol, 2006, 51: 269–285.
33. Moseley DJ, White EA, Wiltshire KL, *et al*. Comparison of localization performance with implanted fiducial markers and cone-beam computed tomography for on-line image-guided radiotherapy of the prostate. Int J Radiat Oncol Biol Phys, 2007, 67: 942–953.
34. Serago CF, Buskirk SJ, Igel TC, *et al*. Comparison of daily megavoltage electronic portal imaging or kilovoltage imaging with marker seeds to ultrasound imaging or skin marks for prostate localization and treatment positioning in patients with prostate cancer. Int J Radiat Oncol Biol Phys, 2006, 65: 1585–1592.
35. Van den Heuvel F, Fugazzi J, Seppi E, *et al*. Clinical application of a repositioning scheme, using gold markers and electronic portal imaging. Radiother Oncol, 2006, 79: 94–100.
36. Kuban DA, Tucker SL, Dong L, *et al*. Long-term results of the M. D. Anderson randomized dose-escalation trial for prostate cancer. Int J Radiat Oncol Biol Phys, 2008, 70: 67–74.
37. Peeters ST, Heemsbergen WD, Koper PC, *et al*. Dose-response in radiotherapy for localized prostate cancer: results of the Dutch multicenter randomized phase III trial comparing 68 Gy of radiotherapy with 78 Gy. J Clin Oncol, 2006, 24: 1990–1996.
38. Zelefsky MJ, Fuks Z, Hunt M, *et al*. High dose radiation delivered by intensity modulated conformal radiotherapy improves the outcome of localized prostate cancer. J Urol, 2001, 166: 876–881.
39. Zelefsky MJ, Levin EJ, Hunt M, *et al*. Incidence of late rectal and urinary toxicities after three-dimensional conformal radiotherapy and intensity-modulated radiotherapy for localized prostate cancer. Int J Radiat Oncol Biol Phys, 2008, 70: 1124–1129.
40. Mock U, Bogner J, Georg D, *et al*. Comparative treatment planning on localized prostate carcinoma conformal photon- versus proton-based radiotherapy. Strahlenther Onkol, 2005, 181: 448–455.
41. Bos LJ, van der Geer J, van Herk M, *et al*. The sensitivity of dose distributions for organ motion and set-up uncertainties in prostate IMRT. Radiother Oncol, 2005, 76: 18–26.
42. Wachter S, Gerstner N, Goldner G, *et al*. Rectal sequelae after conformal radiotherapy of prostate cancer: dose-volume histograms as predictive factors. Radiother Oncol, 2001, 59: 65–70.
43. Fiorino C, Cozzarini C, Vavassori V, *et al*. Relationships between DVHs and late rectal bleeding after radiotherapy for prostate cancer: analysis of a large group of patients pooled from three institutions. Radiother Oncol, 2002, 64: 1–12.
44. Foppiano F, Fiorino C, Frezza G, *et al*. The impact of contouring uncertainty on rectal 3D dose-volume data: results of a dummy run in a multicenter trial (AIROPROS01-02). Int J Radiat Oncol Biol Phys, 2003, 57: 573–579.
45. Vargas C, Martinez A, Kestin LL, *et al*. Dose-volume analysis of predictors for chronic rectal toxicity after treatment of prostate cancer with adaptive image-guided radiotherapy. Int J Radiat Oncol Biol Phys, 2005, 62: 1297–1308.

**DOI 10.1007/s10330-018-0297-7**
**Cite this article as:** Metwally HM. Comparison of bone alignment and fiducial marker alignment for online cone-beam computed tomography-guided radiation therapy for prostate cancer. Oncol Transl Med, 2019, 5: 131–136.

Oncology and Translational Medicine
DOI 10.1007/s10330-019-0353-3
June 2019, Vol. 5, No. 3, P137–P146

ORIGINAL ARTICLE

# The combined prognostic value of pretreatment neutrophil-to-lymphocyte ratio, lymphocyte-to-monocyte ratio, and platelet-to-lymphocyte ratio in stage IE/IIE extranodal natural killer/T-cell lymphoma

**Xiaoying Quan (✉)**

Department of Medical Oncology, The Sixth People's Hospital of Chengdu, Chengdu 610051, China

## Abstract

**Objective** This study aimed to explore the combined prognostic value of pretreatment neutrophil-to-lymphocyte ratio (NLR), lymphocyte-to-monocyte ratio (LMR), and platelet-to-lymphocyte ratio (PLR) in newly diagnosed IE/IIE extranodal natural killer/T-cell lymphoma (ENKTL) treated with a P-Gemox regimen combined with radiotherapy or radiotherapy alone.

**Methods** A total of 132 patients from 2009 to 2017 at the Sichuan Cancer Hospital were enrolled in the study. The cutoff values of NLR, LMR, and PLR using overall survival (OS) rate as an endpoint were obtained by the receiver operating curve.

**Results** The cutoff value of NLR was 3.5. Patients with high NLR had significantly shorter progression-free survival (PFS) ($P < 0.001$) and OS ($P < 0.001$) than those with low NLR. Similarly, the cutoff value of LMR was 3.0. The high LMR group had significantly longer PFS ($P=0.001$) and OS ($P < 0.001$) than the low LMR group. Similarly, the cutoff value of PLR was 191.7. The high PLR group was significantly associated with poor PFS ($P < 0.001$) and OS ($P < 0.001$) than the low PLR group. Furthermore, combining NLR, LMR, and PLR to build a new model to stratify patients into low-, intermediate-, intermediate-high-, and high-risk groups, there were also significant differences in PFS ($P < 0.001$) and OS ($P < 0.001$). The univariate analysis showed that presenting B symptoms, stage IIE, local tumor invasion, Eastern Cooperative Oncology Group score ≥ 2, elevated lactate dehydrogenase level, elevated NLR, decreased LMR, and elevated PLR were significantly associated with poor survival. The multivariate analysis demonstrated that PLR was an independent prognostic factor for both PFS (hazard ratio [HR] = 2.073, 95% confidence interval [CI] = 1.080–3.981, $P = 0.028$) and OS (HR = 2.127, 95% CI = 1.102–4.107, $P = 0.025$).

**Conclusion** Elevated pretreatment PLR was a novel simple predictor of poor survival in patients with stage IE/IIE ENKTL. Combining NLR, LMR, and PLR could provide additional stratification.

**Key words:** extranodal natural killer/T-cell; neutrophil-to-lymphocyte ratio; lymphocyte-to-monocyte ratio; platelet-to-lymphocyte ratio; prognosis

Received: 6 May 2019
Revised: 17 June 2019
Accepted: 23 June 2019

Extranodal natural killer/T-cell lymphoma (ENKTL) of the nasal type, is a rare type of non-Hodgkin lymphoma (NHL) with a highly heterogeneous and invasive disease characterized by "lethal midline granuloma" and more commonly observed in Asia than Western countries [1]. Its main histologic changes are shown as obvious vascular destruction, tissue necrosis, and cytotoxic phenotype and closely associated with Epstein-Barr virus infection [2]. Although most patients with ENKTL were diagnosed with stage IE/IIE, previous studies confirmed that quite a few cases were correlated with unsatisfactory treatment outcomes because of highly aggressive biological behavior, rapid disease progression, and recurrence [3–5]. So far, unified treatment strategies have not yet been established for this disease. Though the International Prognostic Index (IPI) and Korean Prognostic Index (KPI)

✉ Correspondence to: Xiaoying Quan. Email: 1193084163@qq.com

have been proved to assess prognosis in patients with ENKTL, the prognostic value remained controversial [6–7] because IPI and KPI scores were based on patients treated with anthracycline-based regimens. Recently, the prognostic index of natural killer/T-cell lymphoma (PINK) [8] was validated to predict prognosis in patients with ENKTL, but a number of patients diagnosed with ENKTL were categorized into low-risk group due to unbalanced distribution, and it may be further modified by other laboratory parameters. Therefore, great efforts have been made to establish a novel predictor for patients with ENKTL.

Recently, emerging evidence [9–12] has revealed the relationship between inflammation and tumor progression. The results have suggested that inflammation mediators (e.g., chemokines, cytokines, free radicals) in the tumor microenvironment created a favorable condition for tumor cells to promote tumor cell growth, proliferation, progression, and metastatic dissemination, as well as treatment resistance and poor prognosis. Presently, meta-analyses have demonstrated that inflammation-based markers, such as neutrophil-to-lymphocyte ratio (NLR) [13], lymphocyte-to-monocyte ratio (LMR) [14], and platelet-to-lymphocyte ratio (PLR)[15], are significantly correlated with poor survival in solid tumors. Meanwhile, the results of clinical studies have also proved that lymphocytes [16], monocytes [17], LMR [18], and PLR [19] are prognostic factors in patients with ENKTL. Until now, no study has been performed to evaluate the combined prognostic value of NLR, LMR, and PLR in patients with ENKTL. Therefore, we retrospectively conducted this study to evaluate the combined prognostic value of NLR, LMR, and PLR in patients with ENKTL treated with P-Gemox regimen combined with radiotherapy or radiotherapy alone.

## Material and methods

### Patients

A total of 132 patients with upper aerodigestive tract ENKTL at Sichuan Cancer Hospital from 2009 to 2017, who were histologically diagnosed based on the 2016 World Health Organization criteria [20] and clinical stage according to the Ann Arbor staging system [21], were recruited. All patients included in this study met the following criteria: (1) new diagnosis of pathologically and immunohistochemically confirmed ENKTL; (2) clinical stage classified as stage I/IIE; (3) no current antitumor therapy; and (4) available clinical follow-up data. Patients with infection or symptoms of inflammation were excluded. We collected the following pretreatment information for the analysis: age, sex, Eastern Cooperative Oncology Group (ECOG) score, B symptoms, and serum lactate dehydrogenase (LDH), neutrophil, lymphocyte, monocyte, and platelet levels. Moreover, to evaluate the stage, bone marrow examination, magnetic resonance imaging or computed tomography (CT) of the head and neck, and CT of the chest and whole abdomen were performed. Peripheral blood sample was collected from each patient using an ethylenediamine tetraacetic acid-treated tube, and calculation of neutrophil, lymphocyte, monocyte, and platelet levels was conducted using the automated hematology system Mindray BC5800 (Mindray, Shenzhen, China).

### Treatments

The treatment strategies for all patients are as follows: 49 patients received P-Gemox sandwich radiotherapy (defined as two or three cycles of chemotherapy followed by radiotherapy and then two or three cycles of original chemotherapy), 42 patients received P-Gemox regimen sequential radiotherapy (defined as two or three cycles of chemotherapy followed by radiotherapy), and 41 patients were treated with radiotherapy alone. P-Gemox (PEG-asparaginase 2500 IU/m$^2$ intramuscular injection on day 1 + gemcitabine 800–1000 mg/m$^2$ intravenous drip on days 1 and 8 + oxaliplatin 130 mg/m$^2$ intravenous drip on day 1). Radiotherapy for the involved field was performed using 6-MeV linear accelerator, intensity modulated radiotherapy, with a dose range of 50–60 Gy (median dose, 56 Gy) for gross tumor volume in daily fractions of 1.8–2.0 Gy, 5 days per week.

### Statistical analysis

Progression-free survival (PFS) was defined as the time interval from the disease diagnosis to the first documented disease progression, or relapse, or death, or until the last follow-up visit. Overall survival (OS) was defined as the time interval from the disease diagnosis to death from any cause or the last follow-up visit. NLR was defined as the neutrophil count to the lymphocyte count ratio; LMR was defined as the lymphocyte count to the mononuclear count ratio; and PLR was defined by the platelet count to the lymphocyte count ratio. The receiver operating curve (ROC) and Youden index (maximum [sensitivity+specificity-1]) were used to determine the optimal cutoff values for NLR, LMR, and PLR. The chi-square test was used to compare the differences between the groups. The Kaplan-Meier method was performed in the survival curve analysis, and the log-rank test was conducted in the univariate analysis. When the *P*-value was < 0.05, the corresponding factor was added into the multivariate analysis. A multivariate analysis was conducted using the Cox regression model. All data were analyzed using SPSS software version 17.0 (SPSS Inc., Chicago, IL). A *P*-value <0.05 was considered statistically significant, and all *P*-values correspond to two-sided significance tests.

## Results

### Optimal cutoff values for NLR, LMR, and PLR

Using OS as an endpoint, stratification based on the NLR, LMR, and PLR was conducted by analyzing the ROC and area under curve (AUC). The optimal cutoff values were 3.5 for NLR (AUC = 0.617, sensitivity = 49.1%, specificity = 77.2%), 3.0 for LMR (AUC = 0.665, sensitivity = 57.0%, specificity = 75.5%), 191.7 for PLR (AUC = 0.652, sensitivity = 52.8%, specificity = 79.7%) (Fig. 1).

### Patient characteristics

The baseline characteristics of 132 patients are shown in Table 1. This study included 92 men and 40 women (ratio, 2.3:1). The median age was 46 years (range, 15–86 years), and 26 patients (19.7%) were aged > 60 years. Of the patients, 77 (58.3%) had stage IE, 35.6% had elevated serum LDH level, 61.4% presented with B symptoms, and 48.5% had local tumor invasion. The majority of patients (75.0%) had an ECOG score of 0–1, and 77.3% had a PINK score of 0. Moreover, 66.7% of patients were assigned to the low NLR group (NLR < 3.5), and the remaining patients (33.3%) were assigned to the high NLR group (NLR ≥ 3.5). Of the patients, 56.1% were categorized into the low LMR group (LMR < 3.0), and 43.9% patients into the high LMR group (LMR ≥ 3.0). Furthermore, 67.4% of the patients were classified as the low PLR group (PLR < 191.7), and the remaining patients (32.6%) as the high PLR group (PLR ≥ 191.7). Forty-nine patients (37.1%) received P-Gemox sandwich radiotherapy, 42 (31.8%) received P-Gemox regimen sequential radiotherapy, and 41 (31.1%) received radiotherapy alone.

### Survival analysis

In 132 patients, follow-up was conducted until March 2019. The median OS was 37 months (range, 3–114 months). In all patients, the 3-year PFS was 59.9% (Fig. 2a), and the 3-year OS was 67.1% (Fig. 2b).

All patients were divided into the low NLR (< 3.5) and high NLR (≥ 3.5) groups by ROC. The 3-year PFS for the two NLR groups were 69.8% and 39.8%, respectively,

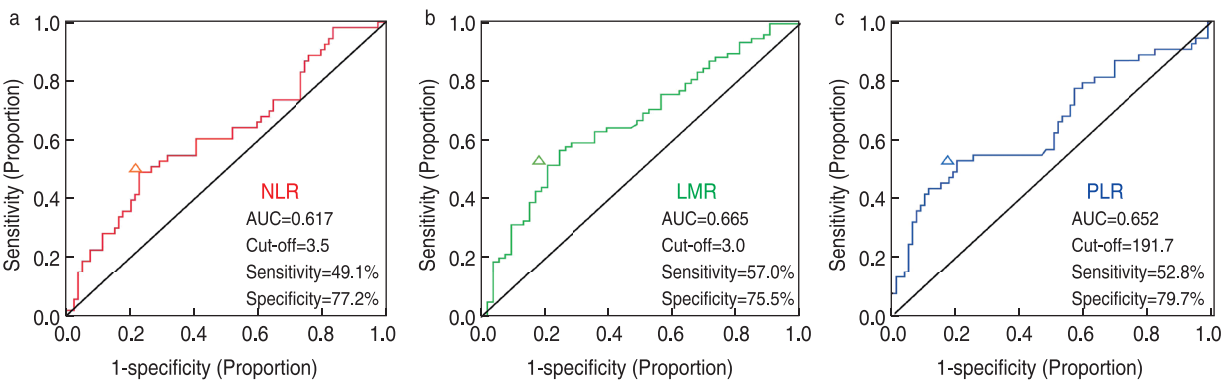


**Fig. 1** The cutoff values of NLR, LMR, PLR obtained by the receiver operating curve using overall survival as endpoint. (a) ROC of NLR; (b) ROC of LMR; (c) ROC of PLR

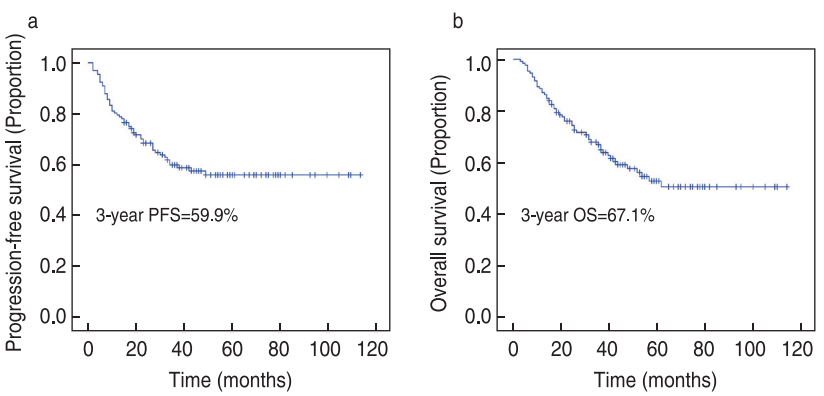


**Fig. 2** Survival curve of the whole patients for PFS and OS. (a) PFS; (b) OS

**Table 1** Baseline clinical characteristics of patients

| Clinical characteristics | No. of patients ($n$ = 132) | Percentage (%) |
|---|---|---|
| Gender | | |
| Male | 92 | 69.7 |
| Female | 40 | 30.3 |
| Age (years) | | |
| ≤ 60 | 106 | 80.3 |
| > 60 | 26 | 19.7 |
| Ann Arbor stage | | |
| IE | 77 | 58.3 |
| IIE | 55 | 41.7 |
| LDH (U/L) | | |
| ≤ 240 | 85 | 64.4 |
| > 240 | 47 | 35.6 |
| B symptoms | | |
| No | 51 | 38.6 |
| Yes | 81 | 61.4 |
| Local tumor invasion | | |
| No | 68 | 51.5 |
| Yes | 64 | 48.5 |
| ECOG | | |
| 0–1 | 99 | 75.0 |
| ≥ 2 | 33 | 25.0 |
| PINK score | | |
| 0 | 102 | 77.3 |
| ≥ 1 | 30 | 22.7 |
| Pretreatment NLR | | |
| < 3.5 | 88 | 66.7 |
| ≥ 3.5 | 44 | 33.3 |
| Pretreatment LMR | | |
| < 3.0 | 58 | 43.9 |
| ≥ 3.0 | 74 | 56.1 |
| Pretreatment PLR | | |
| < 185 | 88 | 66.7 |
| ≥ 185 | 44 | 33.3 |
| Treatment modalities | | |
| P-Gemox sandwich radiotherapy | 49 | 37.1 |
| P-Gemox sequential radiotherapy | 42 | 31.8 |
| Radiotherapy alone | 41 | 31.1 |

and the 3-year OS were 76.8% and 47.0%, respectively. The Kaplan-Meier curve revealed that patients with high NLR had significantly poorer PFS ($\chi^2$ = 12.854, $P$ < 0.001, Fig. 3a) and OS ($\chi^2$ = 14.141, $P$ < 0.001, Fig. 3b). Similarly, all patients were classified into the low LMR (< 3) and high LMR (≥ 3) groups. The 3-year PFS for the two LMR groups were 46.5% and 77.1%, respectively, and the 3-year OS were 58.1% and 78.6%, respectively. Patients with low LMR had significantly shorter PFS ($\chi^2$ = 12.009, $P$ = 0.001, Fig. 3c) and OS ($\chi^2$ = 12.180, $P$ < 0.001, Fig. 3d). All patients were categorized into the low PLR (< 191.7) and high PLR (≥ 191.7) groups. The 3-year PFS for the two PLR groups were 71.6% and 35.2%, respectively, and the 3-year OS were 76.2% and 48.2%, respectively. Patients with high PLR tend to have worse PFS ($\chi^2$ = 18.096, $P$ < 0.001, Fig. 3e) and OS ($\chi^2$ = 19.109, $P$ < 0.001, Fig. 3f) than those with low PLR.

## Survival analysis of combining NLR, LMR, and PLR

Furthermore, combining NLR, LMR, and PLR to establish a new prognostic model (patients with low NLR, high LMR, or low PLR were allocated a score of 0; those with high NLR, low LMR, or high PLR were allocated a score of 1) to stratify patients into the low-risk group (score, 0), intermediate-risk group (score, 1), intermediate-high risk group (score, 2), and high-risk group (score, 3). The 3-year PFS of the four groups were 81.9%, 62.4%, 48.7%, and 23.9%, respectively, and the 3-year OS were 84.0%, 72.4%, 54.6%, and 40.4%, respectively. There were statistically significant difference in PFS ($\chi^2$ = 25.353, $P$ < 0.001, Fig. 4a) and OS ($\chi^2$ = 26.368, $P$<0.001, Fig. 4b) among the four groups.

## Subgroup survival analysis

In the subgroup analysis, when the cutoff values of NLR, LMR, and PLR were added to the group (PINK score 0, 102 patients), patients with high NLR, low LMR, or high PLR had significantly shorter PFS (NLR, $\chi^2$ = 11.648, $P$ = 0.001, Fig. 5a; LMR, $\chi^2$ = 10.336, $P$ = 0.001, Fig. 5c; PLR, $\chi^2$ = 13.640, $P$ < 0.001, Fig. 5e) and OS (NLR, $\chi^2$ = 12.330, $P$ < 0.001, Fig. 5b; LMR, $\chi^2$ = 10.732, $P$ = 0.001, Fig. 5d; PLR, $\chi^2$ = 15.440, $P$ < 0.001, Fig. 5f).

## Prognostic factors for PFS

The results of the univariate and multivariate analyses are presented in Table 2. The univariate analysis showed that B symptoms ($\chi^2$ = 4.572, $P$ = 0.032), stage IIE ($\chi^2$ = 4.324, $P$ = 0.038), local tumor invasion ($\chi^2$ = 5.773, $P$ = 0.016), ECOG score ($\chi^2$ = 28.229, $P$ < 0.001), LDH level ($\chi^2$ = 19.053, $P$ < 0.001), NLR ($\chi^2$ = 12.854, $P$ < 0.001), LMR ($\chi^2$ = 12.009, $P$ = 0.001), and PLR ($\chi^2$ = 18.096, $P$ < 0.001) were significantly associated with PFS. The multivariate analysis demonstrated that ECOG score (HR = 3.371, 95% CI = 1.906–5.961, $P$<0.001), LDH level (HR = 2.298, 95% CI = 1.279–4.128, $P$ = 0.005), and PLR (HR = 2.073, 95% CI = 1.080–3.981, $P$ = 0.028) were independent prognostic factors for PFS.

## Prognostic factors for OS

The results of the univariate and multivariate analyses are shown in Table 3. The univariate analysis demonstrated that B symptoms ($\chi^2$ = 5.018, $P$ = 0.025), stage IIE ($\chi^2$ = 4.248, $P$ = 0.039), local tumor invasion ($\chi^2$ = 5.500, $P$ = 0.019), ECOG score ($\chi^2$ = 29.734, $P$ < 0.001), LDH level ($\chi^2$ = 17.792, $P$ < 0.001), NLR ($\chi^2$ = 14.141, $P$ < 0.001), LMR ($\chi^2$ = 12.180, $P$ < 0.001), and PLR ($\chi^2$ = 19.109, $P$ <

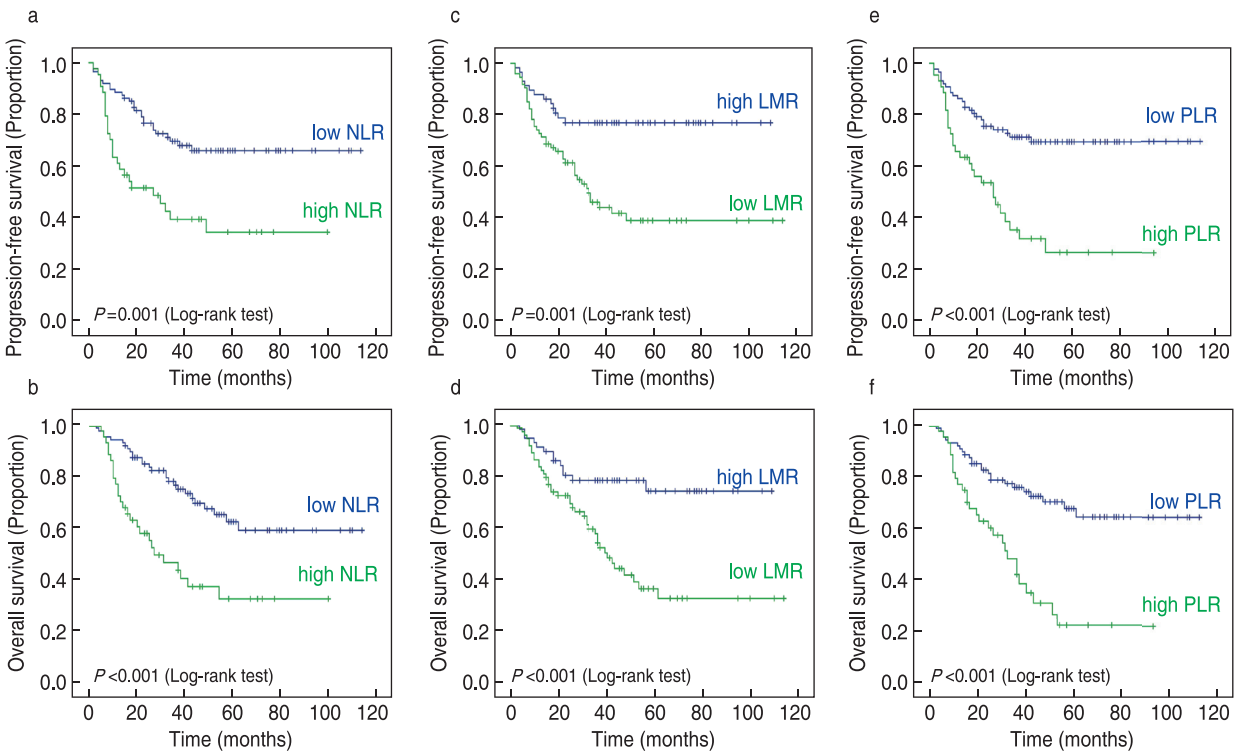


**Fig. 3** Survival curve of the whole patients for NLR, LMR, PLR. (a) PFS curve of ENKTL patients in the two NLR groups (< 3.5 vs ≥ 3.5); (b) OS curve of ENKTL patients in the two NLR groups (< 3.5 vs ≥ 3.5); (c) PFS curve of ENKTL patients in the two LMR groups (< 3.0 vs ≥ 3.0); (d) OS curve of ENKTL patients the two LMR groups (< 3.0 vs ≥ 3.0); (e) PFS curve of ENKTL patients in the two PLR groups (< 191.7 vs ≥ 191.7); (f) OS curve of ENKTL patients in the two PLR groups (< 191.7 vs ≥ 191.7).

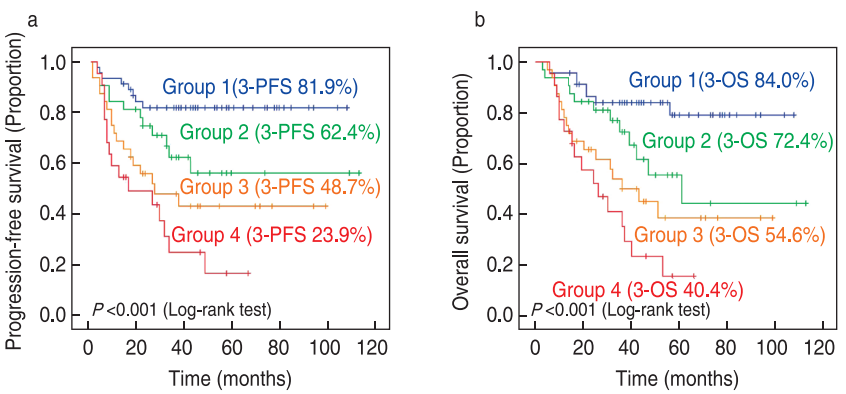


**Fig. 4** Survival curve of combining NLR, LMR and PLR to build a new prognostic model to stratify patients into the low risk group (score 0), intermediate risk group (score 1), intermediate-high group (score 2) and high risk group (score 3). (a) PFS of ENKTL patients in the four groups; (b) OS of ENKTL patients in the four groups

0.001) were significantly related to OS. The multivariate analysis showed that ECOG score (HR = 3.521, 95% CI = 1.984–6.248, $P$<0.001), LDH level (HR = 2.139, 95% CI = 1.197–3.821, $P$ = 0.010), and PLR (HR = 2.127, 95% CI = 1.102–4.107, $P$ = 0.025) were independent prognostic factors for OS.

## Discussion

To our knowledge, ENKTL is a distinct subtype of NHL and is frequently characterized by a prominently heterogeneous disease with poor prognosis. Recently, there are improvements in the validated benefit

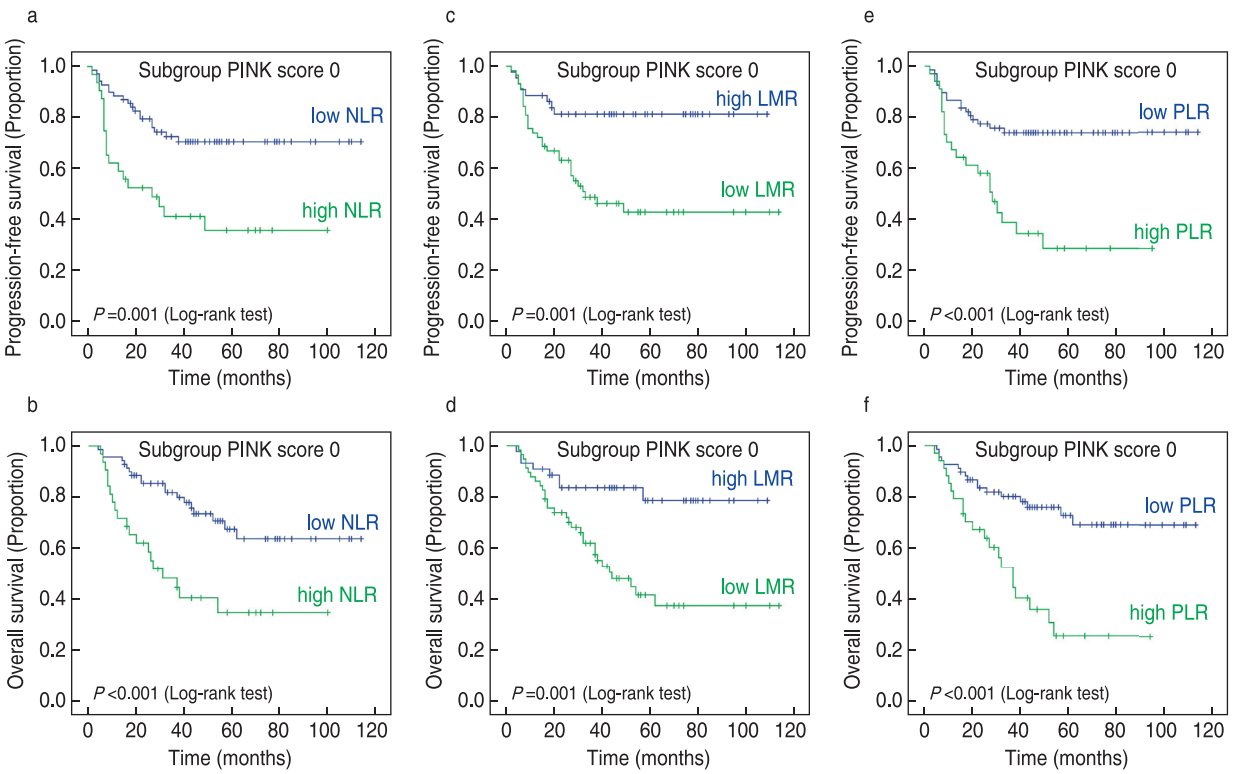


**Fig. 5** Subgroup survival analysis of combining NLR, LMR and PLR to PINK score 0 group. (a) PFS curve of patients with PINK score 0 in the two NLR groups (<3.5 vs ≥3.5); (b) OS curve of patients with PINK score 0 in the two NLR groups (<3.5 vs ≥3.5); (c) PFS curve of patients with PINK score 0 in the two LMR groups (<3.0 vs ≥3.0); (d) OS curve of patients with PINK score 0 in the two LMR groups (<3.0 vs ≥3.0); (e) PFS curve of patients with PINK score 0 in the two PLR groups (<191.7 vs ≥191.7); (f) OS curve of patients with PINK score 0 in the two PLR groups (<191.7 vs ≥191.7)

**Table 2** Prognostic factors analysis of progression free survival

| Clinical characteristics | No. of patients | | | | |
|---|---|---|---|---|---|
| | Univariate | | Multivariate | | |
| | $\chi^2$ | *P* | HR | 95%CI | *P* |
| Gender (male *vs.* female) | 0.067 | 0.795 | – | – | – |
| Age (≤ 60 years *vs.* > 60 years) | 2.043 | 0.153 | – | – | – |
| Stage (IE *vs.* IIE) | 4.324 | 0.038 | 1.021 | 0.481–2.166 | 0.957 |
| LDH (≤ 240 U/L *vs.* > 240 U/L) | 19.053 | < 0.001 | 2.344 | 1.306–4.205 | 0.004 |
| B symptoms (no *vs.* yes) | 4.572 | 0.032 | 0.899 | 0.433–1.869 | 0.776 |
| Local tumor invasion (no *vs.* yes) | 5.773 | 0.016 | 1.328 | 0.595–2.963 | 0.488 |
| ECOG score (0–1 *vs.* ≥2) | 28.229 | < 0.001 | 3.299 | 1.869–5.821 | < 0.001 |
| PINK score (0 *vs.* ≥1 ) | 1.724 | 0.189 | – | – | – |
| NLR (< 3.5 *vs.* ≥3.5) | 12.854 | < 0.001 | 1.195 | 0.594–2.404 | 0.618 |
| LMR (< 3.0 *vs.* ≥3.0) | 12.009 | 0.001 | 1.636 | 0.835–3.202 | 0.151 |
| PLR (< 191.7 *vs.* ≥191.7) | 17.226 | < 0.001 | 1.973 | 1.018–3.824 | 0.044 |

of L-asparaginase-based regimens combined with radiotherapy in patients with early stage ENKTL [22–24]. However, there is still quite a large proportion of patients with stage IE/IIE ENKTL with unappealing outcomes due to disease recurrence or metastasis [3–5]. Therefore, intensive systemic therapy is necessary to prolong survival and improve prognosis in these patients. Previous studies have reported that IPI and KPI scores were initially used to estimate the prognosis of patients with ENKTL but these scores were based on non-asparaginase regimens, and most patients were classified into the low-risk group [6–7]. Recently, the PINK score [8] based on L-asparaginase

**Table 3** Prognostic factors analysis of overall survival

| Clinical characteristics | OS | | | | |
|---|---|---|---|---|---|
| | Univariate | | Multivariate | | |
| | $\chi^2$ | *P* | HR | 95%CI | *P* |
| Gender (male *vs.* female) | 0.104 | 0.747 | – | – | – |
| Age (≤ 60 years *vs.* > 60 years) | 3.324 | 0.068 | – | – | – |
| Stage (IE *vs.* IIE) | 4.248 | 0.039 | 0.923 | 0.438–1.947 | 0.834 |
| LDH (≤ 240 U/L *vs.* > 240 U/L) | 17.792 | < 0.001 | 2.171 | 1.216–3.873 | 0.009 |
| B symptoms (no *vs.* yes) | 5.018 | 0.025 | 1.115 | 0.557–2.231 | 0.759 |
| Local tumor invasion (no *vs.* yes) | 5.500 | 0.019 | 1.177 | 0.532–2.604 | 0.688 |
| ECOG score (0–1 *vs.* ≥ 2) | 29.734 | < 0.001 | 3.464 | 1.955–6.136 | < 0.001 |
| PINK score (0 *vs.* ≥ 1 ) | 3.132 | 0.077 | – | – | – |
| NLR (< 3.5 *vs.* ≥ 3.5) | 14.141 | < 0.001 | 1.381 | 0.684–2.787 | 0.368 |
| LMR (< 3.0 *vs.* ≥ 3.0) | 12.180 | < 0.001 | 1.517 | 0.776–2.969 | 0.223 |
| PLR (< 191.7 *vs.* ≥ 191.7) | 18.525 | < 0.001 | 2.059 | 1.059–4.002 | 0.033 |

chemotherapy showed good prognostic value but this model was mainly based on clinical features and does not completely comprehensively reflect the biological behavior of patients with ENKTL. Therefore, a novel powerful marker to precisely predict the prognosis of patients with ENKTL and appropriately guide the clinical practice is needed.

A mounting body of work [9–12] had been devoted to elucidating the close link between systemic inflammation response and tumor development. The potential explanations that inflammatory cells, proinflammatory cytokines, and chemokines in the tumor microenvironment participated in different pathways of tumor development through facilitated angiogenesis, growth, proliferation, metastasis, and inhibited apoptosis of the malignant cell, leading to worse treatment response, shorter survival, and poorer prognosis. Several studies [13–15] have also confirmed that inflammatory markers such as elevated NLR or PLR and decreased LMR were associated with poor survival in various solid tumors, including ENKTL [18–19]. However, the specific mechanism behind poor tumor prognosis, which might be influenced by NLR, LMR, or PLR, remained completely unclear. Several potential explanations might account for this as follows:

Neutrophil, an inflammatory cell, is an important component of the inflammatory response, and is capable of defense against microorganisms. A high neutrophil count is classically associated with the process of tumor development and likely reflects an increased inflammatory reaction and decreased antitumor immune response [25]. A study by Tecchio *et al* [26] confirmed that production of cytokines by neutrophils (including transforming growth factor-β, oncostatin M) was involved in promoting tumor cell growth and proliferation, as well as invasion. Moreover, accumulating evidence [27–28] showed that neutrophils could promote angiogenesis of tumor cells due to the release of several angiogenic factors (e.g., vascular endothelial growth factor, fibroblast growth factor-2, and angiopoietin-1). Recently, the study conducted by Szczerba *et al* [29] also reported that neutrophils help circulating tumor cells to act on cell cycle progression, resulting in a more efficient metastasis. As already discussed, this might partially indicate why neutrophils have been associated with tumor development. Lymphocytes, a key part in immune response, are responsible for immunosurveillance to remove tumor cells. A series of studies [30–33] have shown that lymphocytes could suppress tumor progression by producing various cytokines (e.g., interferon, tumor necrosis factor, and interleukin-2). Thus, lymphopenia, a reduction in the ability to respond against tumors, is regarded as an indicator of immunosuppression. Therefore, based on these findings and knowledge, it is not surprising that low lymphocyte levels were an independent risk factor for unsatisfactory survival in patients with ENKTL [34–35].

Monocyte is also a type of inflammatory cell from the peripheral blood. Many studies have indicated that tumor-associated macrophages are considered relevant with unfavorable prognosis in tumors, which could secrete monocyte chemoattractant protein-1 to promote tumor angiogenesis, progression, growth, invasion, and distant metastasis through the production of cytokines, chemokines, and proteases (tumor necrosis factor-α, interleukin-1, and interleukin-6) [36–38]. Therefore, monocytes, which play an opposite role to that of lymphocytes, are likely to stimulate and mediate tumor development. A study conducted by Huang *et al* [39] showed that increased monocyte levels were considered as a poor prognostic factor in patients with ENKTL. Platelets, another population of proinflammatory cells

in charge of blood coagulation functions, directly or indirectly participate in the inflammatory response. Thus, thrombocytosis might represent a nonspecific response. Some studies have revealed that activated platelets released a variety of growth factors, chemokines, adhesion molecules, proangiogenic regulatory proteins, and microparticles within the tumor microenvironment to compromise the antitumor ability of natural killer cells and promote tumor cell angiogenesis, growth, proliferation and invasion, and metastasis [40–43]. Moreover, Buergy *et al* [44] reported that increased pretreatment platelet levels were correlated with unfavorable prognosis in different types of tumors.

In this way, inflammation-based markers such as NLR, LMR, and PLR were significant predictors of survival in various types of cancer [13–15]. It was considered that elevated NLR or PLR and decreased LMR were often caused by an imbalance between two types of cells, violating antitumor immune response and tumor-promoting inflammation. Undoubtedly, they may have an impact on survival of patients with cancer patients by affecting the tumor microenvironment and immune system. Meanwhile, NLR, LMR, and PLR, as the ratio of absolute counts between two types of cells, have more relative stability than one type of cell alone. Therefore, in this study, our results also confirmed that a relatively elevated NLR or PLR and decreased LMR were associated with short survival in patients with ENKTL, consistent with the findings of a previous study [18–19]. We further combined NLR, LMR, and PLR to establish a new prognostic model to stratify patients into four risk groups, and there were significant differences in PFS and OS. This might partially explain that, in patients with ENKTL with elevated NLR or PLR and decreased LMR, the balance was tipped toward tumor-promoting inflammation, promoting tumor cell growth, proliferation, and metastasis, compromising the antitumor ability, and resulting in poor treatment outcome and prognosis. Our results are consistent with those of a previous study that increased PLR was an independent risk factor for ENKTL [19]. However, our study indicated that both NLR and LMR were not independent prognostic factors, which was not concluded in the previous study [18]. This may be because, with the simultaneous addition of NLR, LMR, and PLR in the multivariate analysis, PLR might have an influence on NLR or LMR, or the impact of the interaction among the three factors or the confounding effect of other factors could not be completely abolished. Efforts are needed to determine the underlying mechanism. Therefore, NLR or LMR may be a complement prognostic factor for PLR in patients with ENKTL. It is important to note that the cutoff values for LMR and PLR in the ROC of our study were 3.0 and 191.7, respectively, and were different from those of other studies [18–19] (LMR = 3.5, PLR = 185). This variation may be explained by the nature of NLR, LMR, and PLR as nonspecific markers or different treatment regimens, inclusion criteria, or sample sizes. Thus, a consensus on cutoff values for NLR, LMR, and PLR is still to be determined.

Previous studies showed that ECOG score, LDH level, B symptoms, stage, and local tumor invasion were independent prognostic markers in patients with ENKTL [6–8, 16–19]. As expected, our results showed that ECOG score, LDH level, B symptoms, stage, and local tumor invasion were associated with poor prognosis, consistent with the findings of previous studies. Based on previous studies, the multivariate analysis revealed that ECOG score and LDH level remained to be independent prognostic indicators for both PFS and OS. However, it is worth noting that B symptoms, stage, and local tumor invasion were not independent prognostic factors. The reasons for this might be the diagnosis of early stage ENKTL in all patients, retrospectively small sample size, and short-term follow-up. Surprisingly, in the univariate analysis of the current study, no statistical significance was observed in age in the prediction of survival. This might be because all patients with localized lesions had favorable general health status, could develop toxicities with P-Gemox regimens, and were also sensitive to radiotherapy. Although the PINK score was an important prognostic model in patients with ENKTL, our study found that it was not correlated with survival because of the unbalanced distribution, resulting in classification of most patients into the low-risk group. This might partially explain why the PINK score was inapplicable to patients with stage I/IIE. Moreover, we determine whether a new prognostic model is equivalent or superior to other validated prognostic models. We further performed s subgroup analysis. When the cutoff value of NLR, LMR, or PLR was added to the group with PINK score of 0, NLR, LMR, and PLR enabled us to statistically significantly distinguish patients who belong to the “low-risk group”. Therefore, patients with early stage ENKTL needed to be further subdivided to accurately predict the prognosis and appropriately guide the clinical practice. Thus, NLR, LMR, and PLR are useful complements to patients with PINK score 0 to make discrimination of patients into the low-risk group possible. Meanwhile, NLR, LMR, and PLR have the advantage of low cost and ease of access in routine blood examination in clinical practice.

## Conclusion

This study was a single-center, retrospective analysis, and the sample size was small. Despite these limitations, PLR appeared to be a promising marker for early stage ENKTL. NLR and LMR were useful complements to PLR. In the future, large-scale prospective studies are necessary to fully verify the utility of PLR in a clinical setting.

## Conflicts of interest

The author declare no potential conflicts of interest.

## References


1. Liao Y, Du XB, Zou QF. Extranodal natural killer/T-cell lymphoma,nasal type: epidemiology study. Oncol Transl Med, 2012, 11: 290–293.
2. Qian F, Xiao KT, Jing W, *et al*. Prognostic significance of Epstein–Barr virus DNA in NK/T-cell lymphoma: a meta-analysis. Onco Targets Ther, 2018, 11: 997–1004.
3. Lin TC, Chen SU, Chen YF, *et al*. Intramucosal variant of nasal natural killer (NK)/T cell lymphoma has a better survival than does invasive variant: implication on loss of E26 transformation-specific sequence 1 (ETS-1) and T-box expressed in T cells (T-bet) with invasion. Histopathology, 2011, 60: 287–295.
4. Hua W, Pengfei L, Xinke Z, *et al*. Histological vascular invasion is a novel prognostic indicator in extranodal natural killer/T-cell lymphoma, nasal type. Oncol Lett, 2016, 12: 825–836.
5. Makita S, Tobinai K. Clinical features and current optimal management of natural killer/T-cell lymphoma. Hematol Oncol Clin North Am, 2017, 31: 239–253.
6. Chim CS, Ma SY, Au WY, *et al*. Primary nasal natural killer cell lymphoma: long-term treatment outcome and relationship with the international prognostic index. Blood, 2004, 103: 216–221.
7. Au WY, Weisenburger DD, Intragumtornchai T, *et al*. Clinical differences between nasal and extranasal natural killer/T-cell lymphoma: a study of 136 cases from the International Peripheral T-Cell Lymphoma Project. Blood, 2009, 113: 3931–3937.
8. Kim SJ, Yoon DH, Jaccard A, *et al*. A prognostic index for natural killer cell lymphoma after non-anthracycline-based treatment: a multicentre, retrospective analysis. Lancet Oncol, 2016, 17: 389–400.
9. Mantovani A, Allavena P, Sica A, *et al*. Cancer-related inflammation. Nature, 2008, 454: 436–444.
10. Grivennikov SI, Greten FR, Karin M. Immunity, Inflammation, and Cancer. Cell, 2010, 140: 883–899.
11. Schreiber RD, Old LJ, Smyth MJ. Cancer immunoediting: integrating immunity's roles in cancer suppression and promotion. Science, 2011, 331: 1565–1570.
12. Diakos CI, Charles KA, Mcmillan DC, *et al*. Cancer-related inflammation and treatment effectiveness. Lancet Oncol, 2014, 15: e493–e503.
13. Templeton AJ, McNamara MG, Seruga B, *et al*. Prognostic role of neutrophil-to-lymphocyte ratio in solid tumors: a systematic review and meta-analysis. J Natl Cancer Inst, 2014, 106: dju124.
14. Nishijima TF, Muss HB, Shachar SS, *et al*. Prognostic value of lymphocyte-to-monocyte ratio in patients with solid tumors: A systematic review and meta-analysis. Cancer Treat Rev, 2015, 41: 971–978.
15. Templeton AJ, Ace O, Mcnamara MG, *et al*. Prognostic role of platelet to lymphocyte ratio in solid tumors: a systematic review and meta-analysis. Cancer Epidem Biomar, 2014, 23: 1204–1212.
16. Huang JJ, Jiang WQ, Lin TY, *et al*. Absolute lymphocyte count is a novel prognostic indicator in extranodal natural killer/T-cell lymphoma, nasal type. Ann Oncol, 2011, 22: 149–155.
17. Huang JJ, Li YJ, Xia Y, *et al*. Prognostic significance of peripheral monocyte count in patients with extranodal natural killer/T-cell lymphoma. BMC Cancer, 2013, 13: 222.
18. Wang QX, Li SH, Ji BY, *et al*. Lymphocyte/monocyte ratio is a novel predictor for early stage extranodal natural killer/T-cell lymphoma, Nasal Type. J Cancer, 2017, 8: 1030–1037.
19. Wang KF, Chang BY, Chen XQ, *et al*. A prognostic model based on pretreatment platelet lymphocyte ratio for stage IE/IIE upper aerodigestive tract extranodal NK/T cell lymphoma, nasal type. Med Oncol, 2014, 31: 318.
20. Swerdlow SH, Campo E, Pileri SA, *et al*. The 2016 revision of the World Health Organization classification of lymphoid neoplasms. Blood, 2016, 127: 2375–2390.
21. Cheson BD, Fisher RI, Barrington SF, *et al*. Recommendations for initial evaluation, staging, and response assessment of Hodgkin and non-Hodgkin lymphoma: the Lugano classification. J Clin Oncol, 2014, 32: 3059–3068.
22. Wang J, Wang H, Wang Y, *et al*. Analysis of the efficacy and safety of a combined gemcitabine, oxaliplatin and pegaspargase regimen for NK/T-cell lymphoma. Oncotarget, 2016, 7: 35412–35422.
23. Wei W, Wu P, Li L, *et al*. Effectiveness of pegaspargase, gemcitabine, and oxaliplatin (P-GEMOX) chemotherapy combined with radiotherapy in newly diagnosed, stage IE to IIE, nasal-type, extranodal natural killer/T-cell lymphoma. Hematology, 2017, 22: 320–329.
24. Li JW, Li YJ, Zhong MZ, *et al*. Efficacy and tolerance of GELOXD/P-GEMOXD in newly diagnosed nasal-type extranodal NK/T-Cell lymphoma: A multicenter retrospective study. Eur J Haematol, 2018, 100: 247–256.
25. Coolslartigue J, Spicer J, Mcdonald B, *et al*. Neutrophil extracellular traps sequester circulating tumor cells and promote metastasis. J Clin Invest, 2013, 123: 3446–3458.
26. Tecchio C, Scapini P, Pizzolo G, *et al*. On the cytokines produced by human neutrophils in tumors. Semin Cancer Biol, 2013, 23: 159–170.
27. Tecchio C. Neutrophil-derived cytokines involved in physiological and pathological angiogenesis. Chem Immunol Allergy, 2014, 99: 123–137.
28. Galdiero MR, Varricchi G, Loffredo S, *et al*. Roles of neutrophils in cancer growth and progression. J Leukoc Biol, 2017,103: 457–464.
29. Szczerba BM, Castro-Giner F, Vetter M, *et al*. Neutrophils escort circulating tumour cells to enable cell cycle progression. Nature, 2019, 566: 553–557.
30. Salazaronfray F, López MN, Mendozanaranjo A. Paradoxical effects of cytokines in tumor immune surveillance and tumor immune escape. Cytokine Growth Factor Rev, 2007, 18: 171–182.
31. Gooden MJM, De Bock GH, Leffers N, *et al*. The prognostic influence of tumour-infiltrating lymphocytes in cancer: a systematic review with meta-analysis. Br J Cancer, 2011, 105: 93–103.
32. Hsieh CL, Hsu SC, Shen CR, *et al*. Increased expression of IL-21 reduces tumor growth by modulating the status of tumor-infiltrated lymphocytes. Immunobiology, 2011, 216: 491–496.
33. Braumüller, Heidi, Wieder T, Brenner E, *et al*. T-helper-1-cell cytokines drive cancer into senescence. Nature, 2013, 494: 361–365.
34. Huang JJ, Jiang WQ, Lin TY, *et al*. Absolute lymphocyte count is a novel prognostic indicator in extranodal natural killer/T-cell lymphoma, nasal type. Ann Oncol, 2011, 22: 149–155.
35. Zhang YP, Zhang R, Zhu HY, *et al*. Circulating low absolute CD4+ T cell counts may predict poor prognosis in extranodal NK/T-Cell lymphoma patients treating with pegaspargase-based chemotherapy. Cancer Res Treat, 2018, 51: 368-377.
36. Ishii H, Takahara M, Nagato T, *et al*. Monocytes enhance cell proliferation and LMP1 expression of nasal natural killer/T-cell lymphoma cells by cell contact-dependent interaction through membrane-bound IL-15. Int J Cancer, 2012, 130: 48–58.
37. Galdiero MR, Garlanda C, Jaillon S, *et al*. Tumor associated macrophages and neutrophils in tumor progression. J Cell Physiol,

2013, 228: 1404–1412.
38. Rhee I. Diverse macrophages polarization in tumor microenvironment. Arch Pharm Res, 2016, 39: 1588–1596.
39. Huang JJ, Li YJ, Xia Y, *et al*. Prognostic significance of peripheral monocyte count in patients with extranodal natural killer/T-cell lymphoma. BMC Cancer, 2013, 13: 222–222.
40. Bambace NM, Holmes CE. The platelet contribution to cancer progression. J Thromb Haemost, 2011, 9: 237–249.
41. Sharma D, Brummel-Ziedins KE, Bouchard BA, *et al*. Platelets in tumor progression: a host factor that offers multiple potential targets in the treatment of cancer. J Cell Physiol, 2014, 229: 1005–1015.
42. Amo L, Tamayo-Orbegozo E, Maruri N, *et al*. Involvement of platelet-tumor cell interaction in immune evasion. Potential role of podocalyxin-like protein 1. Front Oncol, 2014, 4: 245.
43. Tesfamariam B. Involvement of platelets in tumor cell metastasis. Pharmacol Ther, 2016, 157: 112–119.
44. Buergy D, Wenz F, Groden C, *et al*. Tumor–platelet interaction in solid tumors. Int J Cancer, 2012, 130: 2747–2760.

**DOI 10.1007/s10330-019-0353-3**
**Cite this article as:** Quan XY. The combined prognostic value of pretreatment neutrophil-to-lymphocyte ratio, lymphocyte-to-monocyte ratio, and platelet-to-lymphocyte ratio in stage IE/IIE extranodal natural killer/T-cell lymphoma. Oncol Transl Med, 2019, 5: 137–146.

Oncology and Translational Medicine
DOI 10.1007/s10330-019-0346-6

June 2019, Vol. 5, No. 3, P147–P151

REVIEW ARTICLE

# Regulatory mechanisms of long non-coding RNAs

**Zhigang Luo (✉)**

Department of Oncology, People's Hospital of Jianyang, Jianyang 644000, China

## Abstract

Long non-coding RNAs (lncRNAs) belong to a large and complex family of RNAs, which play many important roles in regulating gene expression. However, the mechanism underlying the dynamic expression of lncRNAs is still not very clear. In order to identify lncRNAs and clarify the mechanisms involved, we collected basic information and highlighted the mechanisms underlying lncRNA expression and regulation. Overall, lncRNAs are regulated by several similar transcription factors and protein-coding genes. Epigenetic modification (DNA methylation and histone modification) can also downregulate lncRNA levels in tissues and cells. Moreover, lncRNAs may be degraded or cleaved via interaction with miRNAs and miRNA-associated protein complexes. Furthermore, alternative RNA splicing (AS) may play a significant role in the post-transcriptional regulation of lncRNAs.

Received: 28 March 2019
Revised: 7 May 2019
Accepted: 7 June 2019

**Key words:** long non-coding RNAs (lncRNAs); regulatory mechanisms; transcriptional factors; chromatin state, alternative splicing; RNA editing, microRNA (miRNA)

Eukaryotic genomes do not act as well-ordered substrates for gene transcription in a conventional manner, and are more complex than was once believed. A fine case in point is that although more than 70% of the human genome is transcribed, only approximately 2% of the transcripts produced may be translated into proteins, as revealed by the ENCODE (Encyclopedia of DNA Element) project [1–2]. Comprehensive testing and examination of RNA species in mammalian cells, as well as studies conducted on genome transcription, have revealed that the transcriptome is extremely complex. Many alternative products are generated during the biogenesis of protein-coding genes. Numerous non-coding RNA (ncRNA) transcripts that are included in the transcriptional background called "noise," are grouped into 2 major classes based on their mode of expression: housekeeping non-coding RNAs and regulatory non-coding RNAs. Transfer, ribosomal, small nuclear, and small nucleolar RNAs, which are usually constitutively expressed, are all classified as housekeeping non-coding RNAs. Regulatory non-coding RNAs include microRNAs (miRNAs), Piwi-interacting RNAs (piRNAs), small interfering RNAs (siRNAs), and long non-coding RNAs (lncRNAs). Unlike the short non-coding RNAs (< 200 nucleotide), lncRNAs range from 200 bp to several kilobases in size, with similar histone-modification profiles, exon/intron lengths and splicing signals to those of protein-coding genes [3–4]. Although lncRNAs share many structural features with protein-coding mRNAs, lncRNAs are often poorly conserved and cannot be translated into proteins. Therefore, only a few lncRNAs have been studied in depth. However, lncRNAs need to be studied further and their genome transcription functions must be well-understood.

## Categories

Based on their genomic loci, lncRNAs may be divided into 5 or more categories: (1) sense; (2) antisense (if the lncRNA transcript overlaps one or more exons of another transcript); (3) intronic (if the lncRNA transcript is present within an intron of a second transcript, which sometimes may encode a protein); (4) bidirectional (if the transcripts of a lncRNA and a neighboring protein coding gene are initiated in close genomic proximity); and (5) intergenic, also called long intervening non-coding RNAs or lincRNAs (if the lncRNA transcript does not overlap exons of protein-coding and other non-coding RNA gene types).

## Cellular localization

To predict the potential function of lncRNAs, its subcellular localization must be considered. The cellular

✉ Correspondence to: Zhigang Luo. Email: 358424970@qq.com

localization of lncRNAs is the same as protein-coding genes. Derrien *et al*, sequenced RNA from nuclear and cytoplasmic cellular fractions and reported that lincRNAs were mainly localized in the chromatin and the nuclei [5]. Moreover, using in situ hybridization analysis data from the Allen Mouse Brain Atlas, Mercer *et al*, identified over 800 non-coding RNAs and found that these RNAs were localized to either certain specific neuroanatomical regions of the nucleus or cytoplasm or to several foci of adult cerebellar Purkinje cells [6]. Certain well-studied lncRNAs, such as Malat 1, Xist, Miat, and Neat 1, mainly localize to the nucleus [7–10]. However, some lncRNAs showing special localization patterns, such as Gomafu (meaning "spotted pattern" in Japanese), which is associated with nuclear speckles, have been identified [8].

## Origins

Unlike protein-coding genes, most long-non-coding RNA sequences are weakly conserved, and only a few exhibit sequence conservation among species. As previously mentioned, many lncRNAs have been verified as being functional, but mechanisms underlying such functions remain unclear. Therefore, it is felt that further studies on the emergence of lncRNA are needed in order to better understand their regulatory functions.

Here, we present a few evolutionary scenarios that may explain the emergence of lncRNAs. The first scenario indicates that lncRNA genes may have metamorphosized from certain protein-coding genes. For example, lncRNA Xist originated by metamorphosizing from a previously protein-coding gene, Lnx3, while including a transposable element [11]. Alternatively, lncRNAs may evolve from other lncRNAs. Duplication of a non-coding gene by retrotransposition may produce either a new functional lncRNA or a nonfunctional retropseudogene. An example of this is mouse nuclear enriched abundant transcript 2 (Neat2), which is paralogous to a mouse testis-derived lncRNA (AK019616) [9]. Another possibility is that some lncRNAs may form following insertion of transposable element sequences. This can be observed in 2 lncRNAs, BC200 (brain cytoplasmic RNA 200-nucleotide) and BC1 (brain cytoplasmic RNA1), which, despite lack of a common origin, play similar roles in translational regulation [12–14].

## Regulation by transcription factors

Some studies have reported that the same transcription factors may act on lncRNAs and protein-coding genes. A recent study found that the Sp1 motif "GGGGCGGGGT" is abundant in bidirectional promoters and that a majority of lncRNAs are transcribed from these promoters [15]. Therefore, SP1 may exert a crucial effect on lncRNA expression. Another study found that among the 1,273 lncRNAs identified using RNA-seq of ribosome-depleted RNA in P493-6 human B-cells, 534 were either up- or down-regulated following MYC over-expression, and that MYC directly binds TSS in 48% lncRNAs. Thus, it may be inferred that the lncRNAs exhibiting a change in production are direct MYC targets [16]. Moreover, by combining luciferase reporter systems and chromatin immunoprecipitation (CHIP) experiments, Huarte *et al*, confirmed that P53 directly binds to the theoretical promoter of lincRNA-P21 (15 kb upstream of CDKN1A) and induces its expression [17]. Another study revealed that P53 may also increase the expression of the lincRNA PANDA, which is located closer to CDKN1A, compared with that of lincRNA-P21 [15]. Furthermore, by using high-density oligonucleotide arrays to map *in vivo* binding sites for Sp1, c-Myc, and p53 in an unbiased manner, Cawley et al., found that approximately 36% of the transcription factor binding sites (TFBS) are located within or immediately 3' to well-characterized genes, the expression levels of which are significantly correlated with those of lncRNAs [18].

In addition, other important transcription factors also play a significant role in the regulation of lncRNAs. It was revealed that 2 newly found lncRNAs that are dysregulated in fatal cardiac tissues with ventricular septal defect, possess TFBS motifs of AP-1 (activating protein-1) or SRF (serum response factor) [19]. Furthermore, there are 5 NF-Kβ binding sites in the promoter region of lncRNA AK019103, and inhibition of NF-Kβ activity significantly reduces AK019103 expression [20].

Recently, some studies have reported that in humans, mice, and zebrafish, transposable elements (TEs) are enriched in both mature lncRNA transcripts and in the vicinity of lncRNA genes, while rarely occurring in protein-coding genes. Moreover, different TE classes are enriched in these 3 species [21]. While the ERV I subclass (alpha retrovirus) is mostly enriched in human lncRNAs, the ERV 2, ERV 3, and ERV K subclasses are enriched in mice [22]. TEs can move and spread in genomes in a lineage-specific fashion and, thus, introduce regulatory elements upon chromosomal insertion. Mammalian TEs have been documented to represent several cis-regulatory sequences of protein-coding genes [23]. One recent finding indicates that TEs located in the vicinity of lncRNAs may contribute to their transcriptional regulation [21]. Although some debate exists with regard to the two scenarios, "lncRNA first" or "TE first," it appears that TEs play an important role in the expression and evolution of lncRNAs.

## Epigenetic modification

In general, epigenetic modification accounts for trait variation in cellular and physiological processes that are not caused by DNA sequence changes, but by dynamic

alterations in the transcriptional potential of a cell. These modifications, including DNA methylation and histone modification, each of which alters gene expression without altering underlying DNA sequences, may or may not be heritable. Once repressor or activator proteins attach to specific regions of the DNA, the expression of downstream genes may change. These epigenetic changes may last through cell divisions for the duration of the cell, and may also last for multiple generations even though they do not involve changes in the underlying DNA sequence of the organism [24–25]. DNA methylation is stable and heritable, but histone modification (methylation or acetylation) may change quickly under the influence of the regulatory networks of cells.

Evidence demonstrates that distinct properties of lincRNAs (low expression levels and cell/tissue type specificity) are directly associated with DNA methylation and histone modification. Some studies examined the expression profile of lncRNAs in embryonic stem cells (ESCs), lineage-restricted neuronal progenitor cells (NPCs), and terminally differentiated fibroblasts, and found that the expression levels of many lncRNAs in these cell types changed. Additionally, promoter histone 3 lysine 4 trimethylation (H3K4me3) and promoter histone 3 lysine 27 trimethylation (H3K27me3) were altered. Further studies have indicated that the knockdown of the H3K27me3 methyltransferase Ezh2 may cause previously repressed lncRNAs to be re-expressed in ES [26]. Therefore there is reason to infer that lncRNAs may be subject to epigenetic regulation in a manner similar to that of protein coding genes.

It is believed that CpG dinucleotides are a remarkable reflection of the DNA methylation level. Mammalian promoters can be classified into two classes: low CpG (LCG); and high DpG (HCG) [27]. As implied by the name, genes that belong to the LCG class may be expressed at lower levels than those that belong to the HCG class. Most lncRNAs are transcribed from LCG promoters and are, thus, frequently expressed at low levels. A recent study indicated that in human sporadic insulinomas (insulin secreting PNETs), a lncRNA maternally expressed gene 3 (Meg3) was altered by hypermethylation at its promoter's CRE-sites. Moreover, in pancreatic neuroendocrine tumors (PNETs), Meg3 can be activated by the protein menin through H3K4me3 and CpG hypomethylation at the Meg3 promoter's CRE site [28]. Meg3 was also markedly reduced upon promoter hypermethylation in 4 human hepatocellular carcinoma (HCC) cell lines [29]. Moreover, 2 well known lncRNAs, XIST and HOTAIR, are targets for site-specific cytosine methylation *in vivo*, and this modification affects the protein binding ability of XIST in the least [30].

Simultaneously, histone methylation or deacetylation is involved in low lncRNA expression and even silencing. It was found that the lncRNA-LET (Low Expression in Tumor) can be repressed via hypoxia-induced histone deacetylase 3 (HDAC3) by reducing the histone acetylation-mediated modulation of the lncRNA-LET3 promoter. This may explain the downregulation of lncRNA-LET observed in colorectal cancers, hepatocellular carcinomas, and squamous cell lung carcinomas [31]. Furthermore, many large intergenic non-coding RNAs (lincRNAs) were identified in the intergenic K4-K36 domain, which not only contains a short region with histone H3K4me3, but also a longer region with histone H3 lysine 36 trimethylation (H3K36me3), indicating that the expression of these lincRNAs may be associated with histone methylation [32–33].

In conclusion, DNA methylation and histone modification determine the low and cell/tissue specific expression of lncRNAs and affect the generation of lncRNAs. The aberrant expression of lncRNAs seen in many diseases results from an abnormal chromatin state.

## Post-transcriptional regulation of lncRNAs

The expression of lncRNAs following transcription is affected by other forms of post-transcriptional pressure, such as degradation by some RNA-binding proteins and the intrinsic half-lives of lncRNAs [34–35]. One study showed that the protein-RNA complex including HuR and let7i/Ago2 may reduce lncRNA HOTAIR's stability in HeLa cells [36], while another study revealed that, in renal carcinoma cells, HOTAIR may bind miR-141 in a sequence-specific way and then be cleaved in an Ago2-dependent manner [37]. Other studies have demonstrated that miRNAs often interact with lncRNAs to regulate their expression strongly.

In addition, RNA provides further means to affect lncRNAs at the post-transcriptional level. LncRNAs often fold into secondary structures or form dsRNAs with target mRNAs and act as candidate substrates for adenosine deaminase acting on RNA (ADAR) [38]. Adenosine to inosine (A-to-I) RNA editing is the most common form of editing in animals. It converts adenosine to inosine in double-stranded RNA regions via the action of ADAR proteins. Most of these specific edits occur in non-coding regions, including non-coding RNAs. A-to-I editing may influence gene expression via nuclear degradation, retention, and alternative splicing. Yang *et al*, found that similar to miRNA editing, lncRNA editing may occur through different processes, such as Tudor-SN mediated degredation [39].

Furthermore, alternative RNA splicing (AS) is a significant post-transcriptional regulatory mechanism active in long intergenic non-coding RNAs (lincRNAs). Several studies reported that annotated human lincRNAs with multiple exons are alternatively spliced

[40–43]. A recent study, compared sequence evolution and biological features of single-exonic lincRNAs and multi-exonic lincRNAs (SELs and MELs, respectively) present in hominoids or conserved in primates, and found that SELs and MELs differed in primary sequence evolution, exon/transcript length, expression breadth and proximity to the nearest coding gene. Thus, SELs and MELs may represent 2 biologically distinct gene groups. Notably, splicing by deletion appears to be disfavored in SELs, compared with MELs. These findings suggest that AS may be associated with the expression levels and functionality of lincRNAs [44].

## Conclusion

As an important factor affecting the regulatory network of gene expression, miRNAs have been studied in detail in recent times. However, the exploration of lncRNAs has just begun. To date, several studies have revealed that lncRNAs may play important roles in the transcriptional regulation of some genes [45–48] as well as in epigenetics [49–51] and are closely associated with human diseases [14, 52–55]. Although the biological function and mechanisms underlying lncRNA regulation remain unclear, growing evidence suggests that lncRNA investigation in human cells has a bright and promising future.

## References


1. Fatica A, Bozzoni I. Long non-coding RNAs: new players in cell differentiation and development. Nat Rev Genet, 2014, 15: 7–21.
2. Gutschner T, Diederichs S. The hallmarks of cancer: a long non-coding RNA point of view. RNA Biol, 2012, 9: 703–719.
3. ENCODE Project Consortium, Birney E, Stamatoyannopoulos JA, *et al*. Identification and analysis of functional elements in 1% of the human genome by the ENCODE pilot project. Nature, 2007, 447: 799–816.
4. Carninci P, Kasukawa T, Katayama S, *et al*. The transcriptional landscape of the mammalian genome. Science, 2005, 309: 1559–1563.
5. Derrien T, Johnson R, Bussotti G, *et al*. The GENCODE v7 catalog of human long non-coding RNAs: analysis of their gene structure, evolution, and expression. Genome Res, 2012, 22: 1775–1789.
6. Mercer TR, Dinger ME, Sunkin SM, *et al*. Specific expression of long noncoding RNAs in the mouse brain. Proc Natl Acad Sci U S A, 2008, 105: 716–721.
7. Clemson CM, Hutchinson JN, Sara SA, *et al*. An architectural role for a nuclear non-coding RNA: NEAT1 RNA is essential for the structure of paraspeckles. Molecular Cell, 2009, 33: 717–726.
8. Sone M, Hayashi T, Tarui H, *et al*. The mRNA-like non-coding RNA Gomafu constitutes a novel nuclear domain in a subset of neurons. J Cell Sci, 2007, 120: 2498–2506.
9. Hutchinson JN, Ensminger AW, Clemson CM, *et al*. A screen for nuclear transcripts identifies two linked non-coding RNAs associated with SC35 splicing domains. BMC Genomics, 2007, 8: 39.
10. Brown CJ, Hendrich BD, Rupert JL, *et al*. The human XIST gene: analysis of a 17 kb inactive X-specific RNA that contains conserved repeats and is highly localized within the nucleus. Cell, 1992, 71: 527–542.
11. Elisaphenko EA, Kolesnikov NN, Shevchenko AI, *et al*. A dual origin of the Xist gene from a protein-coding gene and a set of transposable elements. PLoS One, 2008, 3: e2521.
12. Conley AB, Miller WJ, Jordan IK. Human cis natural antisense transcripts initiated by transposable elements. Trends Genet, 2008, 24: 53–56.
13. Cao X, Yeo G, Muotri AR, *et al*. Non-coding RNAs in the mammalian central nervous system. Annu Rev Neurosci, 2006, 29: 77–103.
14. Zalfa F, Giorgi M, Primerano B, *et al*. The fragile X syndrome protein FMRP associates with BC1 RNA and regulates the translation of specific mRNAs at synapses. Cell, 2003, 112: 317–327.
15. Uesaka M, Nishimura O, Go Y, *et al*. Bidirectional promoters are the major source of gene activation-associated non-coding RNAs in mammals. BMC Genomics, 2014, 15: 35.
16. Hart JR, Roberts TC, Weinberg MS, *et al*. MYC regulates the non-coding transcriptome. Oncotarget, 2014, 5: 12543–12554.
17. Huarte M, Guttman M, Feldser D, *et al*. A large intergenic non-coding RNA induced by p53 mediates global gene repression in the p53 response. Cell, 2010, 142: 409–419.
18. Cawley S, Bekiranov S, Ng HH, *et al*. Unbiased mapping of transcription factor binding sites along human chromosomes 21 and 22 points to widespread regulation of noncoding RNAs. Cell, 2004, 116: 499–509.
19. Song G, Shen Y, Zhu J, *et al*. Integrated analysis of dysregulated lncRNA expression in fetal cardiac tissues with ventricular septal defect. PLoS One, 2013, 8: e77492.
20. Wan G, Hu X, Liu Y, *et al*. A novel non-coding RNA lncRNA-JADE connects DNA damage signalling to histone H4 acetylation. EMBO J, 2013, 32: 2833–2847.
21. Kapusta A, Kronenberg Z, Lynch VJ, *et al*. Transposable elements are major contributors to the origin, diversification, and regulation of vertebrate long noncoding RNAs. PLoS Genet, 2013, 9: e1003470.
22. Mouse Genome Sequencing Consortium, Waterston RH, Lindblad-Toh K, *et al*. Initial sequencing and comparative analysis of the mouse genome. Nature, 2002, 420: 520–562.
23. Bourque G, Leong B, Vega VB, *et al*. Evolution of the mammalian transcription factor binding repertoire via transposable elements. Genome Res, 2008, 18: 1752–1762.
24. Ledford H. Language: Disputed definitions. Nature, 2008, 455: 1023–1028.
25. Bird A. Perceptions of epigenetics. Nature, 2007, 447: 396–398.
26. Wu SC, Kallin EM, Zhang Y. Role of H3K27 methylation in the regulation of lncRNA expression. Cell Res, 2010, 20: 1109–1116.
27. Saxonov S, Berg P, Brutlag DL. A genome-wide analysis of CpG dinucleotides in the human genome distinguishes two distinct classes of promoters. Proc Natl Acad Sci U S A, 2006, 103: 1412–1417.
28. Modali SD, Parekh VI, Kebebew E, *et al*. Epigenetic regulation of the lncRNA MEG3 and its target c-MET in pancreatic neuroendocrine tumors. Mol Endocrinol, 2015, 29: 224–237.
29. Braconi C, Kogure T, Valeri N, *et al*. microRNA-29 can regulate expression of the long non-coding RNA gene MEG3 in hepatocellular cancer. Oncogene, 2011, 30: 4750–4756.
30. Amort T, Soulière MF, Wille A, *et al*. Long non-coding RNAs as targets for cytosine methylation. RNA Biol, 2013, 10: 1003–1008.
31. Yang F, Huo XS, Yuan SX, *et al*. Repression of the long non-coding RNA-LET by histone deacetylase 3 contributes to hypoxia-mediated metastasis. Mol Cell, 2013, 49: 1083–1096.
32. Khalil AM, Guttman M, Huarte M, *et al*. Many human large intergenic noncoding RNAs associate with chromatin-modifying complexes

and affect gene expression. Proc Natl Acad Sci U S A, 2009, 106: 11667–11672.
33. Mikkelsen TS, Ku M, Jaffe DB, *et al*. Genome-wide maps of chromatin state in pluripotent and lineage-committed cells. Nature, 2007, 448: 553–560.
34. Yoon JH, Abdelmohsen K, Srikantan S, *et al*. LincRNA-p21 suppresses target mRNA translation. Mol Cell, 2012, 47: 648–655.
35. Clark MB, Johnston RL, Inostroza-Ponta M, *et al*. Genome-wide analysis of long non-coding RNA stability. Genome Res, 2012, 22: 885–898.
36. Yoon JH, Abdelmohsen K, Kim J, *et al*. Scaffold function of long non-coding RNA HOTAIR in protein ubiquitination. Nat Commun, 2013, 4: 2939.
37. Chiyomaru T, Fukuhara S, Saini S, Majid S, *et al*. Long non-coding RNA HOTAIR is targeted and regulated by miR-141 in human cancer cells. J Biol Chem, 2014, 289: 12550–12565.
38. Mercer TR, Mattick JS. Structure and function of long non-coding RNAs in epigenetic regulation. Nat Struct Mol Biol, 2013, 20: 300–307.
39. Yang Y, Zhou X, Jin Y. ADAR-mediated RNA editing in non-coding RNA sequences. Sci China Life Sci, 2013, 56: 944–952.
40. Washietl S, Kellis M, Garber M. Evolutionary dynamics and tissue specificity of human long non-coding RNAs in six mammals. Genome Research, 2014, 24: 616–628.
41. Necsulea A, Soumillon M, Warnefors M, *et al*. The evolution of lncRNA repertoires and expression patterns in tetrapods. Nature, 2014, 505: 635–640.
42. Novikova IV, Hennelly SP, Tung CS *et al*. Rise of the RNA machines: exploring the structure of long non-coding RNAs. J Mol Biol, 2013, 425: 3731–3746.
43. Keren H, Lev-Maor G, Ast G. Alternative splicing and evolution: diversification, exon definition and function. Nat Rev Genet, 2010, 11: 345–355.
44. Chen FC, Pan CL, Lin HY. Functional implications of RNA splicing for human long intergenic non-coding RNAs. Evol Bioinform Online, 2014, 10: 219–228.
45. Hirota K, Miyoshi T, Kugou K, *et al*. Stepwise chromatin remodelling by a cascade of transcription initiation of non-coding RNAs. Nature, 2008, 456: 130–134.
46. Conley AB, Miller WJ, Jordan IK. Human cis natural antisense transcripts initiated by transposable elements. Trends Genet, 2008, 24: 53–56.
47. Ponjavic J, Ponting CP. The long and the short of RNA maps. Bioessays, 2007, 29: 1077–1080.
48. Katayama S, Tomaru Y, Kasukawa T, *et al*. Antisense transcription in the mammalian transcriptome. Science, 2005, 309: 1564–1566.
49. Peters J, Robson JE. Imprinted non-coding RNAs. Mamm Genome, 2008, 19: 493–502.
50. Cai X, Cullen BR. The imprinted H19 non-coding RNA is a primary microRNA precursor. RNA, 2007, 13: 313–316.
51. Chaumeil J, Le Baccon P, Wutz A, *et al*. A novel role for Xist RNA in the formation of a repressive nuclear compartment into which genes are recruited when silenced. Genes Dev, 2006, 20: 2223–2237.
52. Faghihi MA, Modarresi F, Khalil AM, *et al*. Expression of a non-coding RNA is elevated in Alzheimer's disease and drives rapid feed-forward regulation of beta-secretase. Nat Med, 2008, 14: 723–730.
53. Broadbent HM, Peden JF, Lorkowski S, *et al*. Susceptibility to coronary artery disease and diabetes is encoded by distinct, tightly linked SNPs in the ANRIL locus on chromosome 9p. Hum Mol Genet, 2008, 17: 806–814.
54. Mus E, Hof PR, Tiedge H. Dendritic BC200 RNA in aging and in Alzheimer's disease. Proc Natl Acad Sci U S A, 2007, 104: 10679–10684.
55. Moseley ML, Zu T, Ikeda Y, *et al*. Bidirectional expression of CUG and CAG expansion transcripts and intranuclear polyglutamine inclusions in spinocerebellar ataxia type 8. Nat Genet, 2006, 38: 758–769.

**DOI 10.1007/s10330-019-0346-6**
**Cite this article as:** Luo ZG. Regulatory mechanisms of long non-coding RNAs. Oncol Transl Med, 2019, 5: 147–151.

# Call For Papers
# Oncology and Translational Medicine

(CN 42-1865/R, ISSN 2095-9621)

Dear Authors,

*Oncology and Translational Medicine* (OTM), a peer-reviewed open-access journal, is very interested in your study. If you have unpublished papers in hand and have the idea of making our journal a vehicle for your research interests, please feel free to submit your manuscripts to us via the Paper Submission System.

Aims & Scope

- Lung Cancer
- Liver Cancer
- Pancreatic Cancer
- Gastrointestinal Tumors
- Breast Cancer
- Thyroid Cancer
- Bone Tumors
- Genitourinary Tumors
- Brain Tumor
- Blood Diseases
- Gynecologic Oncology
- ENT Tumors
- Skin Cancer
- Cancer Translational Medicine
- Cancer Imageology
- Cancer Chemotherapy
- Radiotherapy
- Tumors Psychology
- Other Tumor-related Contents

Contact Us
Editorial office of Oncology and Translational Medicine
Tongji Hospital
Tongji Medical College
Huazhong University of Science and Technology
Jie Fang Da Dao 1095
430030 Wuhan, China
Tel.: 86-27-69378388
Email: dmedizin@tjh.tjmu.edu.cn;
dmedizin@sina.com

*Oncology and Translational Medicine* (OTM) is sponsored by Tongji Hospital, Tongji Medical College, Huazhong University of Science and Technology, China (English, bimonthly).

OTM mainly publishes original and review articles on oncology and translational medicine. We are working with the commitment to bring the highest quality research to the widest possible audience and share the research work in a timely fashion.

Manuscripts considered for publication include regular scientific papers, original research, brief reports and case reports. Review articles, commentaries and letters are welcome.

About Us

- Peer-reviewed
- Rapid publication
- Online first
- Open access
- Both print and online versions

For more information about us, please visit:
http://otm.tjh.com.cn